Federal Ministry of Education and Research

Ministry of Innovation, Science & Technology

MOST- BMBF Cooperation in Water Technology Research

Status Seminar

25-27 Oct, 2022

Leonardo Plaza Hotel, Ashdod, Israel

Contact

Federal Ministry of Education and Research (BMBF), Germany

Dr. Helmut Löwe
Email: Helmut.Loewe@bmbf.bund.de

Ministry of Innovation, Science and Technology (MOST), Israel

On scientific matters:
Dr. Moshe Ben Sasson
Email: mosheBS@most.gov.il

On administrative matters:
Ms. Shani Edri
Email: shani@most.gov.il

Project Management Agency Karlsruhe (PTKA), Germany

Dr. Leif Wolf
Email: leif.wolf@kit.edu

Dr. Sina Hale
Email: sina.hale@kit.edu

Further information on the German-Israeli cooperation is available at

WWW.COGERIL.DE

OVERVIEW PROGRAM

TUESDAY, OCTOBER 25TH, 2022

08:30 - 09:00 Registration + Coffee and Mingling

09:00 – 09:20 Greetings: MOST and BMBF

09:20 – 10:00 **WT1801** - "Bioaugmentation and Monitoring for Aerobic Chloroethene Biodegradation"

Principal Investigators: Prof. Ariel Kushmaro / Prof. Dr. Andreas Tiehm

10:00 – 10:40 **WT1805** - "PALM-IRRI - Improve date palm irrigation scheduling"

Principal Investigators: Prof. Naftali Lazarovitch / Prof. Dr. Johan A. Huisman

10:40 – 11:00 Coffee Break

11:00 – 11:40 **WT1803** - "Cosmic-Ray Neutron Sensor for quantifying Non-Rainfall Water Inputs (CoNRaWI)"

Principal Investigators: Prof. Nurit Agam / Dr. Martin Schrön

11:40 – 12:20 **WT1804** - "ISCO3 for GW remediation"

Principal Investigators: Dr. Ines Zucker / PD Dr. Uwe Hübner

12:20 – 13:00 **WT1802** - "NanoWater": Pathogen detection by plasmonic nanoarray

Principal Investigators: Prof. Yechezkel Kashi / Prof. Gilad Yossifon / Apl. Prof. Dr. Wolfgang Fritzsche

13:00 – 13:45 Lunch

14:00 – 16:00 Ashdod port ***(Please bring your Passports and comfortable clothing and shoes)***

16:30 – 18:30 Cruise + Happy Hour

20:00 – 21:00 Dinner

WEDNESDAY, OCTOBER 26TH, 2022

08:30 – 09:10 **WT2003** - "CatMemReac: CO_2 reduction in oxidation of micropollutants - energy intensive vs. novel solar based processes"

Principal Investigators: Prof. Hadas Mamane / Dipl.-Ing. Christiane Chaumette

09:10 – 09:50	**WT1901** - "MoDiCon: Online Monitoring and Digital Control in drinking water distribution systems" *Principal Investigators: Prof. Avi Ostfeld / Prof. Dr.-Ing. Mathias Ernst & Prof. Pu Li*
09:50 – 10:30	**WT1902** - "NEMWARE: NanoElectroMembrane processes for micropollutant removal in water reuse" *Principal Investigators: Prof. Daniel Mandler / Prof. Dr. Andrea Schäfer*
10:30– 10:50	Coffee Break
10:50 – 11:30	**WT2001** - "LowGHGWatt: Reduction green-house gas emissions in the water treatment sector by integrated technologies for biofouling mitigation" *Principal Investigators: Dr. Roy Bernstein/ Prof. Dr. Steffen Witzleben*
11:30 – 12:10	**WT2002** - "Red-CO2-PNA: Water technology to reduce the CO2-Footprint of the water sector" *Principal Investigators: Prof. Michal Green / Prof. Dr. Susanne Lackner*
12:10 – 12:50	**WT2004** - "EconWatSim: Developing an economic simulation-modelling framework as a decision-support tool for policymakers in the water sector" *Principal Investigators: Prof. Iddo Kan / Dr. Jonas Luckmann*
12:50 – 13:00	Closing Words
13:00 – 14:30	Lunch
15:00 – 17:30	Cycling + Delphis Center Tour ***(Please bring comfortable clothing and shoes)***
18:00 – 19:00	Preparations at the hotel
19:30	Happy hour + Festive dinner at restaurant

THURSDAY, OCTOBER 27TH, 2022

8:15	Pick up from the Hotel *(Please bring comfortable clothing and shoes)*
09:00 – 10:00	Excursion Talmei Yafe
10:30 – 13:00	Tour in Ashkelon's National Park

Project WT1801

Bioaugmentation and Monitoring for Aerobic Chloroethene Biodegradation (BioChlor)

Ariel KUSHMARO[1*], Asher BRENNER[2], Rita MEJUBOVSKY-MIKHELIS[1]
Andreas TIEHM[3*], Anna WILLMANN[3], Axel MÜLLER[3], Johannes HO[3]

[1]*Avram and Stella Goldstein-Goren Department of Biotechnology Engineering, Ben Gurion University, Israel*
[2] *Department of Civil and Environmental Engineering, Ben-Gurion University, Israel*
[3] *Department of Water Microbiology, DVGW- Technologiezentrum Wasser (TZW), Germany*
**Corresponding authors: andreas.tiehm@tzw.de ; arielkus@bgu.ac.il*

ABSTRACT
Contaminated sites affect groundwater, one of the most important drinking water resource worldwide. Efficient and cost-effective remediation processes for the removal of pollutants from the groundwater and soil are therefore necessary. Chloroethenes frequently contaminate groundwater in Germany and Israel. These compounds are particularly persistent and harmful, making the remediation of groundwater a complex challenge. The collaborative research of the German and Israeli teams has characterized aerobic metabolic degradation pathways that overcome the shortcomings of the hitherto existing anaerobic bioremediation concepts. Microcosm studies were conducted with groundwater samples from different contaminated sites to investigate their intrinsic trichloroethene (TCE) degradation potential as well as stimulation potential through bioaugmentation. The microcosms without inoculum proved the occurrence of aerobic TCE-metabolizing bacteria stimulated by the supply of oxygen in 54 % of the groundwater samples. Degradation started in most cases after adaption times of up to 92 d or the addition of mineral nutrients. The doubling time of 24 d indicated comparatively slow growth of the TCE degrading microorganisms. However, bioaugmentation was successful in all groundwater samples with TCE concentrations below 41 mg/L. The microbial communities of Israeli and German contaminated sites were taxonomically and functionally characterized, and a specific PCR-based detection method is in progress. First steps to develop a monitoring method were successfully carried out. Specific qPCR detection is currently tested with laboratory and field samples.

KEYWORDS
Aerobic biodegradation; Groundwater remediation; Chloroethenes; TCE; Doubling time

INTRODUCTION
The majority of groundwater contaminations is caused by chlorinated hydrocarbons such as chloroethenes. These compounds are persistent in the environment and particularly harmful (Mattes et al. 2010). In general, microbiological remediation processes can provide a sustainable, environmentally friendly and cost-effective alternative to conventional pump-and-treat procedures. Under anaerobic conditions and after addition of organic auxiliary substrates, perchloroethene (PCE) or TCE are transformed via the metabolites dichloroethene (DCE) and vinyl chloride (VC) to ethane (Dolinová et al. 2017). Competing microbial reactions (i.e., methanogenesis or sulfate reduction) can lead to detrimental changes in groundwater quality. In case of the new process of aerobic metabolic degradation, no hazardous metabolites are

formed and no side reactions occur (Schmidt et al. 2014). In addition, the oxygen demand is considerably lower than in aerobic co-metabolic degradation (Gaza et al. 2019). Hence, this degradation pathway is an efficient way to eliminate pollutants. The microorganisms responsible for the aerobic metabolic degradation of chloroethenes have not yet been identified. Furthermore, there are no methods to monitor this degradation process specifically at field sites. In order to develop innovative remediation strategies
and monitoring methods for aerobic chloroethene degradation, studies were conducted to identify
the microorganisms and to stimulate the degradation pathway. Laboratory and field data were evaluated to establish comprehensive remediation concepts for Israeli and German contaminated sites.

METHODS

Microcosm studies were performed to investigate the intrinsic degradation potential as well as the stimulation potential through bioaugmentation with an enrichment culture. Groundwater from several sites contaminated with choroethenes was considered. From each well, samples were inoculated with aerobic TCE degrading enrichment culture in mineral salts medium and immobilized on silica sand. One sample was left unchanged to investigate the intrinsic degradation potential. In addition, copper sulfate was added to one batch as an abiotic control. The headspace contained ambient air so that oxygen was sufficiently available for aerobic degradation at all times. Redox parameters such as oxygen, pH, and temperature were measured during sampling to document environmental conditions. The content of chloroethenes (perchloroethene (PCE), trichloroethene (TCE), cis-dichloroethene (cDCE), vinyl chloride (VC), and ethene) was measured by gas chromatography (ECD and FID). Ion chromatography was used to determine the degradation product chloride as well as nitrate, nitrite, and sulfate. The measurement of DOC was used to check the organic components in groundwater.

Detailed taxonomic and functional characterization of microbial communities in Israeli and German chloroethenes contaminated samples were performed using amplicon of 16S rRNA gene and shotgun metagenomics.

RESULTS AND DISCUSSION

Intrinsic and bioaugmented trichloroethene (TCE) degradation

Surprisingly, 54 % of groundwater samples showed a significant TCE decrease without inoculation. Taking into account losses during sampling and into the increasing gas phase over the experimental period, the sterile controls show relatively constant concentrations of the chloroethenes. Accordingly, abiotic effects such as volatilization can be ruled out and biodegradation processes were demonstrated in the active microcosms. The concentrations or decreases of the other chloroethenes were lower, which excludes co-metabolic degradation of TCE with another chloroethene as the growth substrate. Also, the minor DOC decreases are insufficient as primary substrates in relation to the total amount of TCE degraded. Figure 1 shows the TCE concentration of a microcosm series with comparably high concentrations. Significant TCE decrease compared to the sterile control is evident in the non-inoculated microcosm and could be reproduced after spiking TCE at day 133. Compared to the microcosms with inoculum, which showed rapid TCE degradation after the start of the experiment, degradation without bioaugmentation occurred after a lag time of approximately 70 d. In the other degrading microcosms, lag phases of up to 92 days were observed and one microcosm showed TCE degradation only after the addition of inorganic nutrients. In some microcosms, the background concentration of chloride was low enough and the amount of degraded TCE was high enough to observe significant and nearly stoichiometric formation of the degradation

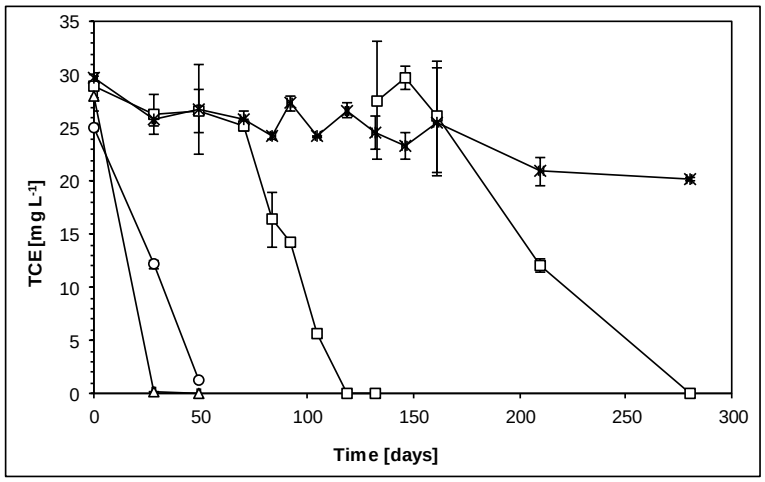

Figure 1: TCE concentrations of a microcosm series showing intrinsic degradation without inoculum (□) as well as accelerated degradation by bioaugmentation with liquid (○) and immobilized culture on silica sand (△) compared to the sterile control (✱).

product chloride, demonstrating aerobic metabolism. From the exponential increase in chloride formation, a doubling time of 24 d was determined.

The bioaugmentation with enrichment culture was successful in all groundwater samples with TCE concentrations up to 41 mg/L. Only the microcosms of one well with chloroethenes beyond 100 mg/L showed no decline in TCE concentration. Figure 2 gives an example of a microcosm series without intrinsic degradation potential. While TCE levels remain relatively constant over the
experimental period in the sterile control and without inoculation, the inoculated microcosms show a significant TCE decrease. TCE degradation could be re-produced after spiking. The initial concentrations of comparatively low 0.02 mg/L were increased to 1 mg/L after 56 days and to 5 mg/L after repeated degradation on day 133. For groundwater samples with intrinsic degradation potential, bioaugmentation resulted in accelerated degradation (Figure 1). Corresponding chloride formation was observed in all microcosms where the TCE decrease was large and the background chloride concentration was low. At the Sindelfingen site, oxygen is infiltrated for stimulation. Stable and efficient TCE degradation has been successfully established even after operational disturbances, system interventions, and expansions, demonstrating remediation applicability under field conditions.

Microbial community analysis

There is a significant difference between the microbial communities present in contaminated groundwater in Israel and Germany. Most of the OTUs in Israeli and German samples are associated with bacteria (> 95 %) and some of the samples contain OTUs associated with archaea (< 2 %). The microbial diversity at the phylum level shows that the most abundant OTUs in Israeli and German samples are related to Proteobacteria (49 – 88 %) which some of its members (alpha, beta and gamma) are capable of degrading chloroethenes via aerobic metabolic or co-metabolic pathway.

Actinobacteria phyla that are considered as chloroethenes degraders are also present (3 – 10 %). Microbial genera that are well known in aerobic metabolic and co-metabolic chloroethenes degrading pathways e.g., *Bacillus, Brevundimonas, Burkholderia, Comamonas, Methylobacter, Methylococcus, Methylocystis, Methylomonas, Mycobacterium, Nitrosomonas, Nocardioides, Polaromonas, Pseudomonas, Ralstonia, Rhodococcus* and *Rhodoferax* were identified.

CONCLUSIONS

For remediation practice, aerobic metabolic TCE degradation has significant advantages over anaerobic dechlorination and aerobic co-metabolism because no auxiliary substrates are required, no competitive reactions occur, and no hazardous metabolites are formed. In addition, the oxygen demand is considerably lower than in aerobic co-metabolic degradation. Inoculation with a degradative culture (bioaugmentation) can be a promising option for contaminated sites, where the responsible microorganisms are not present or not sufficiently active.

ACKNOWLEDGEMENT

This work was carried out as part of the BMBF-MOST project (German-Israeli Cooperation in Water Technology Research) BioChlor (Bioaugmentation and Monitoring Methods Development for Aerobic Chloroethene Biodegradation in Groundwater). The authors would like to thank the German Federal Ministry of Education and Research (BMBF) (grant number 02WIL1520) and the Israeli Ministry of Science, Technology and Space (MOST) (grant number WT-1801) for financial support of the project as well as The German Federal Environmental Foundation for supporting the accompanying dissertation (Anna Willmann).

REFERENCES

Dolinová I, Štrojsová M, Černík M, Němeček J, Macháčková J, Ševců A (2017) Microbial degradation of chloroethenes: A review. Environmental Science and Pollution Research 24:13262–13283. https://doi.org/10.1007/s11356-017-8867-y

Gaza S, Schmidt KR, Weigold P, Heidinger M, Tiehm A (2019) Aerobic metabolic trichloroethene biodegradation under field-relevant conditions. Water research 151:343–348. https://doi.org/10.1016/j.watres.2018.12.022

Mattes TE, Alexander AK, Coleman NV (2010) Aerobic biodegradation of the chloroethenes: Pathways, enzymes, ecology, and evolution. FEMS Microbiology Reviews 34:445–475. https://doi.org/10.1111/j.1574-6976.2010.00210.x

Schmidt KR, Gaza S, Voropaev A, Ertl S, Tiehm A (2014) Aerobic biodegradation of trichloroethene without auxiliary substrates. Water research 59:112–118. https://doi.org/10.1016/j.watres.2014.04.008

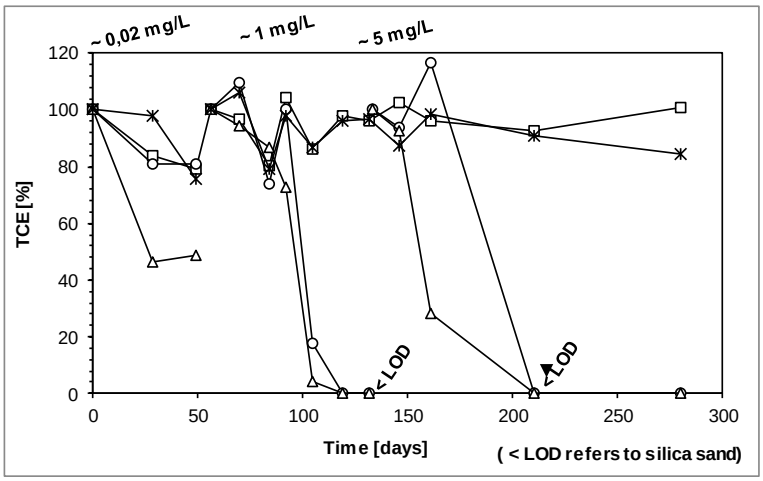

Figure 2: TCE concentrations of a microcosm series without intrinsic degradation (□) and stimulated degradation with liquid (○) and immobilized culture on silica sand (△) compared to sterile control (✱).

Project WT1805: PALM-IRRI

Integrating Electrical Resistivity Tomography and Sap Flow Measurements within Agro-Ecosystem Models to Improve Irrigation Efficiency of Date Palm (PALM-IRRI)

Johan Alexander HUISMAN[1*], Tarig BUKHARY[1], Jingbo ZHEN[2], Perrine MARGUER FERNANDEZ[2], Egon ZIMMERMANN[3], Effi TRIPLER[4], and Naftali LAZAROVITCH[2]

[1]Agrosphere (IBG-3), Institute for Bio- and Geosciences, Forschungszentrum Jülich GmbH, Germany
[2]The French Associates Institute for Agriculture and Biotechnology of Drylands, Jacob Blaustein Institutes for Desert Research, Ben-Gurion University of the Negev, Israel
[3]Electronic systems (ZEA-2), Central Institute of Engineering, Electronics and Analytics, Forschungszentrum Jülich GmbH, Germany
[4]Central- and Northern-Arava Research and Development, Israel
[*]Corresponding author's e-mail: s.huisman@fz-juelich.de

ABSTRACT

The cultivation of date palms is widespread in Israel and exclusively depends on high-frequency irrigation. The overall objective of the PALM-IRRI project is to combine sap flow and electrical resistivity tomography (ERT) measurements to obtain improved estimates of transpiration and stem water content of date palms, and to use this novel sensor combination to calibrate a soil-plant-atmosphere model that will subsequently be used to reduce irrigation water use while maintaining and perhaps even improving agricultural productivity of date palms. To achieve the project aims, a combination of laboratory experiments, field experiments and soil-plant-atmosphere modelling was used. Laboratory experiments were used to improve understanding of the electrical and hydraulic properties of date palm stems. A laboratory set-up was developed that induced flow in a date palm stem segment using vacuum pressure while making time-lapse ERT measurements. It was found that such ERT monitoring allows to visualize changes in radial flow variability due to different flow conditions. The electrical conductivity of the outflow was considerably higher than that of the introduced solution, which suggest the presence of stored salt in the stem segment. The relationship between bulk electrical conductivity and water content of date palm stem segments was investigated on smaller samples using multi-step-outflow (MSO) experiments combined with complex electrical conductivity measurements. The results showed that the water redistribution in the sample was slow after the initial desaturation, which suggests that the water is tightly bound as in a clay soil. The observed relationship between bulk electrical conductivity and saturation could be described with models established for porous media. Both the flow and the MSO experiment did not show additional information content in the imaginary part of the electrical conductivity. Field experiments were focused on combined ERT and sap flow measurements on both juvenile date palm trees growing in lysimeters and mature date palm trees. Initial ERT measurements showed that the spatial distribution of electrical resistivity was highly variable within the stem and changed substantially with time and applied irrigation. To investigate this in more detail, a custom-made EIT measurement system was used to acquire high-speed measurements with a temporal resolution of several minutes. This revealed diurnal changes in the spatial distribution

of the electrical resistivity. An induced drought period for the juvenile date palm in the lysimeter also resulted in noticeable changes in the electrical resistivity. To determine the irrigation amount and timing for date palm trees, a dynamic decision support system (DSS) was conceptualized based on the calibrated and validated soil-plant-atmosphere model CoupModel. This involved a sensitivity analysis to determine the key parameters that require additional calibration with short term measurements. An essential part of the DSS is a response surface analysis based on a set of model runs with a boundary condition that triggers irrigation each time the amount of water in the root zone decreased below a certain threshold. This set of model runs provides a simulated relationship between the amount of carbon gained given a weather forecast and different amounts of applied irrigation, which showed a maximum that can be used for irrigation scheduling.

KEYWORDS
Electrical resistivity tomography; transpiration; sap flow; irrigation

INTRODUCTION
The cultivation of date palms in the hyper-arid Arava and Jordan valleys is widespread and exclusively depends on high-frequency irrigation. Large amounts of water are usually applied for meeting the evapotranspiration demand of date palm, despite local agricultural water quota constraints. To better understand water use of date palms (and many other trees), much attention has been paid to using sap flow measurements with heat dissipation sensors to determine transpiration rates (Sperling *et al.*, 2012). However, the calculation of whole-tree water use from point-scale sap flow measurements is challenging in general due to the empirical sapwood area estimation and the heterogeneous xylem hydraulic conductivity. In addition, date palms are known to have a large internal stem water reservoir that is used for transpiration in daytime when the evaporative demand exceeds the water supplied by roots and recharged at night. This diurnal water allocation in the stem is crucial to the photosynthetic performance of date palms, as it enables optimal vegetative and reproductive growth in hot and dry deserts, but its dynamics are still poorly understood because of a lack of methods to quantify stem water content (Sperling *et al.*, 2015). Previous studies have shown that electrical resistivity tomography (ERT) can be used to separate sapwood from heartwood (e.g., Wang *et al.*, 2016), which is important information for upscaling point-scale sap flow measurements to the tree and stand scale. In subsurface applications, it is well established that ERT can provide water content estimated when appropriate calibration relationships have been established (Mares *et al.*, 2016). Within this context, the overall objective of the PALM-IRRI project is to combine sap flow and measurements to obtain improved estimates of transpiration and stem water content of date palms, and to use this novel sensor combination to calibrate a soil-plant-atmosphere model that will subsequently be used to reduce irrigation water use while maintaining and perhaps even improving agricultural productivity of date palms. To achieve the project aims, this project relied on a combination of laboratory experiments, field experiments and soil-plant-atmosphere modelling. In the following, we briefly summarize key achievements in these three areas.

LABORATORY EXPERIMENTS
A laboratory set-up was developed to investigate whether ERT can be used to investigate radial variability in sap flux in date palm stem segments (Figure 1). For this, a stem segment was obtained from a felled date palm and cleared from barkwood. Next, it was processed in a wood turning machine to a cylindrical shape with a diameter of 0.25 m and a length of 0.50 m. The

outside of the sample was sealed with a liquid plastic coating in multiple layers. A plastic funnel was placed on the top end of the stem and sealed in place using self-expanding sealing foam. The stem segment was positioned in the same orientation as the felled date palm, thus maintaining the same organic flow direction from the bottom up. The bottom of the segment was placed in a water-filled basin. A reservoir containing the flow solution was connected to the basin by means of plastic tubing, and a peristatic pump was used to deliver the solution at a constant rate. A vacuum pump was connected to the top end. Between the vacuum pump and the funnel, a container was used to collect the outflowing solution. The amounts of inflow and outflow were monitored using balances.

Using this set-up, a flow experiment with three flow periods with suctions of -0.3, -0.2, and -0.1 Bar was performed. To enable ERT measurements, two rings of 20 equidistant brass electrodes were used (Figure 1, top left). The electrodes of both rings were connected to the custom-made EIT40 system used for the ERT measurements. Continuous measurements were obtained interchangeably at the two electrode layers using 20 current injections and a total of 340 ERT measurements per electrode ring. After data filtering, the ERT data were inverted using a MATLAB-based customised programme using a 3-D mesh created using the open-source mesh generator Gmsh. The resulting temporal resolution of the ERT images was 4.6 minutes.

The induced flow during each flow period resulted in an increase in the averaged electrical conductivity at both planes (Figure 1, top right). This increase occurred despite the use of a solution with low electrical conductivity, suggesting that the changes are due to differences in saturation of the sample. The measured electrical conductivity of the outflow was considerably higher than the inflow, which is attributed to the release of stored salt, which originated from irrigation water prior to the felling of the tree. The spatial distribution of the electrical conductivity at the two planes showed a clear increase in the centre of the sample that is associated with the induced flow (Figure 1, top middle). The results obtained during this experiment evidently show the potential of ERT as a tool to monitor flow and changes in water content in the stem segment.

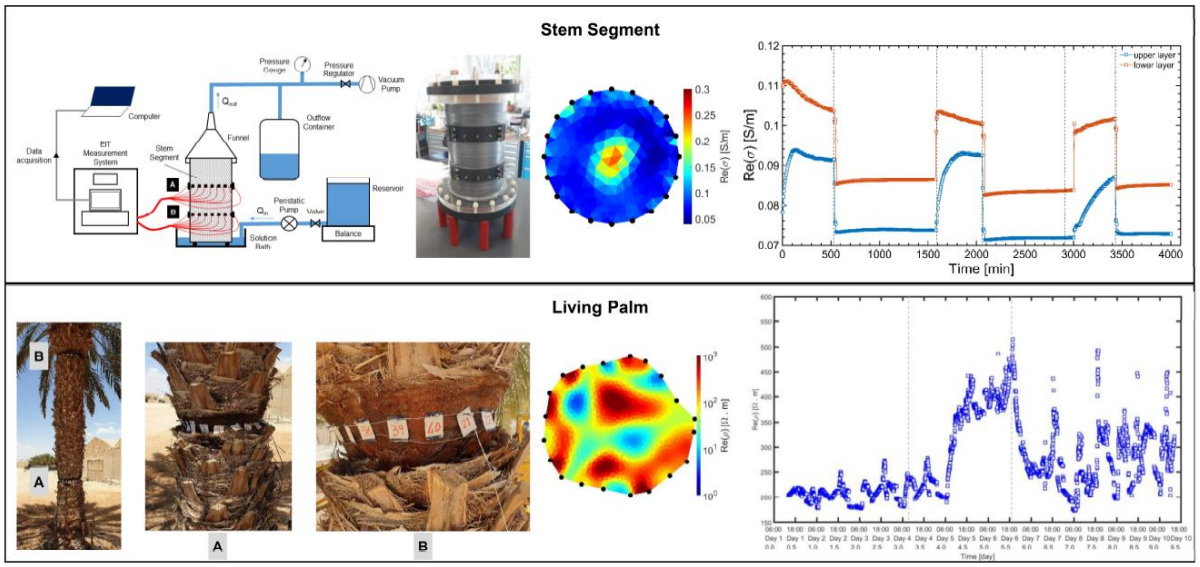

Figure 1: Illustration of experimental set-ups and results for the laboratory and field experiments using ERT measurements to study spatial variation in flow dynamics on stem segments and live trees.

FIELD EXPERIMENTS

The field experiments were conducted at the Yair Experimental Station (30°46′45.3″N 35°14′31.1″E) situated in Israel's Central Arava Valley, 130 m below sea level. The central Arava Valley is characterized by an average annual precipitation of 30 mm and mean daily maximum and minimum temperatures of 40.1 °C (July) and 9.2 °C (January), respectively. Field experiments were focused on combined ERT and sap flow measurements on both juvenile date palm trees growing in lysimeters and mature date palm trees (Zhen et al. 2019). Experimental set-ups are shown in Figure 2. Initial ERT measurements showed that the spatial distribution of electrical resistivity was highly variable within the stem and changed substantially within a diurnal cycle and in response to applied irrigation. Therefore, high-speed ERT monitoring with a temporal resolution of minutes was deemed necessary to investigate the spatio-temporal changes in the electrical conductivity distribution in response to irrigation. For this, a single ring of 20 electrodes was installed in the juvenile date palm tree growing in a lysimeter and two rings of 20 electrodes were installed at the top and bottom of a mature date palm tree (Figure 1, bottom left). The investigated trees were also equipped with sap flow sensors. Initially, normal irrigation conditions were used to establish baseline conditions. After this, the irrigation was suspended for several days. Finally, irrigation was resumed to the normal schedule while closely monitoring the recovery of the date palm. The ERT data acquisition, processing, and inversion followed the same procedures as for the laboratory experiments.

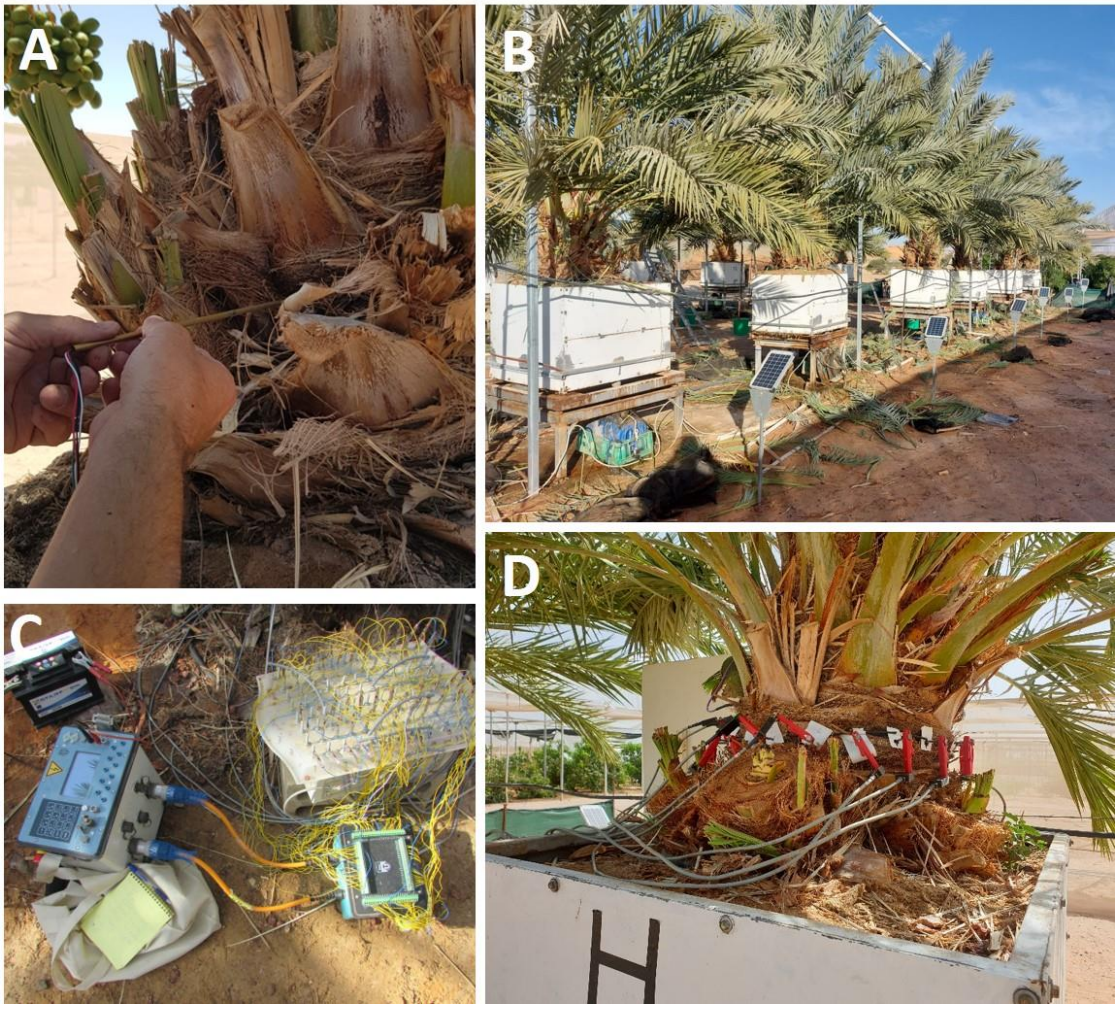

Figure 2: A. Sap flow sensor installation. B. lysimeters with date palm trees. C. ERT cable connections. D. Electrodes installation in a lysimeter.

The high-resolution monitoring of both the juvenile and mature date palm trees confirmed the high spatial variability in electrical resistivity within both the juvenile and mature date palm tree (Figure 1, bottom middle). This has obvious implications for the installation of sap flow sensors, where low-conductivity areas likely indicating regions without flow should be avoided. The monitoring also revealed diurnal changes in the spatial distribution of the electrical resistivity that are associated with the tree response to irrigation. An induced drought period for the juvenile date palm in the lysimeter also resulted in a noticeable increase in the mean electrical resistivity (Figure 1, bottom right) on the second day after irrigation was stopped, which indicates that ERT may also provide an early indicator of water stress.

SOIL-PLANT-ATMOSPHERE MODELLING

The envisioned design of the decision support system (DSS) to determine irrigation amount and timing for date palm trees is shown in Figure 3. CoupModel is the model at the heart of the system.

It simulates water flow and the carbon balance in the soil-plant atmosphere system, and thus can predict plant growth given the boundary conditions (amount and timing of irrigation, weather conditions). The left loop describes the calibration, validation and sensitivity analysis of the model. The first step was to calibrate the model with data coming from lysimeters. These data included the transpiration rate and the quality of the drainage water. After the calibration, a confrontation of the model with real data of the fruit yield was performed. A sensitivity analysis was also performed on the model parameters to understand which parameters require recalibration because of their high sensitivity. The right loop describes operational part of the DSS, where CoupModel is run in a batch mode with meteorological input that allows to determine the potential evapotranspiration. Available data from the last days are used to recalibrate the model if necessary. These data may include actual transpiration estimates from combined sap flow and ERT measurements, estimates of stem water content from a budget approach, and soil water content measurements.

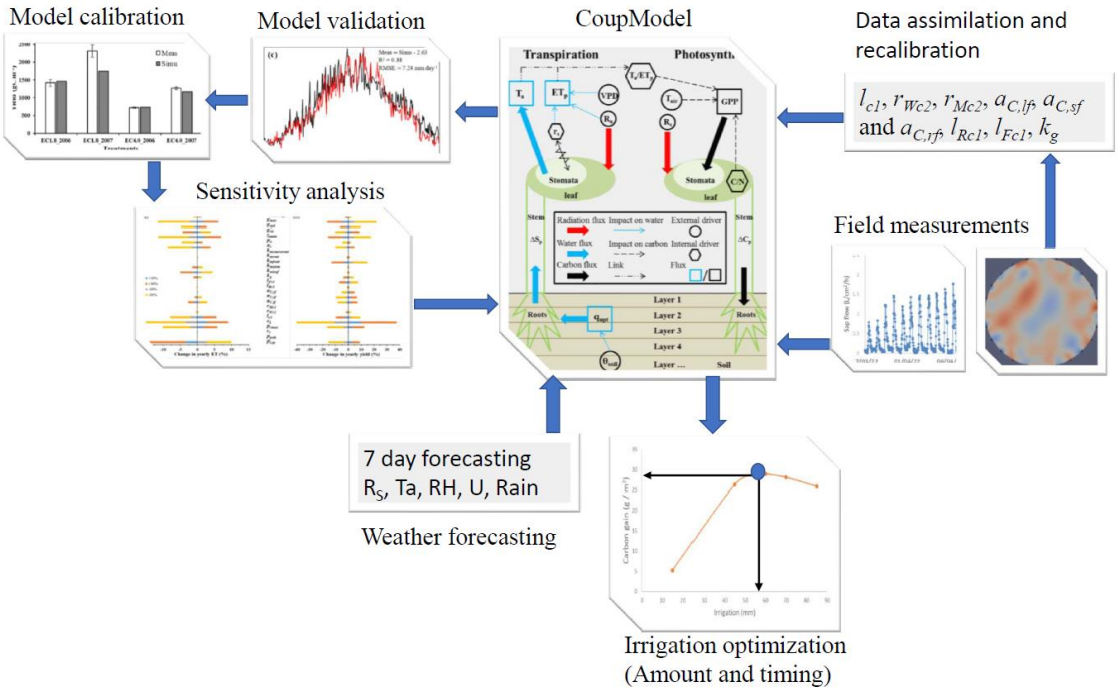

Figure 3: Overview of the concept for the decision support system to determine optimal amount and duration of irrigation.

To optimize irrigation, a response surface analysis using several models runs is proposed once meteorological information becomes available. The response surface is based on a set of model runs using the calibrated CoupModel with a boundary condition that triggers irrigation each time the amount of water in the upper 30 cm of soil decreases below a certain threshold. Every time the threshold is exceeded, an amount of 5 mm is irrigated. This boundary condition is thus system-dependent, and the irrigation timing is provided by the model. The simulations are performed for a period of one week into the future using different thresholds for triggering irrigation. These simulations are providing a simulated relationship between the amount of carbon gained during a one-week period and the amount of applied irrigation that can be used for scheduling. It should be noted that the design of the dynamic DSS allows the use of different response surfaces without much additional effort. For example, the carbon gain could be replaced by fruit yield directly or a monetary assessment of yield versus costs of irrigation depending on what is desired to be optimized.

CONCLUSIONS

Laboratory experiments on stem segments of date palm have confirmed the ability of electrical resistivity tomography (ERT) to determine the radial variability in flow within the stem. Field measurement on juvenile date palms growing in lysimeters and mature date palms showed a high spatial variability in electrical resistivity, which has obvious implications for sap flow sensor installation. Diurnal variations in the electrical resistivity distribution due to irrigation as well as a clear response to water stress were also observed. Finally, a concept for the integration of the sensor information with a soil-plant atmosphere model into a decision support tool for irrigation has been developed.

ACKNOWLEDGEMENTS

This work was funded by the German Federal Ministry of Education and Research (BMBF) with funding code 02WIL1524 and by the Ministry of innovation, science and technology of the State of Israel.

REFERENCES

Mares R., Barnard H.R., Mao D., Revil A. and Singha K. (2016). Examining diel patterns of soil and xylem moisture using electrical resistivity imaging, *J. Hydrol.*, 536, 327–338.

Sperling O., Shapira O., Cohen S., Tripler E., Schwartz S. and Lazarovitch N. (2012). Estimating sap flux densities in date palm trees using the heat dissipation method and weighing lysimeters. *Tree Physiol.*, 32(9), 1171–1178.

Sperling O., Shapira O., Schwartz A. and Lazarovitch N. (2015). Direct in vivo evidence of immense stem water exploitation in irrigated date palms. *J. Exp. Bot.*, 66(1), 333–338.

Wang H., Guan H., Guyot A., Simmons C.T. and Lockington D.A. (2016). Quantifying sapwood width for three Australian native species using electrical resistivity tomography, *Ecohydrology*, 9(1), 83–92.

Zhen J., Tripler E., Pevzner S. and Lazarovitch N. (2019). Impact of fruiting on gas exchange, water fluxes and frond development in irrigated date palms, *Scientia Horticulturae*, 244, 234-241.

Project WT1803: CoNRaWI

Precise measurement of soil water changes using Cosmic-Ray Neutron Sensing (CRNS)

Martin SCHRÖN[1,*], Nurit AGAM[2], Steffen ZACHARIAS[1], Carmen ZENGERLE[1] and Adit ARAZI[2]

[1]Dept. Monitoring and Exploration Technologies, Helmholtz Centre for Environmental Research GmbH – UFZ, 04318 Leipzig, Germany
[2]Blaustein Institutes for Desert Research, Ben-Gurion University of the Negev, Sede Boqer campus, 8499000, Israel
**Corresponding author's e-mail: martin.schroen@ufz.de*

ABSTRACT
In the project on precise measurement of soil moisture, the novel cosmic-ray neutron sensing technology (CRNS) has been transferred to the Negev desert. For the first time, the potential and limitations of CRNS in extremely dry regions have been studied. From the observations we realized that new data processing methods are necessary in arid regions to correct the signal for air humidity and incoming cosmic radiation. We developed new correction methods that allowed us to significantly push forward the hitherto accepted state-of-the-art of the method. With this breakthrough of CRNS data processing in arid and low-latitude environments, we have been able to monitor daily soil moisture variations at the Mashash farm with an unprecedented precision of less than 0.5 Vol%. For mobile applications, we were able to identify wet spots in soils under apparently dry surfaces in various farms, Limans, and Wadis. After the scientific improvements and substantial tests in the field, the method is now ready to be used for hydrological and agricultural applications.

KEYWORDS
Non-rainfall water inputs; desert; dew; soil water content; diurnal water cycle; cosmic-ray neutron sensing, mobile neutron detectors

INTRODUCTION

The spatial soil moisture distribution, as well as its temporal dynamics, are among the key parameters in the prediction of hydrological events and in the planning of agricultural measures. Soil moisture is mainly controlled by precipitation, evapotranspiration, surface runoff, and infiltration. Non-rainfall water inputs (NRWIs) due to fog, dew, and direct water vapor adsorption (Agam and Berliner, 2006 and references therein) also contribute significantly to the hydrologic cycle (Agam and Berliner, 2004). In arid regions, the annual amount of NRWIs can exceed that of precipitation, and in many areas NRWIs are the only source of liquid water during the long, dry summer (e.g., Evenari, 1985; Jacobs et al., 1999; Lange et al., 1998; Lange et al., 1992). However, the small amount of water involved in the formation and evaporation of NRWIs makes accurate measurement very difficult. Given the large heterogeneity of soils, both at local and regional scales, upscaling from small point measurement methods to larger scales is necessary to fully understand the environmental factors that influence soil moisture distribution, dynamics, and the potential influence of NRWIs.

Cosmic-Ray Neutron Sensing (CRNS) is a novel technique for measuring water quantities in the environment (Zreda et al., 2012). Cosmic rays generate neutrons in the atmosphere that reflect off the ground and can be detected above the surface. The measurement principle is unique in three ways: (1) there is scientific evidence that it is sensitive to small changes in near-surface water content particularly under dry conditions, (2) it is non-invasive and insensitive to high temperatures and disturbing electromagnetic fields (in strong contrast to traditional TDR/FDR probes), and (3) the CRNS horizontal footprint is on the order of tens of meters while the sensing depth is tens of decimeters, thus representing a larger area compared to the point-scale detection of traditional methods (Schrön et al., 2017). With the novel CRNS technology, it would be possible not only to efficiently measure general soil moisture changes spatially and with high temporal resolution, but also to capture the subtle dynamics of NRWIs especially during the dry season. We consider the results presented here as a starting point to demonstrate the precision and applicability of CRNS technology. We foresee the establishment of this technology for applied services in arid environments.

The goals of this project were (1) to test and improve CRNS measurement technology to demonstrate increased precision and robustness under extreme climatic conditions, (2) to provide information for practical, operational mapping of soil water content at relevant scales for integration into hydrologic models and for agricultural water management, and (3) to prepare CRNS technology for independent, private-sector operation.

METHODS

Site description. The research was mainly conducted at the Wadi Mashash Experimental Farm of the Blaustein Institutes for Desert Research, Ben-Gurion University of the Negev, in the northern Negev, Israel (31°80'89" N, 34°85'39" E; 400 m above mean sea level, 60 km from the Mediterranean Sea). Precipitation events at the site occur typically between October and May, and the mean long-term annual rainfall at the farm is 115 mm. The long-term maximum and minimum temperatures are 14.78 and 4.88°C for January and 32.48 and 18.68°C for July, respectively. The soil is a sandy loam Aridisol (loess) with 13% clay, 15% silt, and 72% sand, and a porosity of 0.45. The observations related to NRWIs were focused during the dry summer season (May-October), beginning one month after the last rain event and continuing until the first rain of the following wet season. During this dry season, the increase in soil water content can be attributed solely to adsorption of fog and dew. Additional campaigns were conducted at the nearby Yeruham Lake (30° 59’ 20.3” N, 34° 53’ 48.8” E) and in a Jojoba agricultural field near Ashalim (30° 57' 1.5” N, 34° 40' 35.3” E.

CRNS technology. The CRNS instrument has been manufactured by Quaesta Instruments (USA) specifically for the conditions in the Negev desert. Since the construction, delivery, and customs took more time than expected during the pandemic, we sent an existing CRNS system from UFZ Leipzig to start the measurements by January 2021. This sensor was replaced in November 2021 by the new CRNS system. The new system consists of two identical sensors, which can be used, together or independently, for stationary or mobile applications. For the continuous measurements at the Mashash farm, the detector has been placed on 5 cm thick sockets. For mobile mapping of soil moisture, the instruments have been used in the trunk of a car, or if areas were inaccessible, on a hand wagon (Figure 1). The latter configuration has been particularly useful to measure at locations near the lake or in limans.

Figure 1: Cosmic-ray neutron detectors in stationary mode at the research farm (left) and in mobile mode in a car or on a handwagon (right).

RESULTS & DISCUSSION

Sensitivity and corrections

We continuously operated CRNS and soil moisture sensors throughout the years 2021 and 2022 to measure variations of soil moisture at high temporal resolution. The observed measurement precision is indeed high enough to resolve 0.5% changes of water content during the day (Fig. 2).

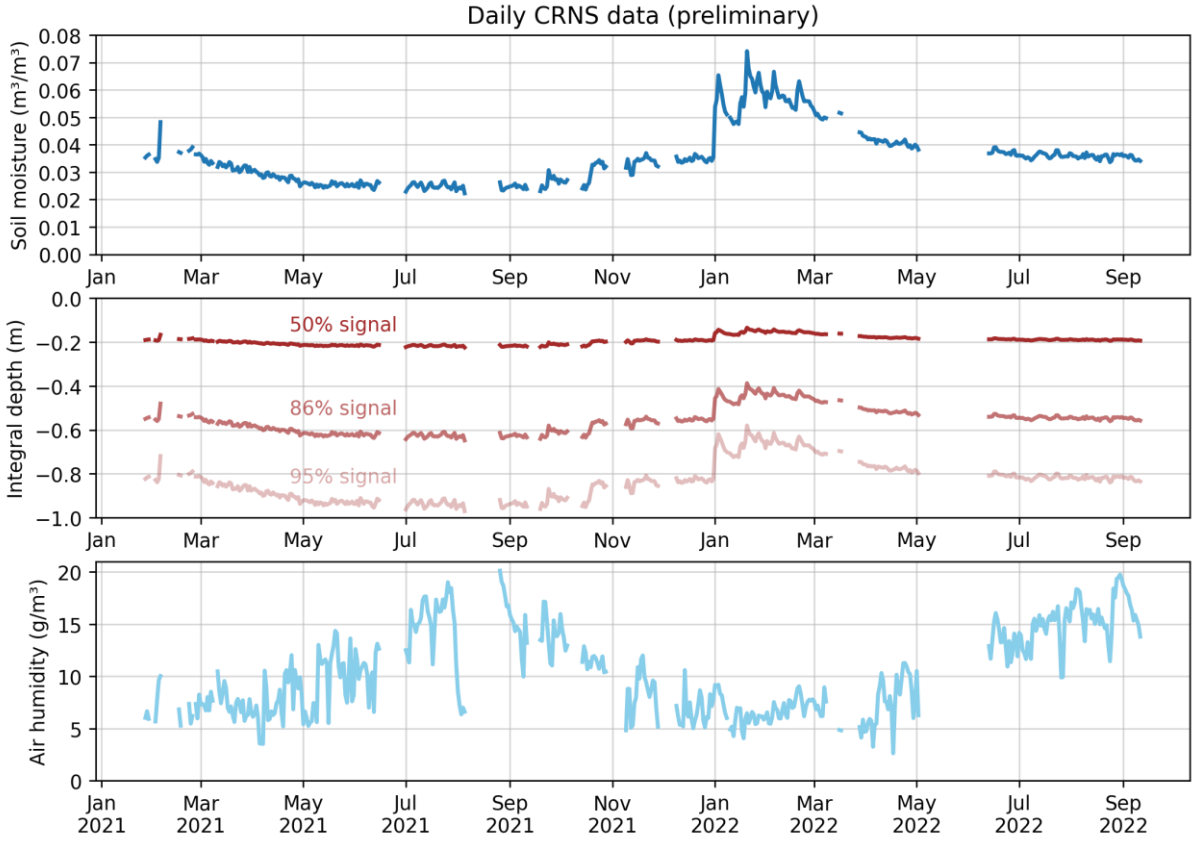

Figure 2: Time series at the research farm showing preliminary data products for volumetric soil moisture (top), integral range of the measurement depth within which most of the signal originates (middle), and absolute air humidity from external sensors (bottom). Data gaps indicate periods when the sensors were used for mobile campaigns elsewhere. The detector type has been exchanged in Nov 2021.

However, we have suspected that the data product is still disturbed by additional influence of atmospheric changes, and we observed an apparent correlation to phase changes (from liquid to vapor) in the air-filled soil pores. We also found that the traditional correction approaches for

incoming cosmic radiation and for air humidity no longer hold in the arid regions of Israel, where the geomagnetic conditions are different to Europe and US, and where air humidity interactions with very dry soil becomes a dominant factor. We worked on new correction approaches based on the theoretical preconsiderations by Schrön et al. (2015) and Köhli et al. (2021). The results showed much better performance in the removal of these external factors (Fig. 3), and the procedures have now been implemented into the processing tools in order to produce more reliable data products.

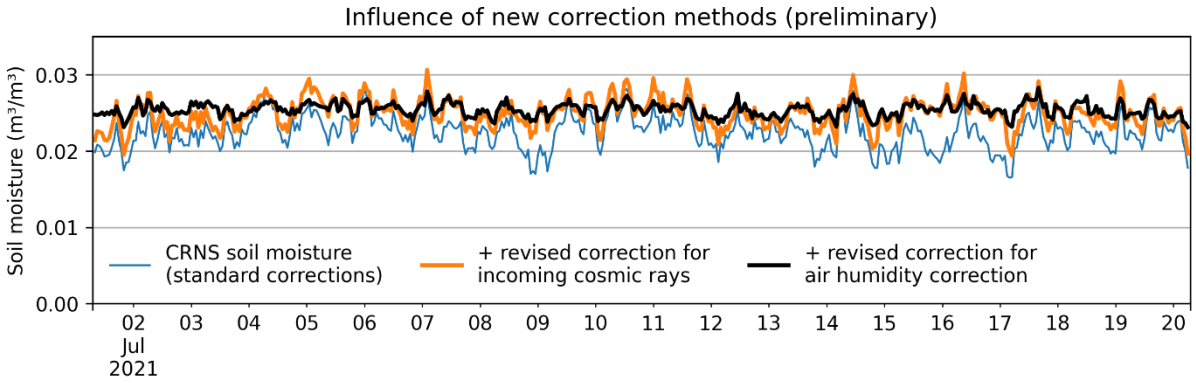

Figure 3: The development of novel methodological approaches was needed in order to properly correct the traditional signal (blue) for incoming cosmic radiation (orange) and air humidity fluctuations (black). The result (preliminary) agrees with the presumably constant soil moisture state during this period within a precision range of ~0.005 m³/m³.

Non-rainfall water input

The potential of detecting non-rainfall water input could then be investigated with better precision using the existing datasets. The sensitivity of the sensor to small changes in water content near the surface was estimated using neutron physics simulations (Köhli et al., 2022). The results show that the neutron count rates may change by 2 to 5%, but include air humidity changes as well. Fig. 4 shows a first and preliminary impression of an experimental evidence for the neutron-NRWI relationship, but the complexity of these processes require further detailed investigation.

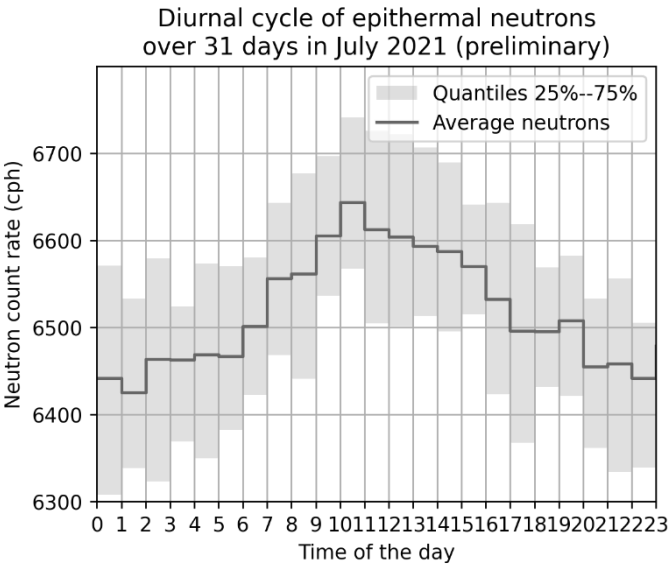

Figure 4: Diurnal variation of measured epithermal neutrons that are suspected to respond to non-rainfall water input (preliminary). Average in quantiles indicate the variation across all 31 days in July 2021.

Soil moisture mapping

The CRNS systems have been successfully used in Israel in a mobile mode (CRNS roving) to detect spatial soil moisture variations several times throughout the years 2021 and 2022. By design, the new system can be split into two independent parts to facilitate more efficient experimentation. In contrast to conventional sensors, the CRNS allows to measure average water content in depths of up to 70 cm, such that wet spots have been identified that were not visible from the surface (e.g, in Wadis, or in a partly irrigated farmland of Jojoba, Fig. 5). In a recent publication, we demonstrated that the achievable level of uncertainty during mobile CRNS measurements is much different for arid and humid climate, and it further depends on speed of the rover and its altitude (Schrön, et al. 2021).

Figure 5: Mobile CRNS measurement to map the spatial soil moisture variations in the partly irrigated Jojoba farm. The preliminary data suggests the occurance of dry areas and wet spots.

Data processing toolbox

In order to facilitate sustainable transfer of technology and knowledge, we have continuously developed a visually guided and highly configurable processing tool during the project and adapted it to the specific conditions in Israel (Corny, https://git.ufz.de/CRNS/cornish_pasdy). In the meantime, the tool has been applied also by other researchers (Kasner, et al. 2022; Schrön, et al. 2022) and used in the processing of 64 European CRNS sites, which helped to demonstrate further evidence of the recent continental drought events (Bogena, et al. 2022).

CONCLUSIONS & OUTLOOK

In this project we demonstrated that CRNS technology will be able to resolve subtle changes in water content in arid environments and provide informative maps of soil moisture in farmland environments. One of the most important findings is that the dependency of neutrons on soil moisture is related to air humidity and incoming radiation in a different way than hitherto known. We made use of various field experiments and physics simulations in order to identify,

quantify, and find corrections for this problem, while the methodological advancement will be substantial for any future applications of CRNS in arid regions and at low latitudes. We believe that prior quantification of sensor performance and its reliability are prerequisites before further applications and demonstrations with partners can be made. Therefore we have achieved significant steps forward to improve the quality of the data specifically for arid conditions, and we will now continue approaching further partners to support science, industry, and society. The method would allow users to better support informed management decisions and increase the resilience of desert ecosystems under extreme climatic conditions. The established method is now transferable to other semi-arid regions and could become a key technology for integrated water resource management. CRNS measurements can also contribute to improving process understanding in hydrological models and potentially identifying missing components of the hydrological cycle.

ACKNOWLEDGEMENTS

The authors wish to express their gratitude to the Joint German-Israeli Water Technology Research Program by the Federal Ministry of Education and Research (BMBF), Germany and the Ministry of Science, Technology and Space (MOST), Israel, for funding this research (German project number 02WIL1522, Israeli project number 15877-3).

REFERENCES

Agam N. and Berliner P.R. 2004. Diurnal water content changes in the bare soil of a coastal desert. Journal of Hydrometeorology, 5, 922-933.

Agam N. and Berliner P.R. 2006. Dew formation and water-vapor adsorption in semi-arid environments - A review. Journal of Arid Environments, 65, 572-590.

Boeing F, Rakovech O, Kumar R, Samaniego L, Schrön M, Hildebrandt A, Rebmann C, Thober S, Müller S, Zacharias S, et al. 2021. High-resolution drought simulations and comparison to soil moisture observations in Germany. Hydrol. Earth Syst. Sci. Discuss., 2021, 1-35.

Bogena HR, Schrön M, Jakobi J, Ney P, Zacharias S, Andreasen M, Baatz R, Boorman D, Duygu MB, Eguibar-Galán MA, et al. 2022. COSMOS-Europe: a European network of cosmic-ray neutron soil moisture sensors. Earth Syst. Sci. Data, 14, 1125-1151.

Evenari, M., 1985. Adaptations of plants and animals to the desert environment, in: Ecosystems of the world. 12A. Hot deserts and arid shrublands. Elsevier, pp. 79-92.

Jacobs, A.F.G., Heusinkveld, B.G. and Berkowicz, S.M., 1999. Dew deposition and drying in a desert system: a simple simulation model. Journal of Arid Environments, 42: 211-222.

Kasner M, Zacharias S, Schrön M. 2022. On soil bulk density and its influence to soil moisture estimation with cosmic-ray neutrons. Hydrol. Earth Syst. Sci. Discuss., 2022, 1-24.

Köhli, M., Weimar, J., Schrön, M., Baatz, R. & Schmidt, U. 2021. Soil Moisture and Air Humidity Dependence of the Above-Ground Cosmic-Ray Neutron Intensity. Frontiers Water 2, 544847 (2021).

Köhli, M., Schrön, M., Zacharias, S., and Schmidt, U., 2022: URANOS v1.0 – the Ultra Rapid Adaptable Neutron-Only Simulation for Environmental Research, Geosci. Model Dev. Discuss. [preprint], doi:10.5194/gmd-2022-93, in review, 2022.

Lange, O.L., Belnap, J. and Reichenberger, H., 1998. Photosynthesis of the cyanobacterial soil-crust lichen Collema tenax from arid lands in southern Utah, USA: Role of water content on light and temperature responses of CO2 exchange. Functional Ecology, 12(2): 195-202.

Lange, O.L. et al., 1992. Taxonomic composition and photosynthetic characteristics of the 'biological soil crusts' covering sand dunes in the western Negev Desert. Functional Ecology, 6(5): 519-527.

Schrön M, Köhli M, Zacharias S. 2022. Signal contribution of distant areas to cosmic-ray neutron sensors - implications on footprint and sensitivity. EGUsphere, 2022, 1-25.

Schrön M, Oswald SE, Zacharias S, Kasner M, Dietrich P, Attinger S. 2021. Neutrons on Rails: Transregional Monitoring of Soil Moisture and Snow Water Equivalent. Geophysical Research Letters, 48

Schrön, M. et al., 2017. Improving calibration and validation of cosmic-ray neutron sensors in the light of spatial sensitivity. Hydrology and Earth System Sciences, 21(10): 5009-5030.

Schrön, M., Zacharias, S., Köhli, M., Weimar, J., Dietrich P., 2015, Monitoring Environmental Water with Ground Albedo Neutrons from Cosmic Rays., PoS(ICRC2015), doi:10.22323/1.236.0231

Zreda, M. et al., 2012. COSMOS: the COsmic-ray Soil Moisture Observing System. Hydrology and Earth System Sciences, 16(11): 4079-4099.

Project WT1804: ISCO3 for GW remediation

$ISCO_3$ – *in-situ* Chemical Oxidation (ISCO) by Passive Dissolution of Ozone Gas using Gas-Permeable Membranes for Remediation of Petroleum-Contaminated Groundwater

Ines ZUCKER[b], Emil BEIN[a], Anwar DAWAS[b], Yinon YECHESKEL[b], Jörg E. DREWES[a], Uwe HUEBNER[a]

[a] Technical University of Munich, Chair of Urban Water Systems Engineering, Am Coulombwall 3, 85748 Garching, Germany.

[b] School of Mechanical Engineering and Porter School of Environmental Studies, Tel Aviv University, Tel Aviv 69978, Israel.

**Corresponding author's e-mail: ineszucker@tauex.tau.ac.il; u.huebner@tum.de*

ABSTRACT

The objective of our research was to develop, test, and optimize a novel *in-situ* ozone-based oxidation process using gas permeable membranes, for the effective removal of organic contamination from water and evaluate the feasibility of such process to replace current groundwater remediation schemes. Based on a literature study, we selected two types of ozone-resistant membranes, polydimethylsiloxane (PDMS) and polytetrafluoroethylene (PTFE), for testing ozone injection into groundwater. A novel approach was developed to indirectly determine ozone mass transfer based on the removal of indicator compounds and ozone exposure calculations. Thus, we are now able to determine *in-situ* ozone delivery at various flow velocities and membrane configurations. Experiments at lab-scale were complemented with operation of a new two-dimensional (2D) system to study ozone passive injection. Our results indicate that *in-situ* contaminant removal can be achieved when the PDMS membrane is operated in permeable reactive barrier (PRB) mode at relatively high water velocities. In addition, we find that concentration of ozone-reactive contaminants and surrounding substances significantly affect ozone diffusion through the PDMS membrane and thus needed to take into consideration once ISCO3 is designed. The elucidation of the passive ozone injection efficiency into porous media was examined considering chemical, hydraulic and physical aspects. We studied the porous media and contaminant interaction with ozone, effect of liquid velocity, and particle size. The findings suggest that soil itself consume large portion of the applied ozone in both catalytic and finite reactions, and demonstrate that soil characterization is beneficial for the design of the $ISCO_3$ process. We also developed numerical and analytical models of ozone transport in porous media which suggest again that higher flow rates than natural groundwater flow are required to enable spatial impact on the groundwater, unless the PRB approach is being used. Furthermore, we investigated the transformation of BTEX (benzene, toluene, ethylbenzene and xylene) by the ozone/H_2O_2 process. Our results indicate that intermediates from initial reaction of hydroxyl radicals with BTEX are rapidly transformed by ozone. Formation of radicals during this reaction can result in a rapid removal of BTEX even without the addition of H_2O_2. This self-enhanced decomposition leads to a fast ozone removal at the membrane surface, and is driven by initial contaminant concentration and radical scavengers in the water including alkalinity. However, analysis of dissolved organic carbon in subsequent batch biodegradation tests with oxidized solutions showed that refractory products remained in the solution after oxidation of monocyclic aromatics. Lastly, we are currently conducting a pilot-scale study of passive ozone injection.

KEYWORDS
in-situ chemical oxidation; ozonation; BTEX; groundwater; passive injection; Gas-permeable membrane

INTRODUCTION
Pollution by petroleum compounds is one of the main problems affecting groundwater in Israel. The methods for remediation of groundwater or contaminated soil are selected specifically for each site, based on the nature of the contaminated site as well as the type and concentration of the pollutants. Advanced oxidation process (AOPs) that produce hydroxyl radicals are particularly effective in the non-selective oxidation of organic compounds such as petroleum constituents benzene, toluene, ethylbenzene, and xylene (BETX).
Among the AOP processes, ozone-based in-situ treatment has high application potential, but its effectiveness is limited due to the injection methods. Most of the methods are using active injection systems for both gaseous and liquid (dissolved) ozone as point sources requiring an efficient ozone transport through the contaminated site. In addition, due to the fast ozone depletion, several injectors are needed for the in-situ chemical oxidation (ISCO) applications with ozone, which causes more energy consumption for ozone supply.
Therefore, there is a growing need to develop large-scale ozone injection methods and overcome the current limitations of point-source injection. More advanced injection methods, such as the *passive* injection of ozone through semi-permeable membranes, may allow for more uniform and efficient dispersion and allow an efficient oxidation process through minimal ozone concentration. Passive techniques provide a cost-effective alternative to *active* injection as they function with minimal energy, operational, and maintenance requirements.
The objective of the proposed research is to develop, test, and optimize a novel in-situ ozone-based oxidation process for the effective removal of organic contamination from water and evaluate the feasibility of such process to replace current groundwater remediation schemes. Core element of the new concept is the passive injection of gaseous ozone by diffusion through gas-permeable membranes. The distribution of ozone over multiple injection points along the membrane surface facilitates spatial distribution in the aquifer and thereby helps to overcome limitations of current point source injection systems. Specific objectives of the project included the fundamental characterization of ozone mass transfer efficiency, the evaluation of oxidants' stability and transport in water and porous media, the mechanistic understanding of reactions at the membrane surface, and the elucidation of the transformation of BTEX in ozone-based AOPs. Lab-scale experiments were using different set-ups including batch reactors, columns, and a 2D system simulating ozone injection into porous media. In addition, the German and Israeli teams—in collaboration will LDD ltd.—designed an ozone treatment process based on passive membrane injection for a BTEX contaminated well at a fuel station in Netanya, Israel. The system is already running for a couple of months, and will be operated until the last month of our project (Dec 2022).

RESULTS
Fundamental characterization of oxidant mass transfer into a liquid phase
Assessing ozone mass transfer at low liquid flow velocities poses a challenge due to the characteristics of ozone (short lifetime and reactivity with various substances). We developed a novel approach to indirectly determine ozone mass transfer based on removal of indicator compounds and ozone exposure calculations. Results enable us to estimate ozone delivery at different flow velocities and ozone-resistant membrane types (PDMS and PTFE) that were also selected based on a literature review (Bein et al. 2021).

Elucidation of ozone-injection efficiency into porous media

Ozone consumption by two main soil types of Israeli coastline aquifer was examined. Iron-rich soil showed considerably higher reactivity than did calcareous soil. The effect of both physical and chemical soil characteristics on finite and catalytic ozone decay, hydroxyl-radical formation, and ozone transport behavior was investigated. The ozone consumption increased by >90% in the presence of fine soil particles (<100 µm) resulting from the large number of reactive sites and the higher content of ozone consumers compared to coarse soil particles. In batch experiments, soil

organic matter consumed ozone twice as fast as iron components, promoted radicals formation at higher rates, and mainly acted as a finite ozone consumer. In contrast, the ozone consumption in a continuously-fed column with porous media was dominated by catalytic reactions with iron components in soil (Figure 1). Overall, these findings demonstrate that the characterization of ozone reactions in soil can be helpful in evaluating the feasibility and efficiency of $ISCO_3$ and inform the design of this treatment, e.g., the need to inject additional radical promoters. This part of the project was accomplished and published in the American Chemical Society Journal "ES&T Water" (Ying et al. 2021).

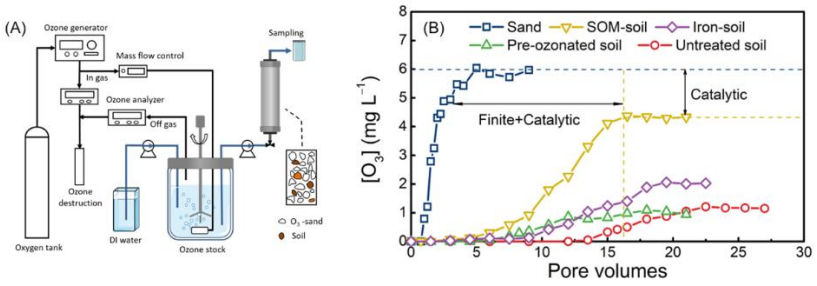

Figure 1: *(A) Schematic illustrating the column experiments. An ozone stock solution was injected upward into a vertical column filled with porous media. (B) Breakthrough curves of ozone in porous media. Dashed lines mark the steady state concentrations as well as the relative contribution of finite and catalytic reactions. Experiments were conducted with 100 g sand, sand-soil mixture (95/5 wt %), and modified sand-soil mixture and 28 mg* L^{-1} *inlet ozone concentration at 2 mL* min^{-1} *flow rate.*

Numerical and analytical models were developed to describe the observed ozone transport in column experiments and expected travel distances. Our findings demonstrated the necessity of higher flow rates than the characteristic flow rates of natural groundwater, to enable reasonable spatial impact on the groundwater. We also demonstrated that the maximum travel distance is largely affected by the initial ozone concentration and that the requirement of high ozone outlet concentration is limited to a short maximum travel distance. Therefore, the PRB approach may be more efficient for $ISCO_3$ processes using membranes. In this treatment method, the ozonation process occurs in a certain zone where the contaminated water flows through this zone either naturally or forced by the pumping/injecting process.

A 2D lab-scale set-up simulating in-situ ozonation treatment (Figure 2A) was designed to analyse more in depth ozone travel distances from the point of injection as well as the removal of indicator compounds with different ozone reactivity. A cylindrical PDMS membrane was used for the ozone injection. Carbamazepine (CBZ) and nitrite were used as model contaminants, where the latter is used to demonstrate behaviour of fast-reacting compounds at elevated concentrations. Increasing liquid velocity was found to noticeably enhance the ozone diffusion rates through the membrane into the water. Based on observed CBZ removal, we conclude that transformation of ozone-reactive contaminants occurrs at the membrane surface, resulting in immediate consumption of ozone in the injection area (Figure 2B-D). The lowest

residual concentration of CBZ (~20%) was observed at the lowest liquid velocity (340 cm day^{-1}). Increasing nitrite concentrations from 0.46 to 25 mM enhanced ozone diffusion rate at all tested velocities, with a maximal ozone diffusion rate of 6-8 µmol sec^{-1} m^{-2}. Overall, our findings confirm that ozone concentration in the injection area, retention time in the porous media, and water quality determine the residual ozone concentration at a distance from the injection source.

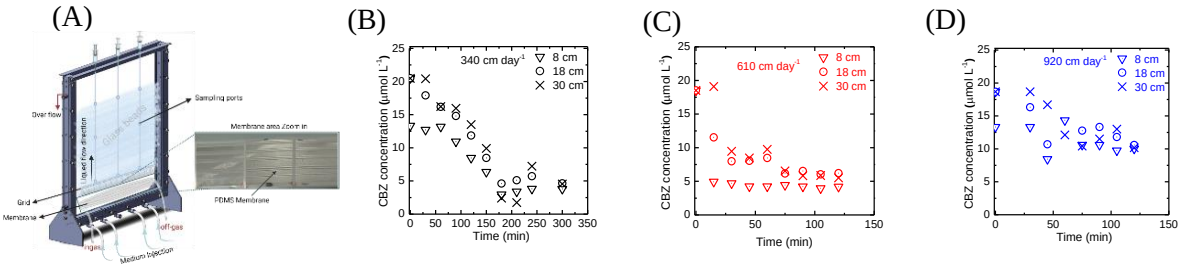

Figure 2: *(A) Schematic illustrating the two-dimensional (2D) lab-scale system. The system was separated by a Teflon grid into two parts, the upper part with nine sampling points fixed through glass beads at different distances from the bottom and across the system, and the lower part with the liquid injection area and the fixed membrane. (B-D) Carbamazepine* ***(****CBZ) removal in the 2D system at liquid velocities of 340, 610, and 920 cm day^{-1} at different heights (experiments with 5 mg L^{-1} (21µM) CBZ).*

Mechanistic understanding of reactions at the membrane surface

We further evaluated the effect of initial compound concentration and water matrix on the removal of monocyclic aromatic compounds by ozone. Batch kinetic experiments with para-chlorobenzoic acid (pCBA) as a model monocyclic aromatic contaminant indicate that the addition of H_2O_2 might not be needed for remediation of BTEX contaminated sites, because resulting intermediates are highly reactive with ozone and initiate a radical chain reaction (self-enhancement), which results in rapid decomposition of the parent compound (Huang et al. 2015). In addition, our findings showed a strong effect of alkalinity and initial concentration of pCBA on its self-enhancement.

With the aim to assess removal of compounds through membrane ozonation and oxidant travel in porous media, we compared two ozone-resistant compounds (benzoic acid and 1,4-dioxane) in a bench scale set-up at near-groundwater velocity (1.5 m/d). Benzoic acid served as non-volatile model compound throughout our study to overcome difficulties working with volatile BTEX. As a monocyclic and aromatic compound, it shows similar self-enhanced decomposition in presence of ozone as observed for pCBA. 1,4-Dioxane is ozone-resistant but does not contain double bonds which trigger follow-up reactions of intermediate products, thus serves as reference to highlight the impact of ozone injection (passive membrane release) and compound properties on ozone travel distances in porous media. Different porous media layers (including non-reactive baked sand, Mn92 and reactive soil) were installed after the membrane barrier. The measured ozone concentration after the soil layer clearly shows advective transport of ozone in the presence of 1,4-dioxane (Figure 3), while ozone consuming reactions by benzoic acid and its intermediates take place immediately at the membrane surface and no ozone was detected in the effluent (data not shown). Additionally, the injection type seems to impact removal efficiencies due to mass transfer limitations, which is currently under investigation.

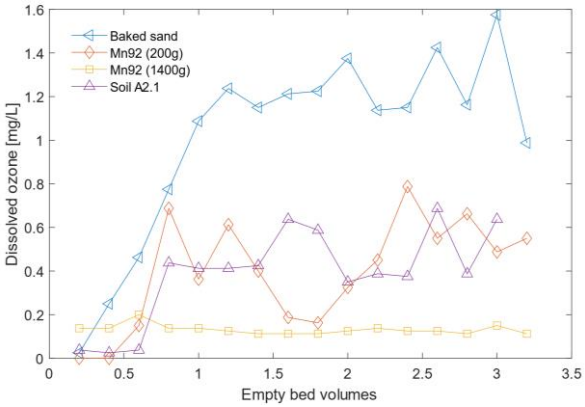

Figure 3: *Effluent dissolved ozone concentrations taken at a sampling port after the membrane barrier (PDMS, 2.6 m tubing length) and the porous media layer during 1,4-dioxane experiments after different empty bed volumes with different porous media configurations.*

Tracking transformation of BTEX by peroxone treatment

To investigate the effects of ozone-reactions on BTEX transformation and biodegradability of residual organic matter, we compared the transformation of BTEX compounds during ozone/H_2O_2 with UV/H_2O_2 treatment as radical generating control without ozone. Our results demonstrate exist synergies of ozone and generated hydroxyl radicals compared to other AOPs where only hydroxyl radicals are present. A build-up of hydroxylated transformation products of BTEX was only detected for UV/H_2O_2, while those compounds were not detected during O_3/H_2O_2 due to rapid reaction with ozone. A full follow-up study on biological degradation after oxidation was conducted using benzoic acid. Biological degradation was assessed by measuring DOC over treatment time (mineralization), but also using high-resolution MS to check for potential persistent products. The results confirmed observations made during BTEX experiments (beneficial effects of ozone), however, refractory DOC remained present after biological degradation, suggesting that some of the compounds formed during chemical oxidation could not be metabolized.

CONCLUSIONS

This project exhibited the potential of using a gas permeable membrane for passive injection in ISCO$_3$ treatments. The advantages of such a system are the controlled (passive) and uniform ozone diffusion which can be used to design a process with efficient use of ozone gas. Our published literature review provides valuable information for the selection and design of appropriate gas permeable membranes for ozone delivery. The developed mathematical model in this research enables to estimate ozone delivery at different flow velocities and ozone-resistant membrane types (PDMS and PTFE). We further demonstrated that the characterization of ozone reactions in soil can be helpful in evaluating the feasibility and efficiency of ISCO$_3$ and inform the design of this treatment. In addition, our findings indicated an efficient transformation of BTEX using ozone/H_2O_2, because intermediates from the initial reaction of hydroxyl radicals with BTEX are rapidly transformed by ozone. The formation of radicals during this reaction can result in the rapid removal of BTEX (self-decomposition) even without the addition of H_2O_2. The relevance of the self-enhanced decomposition for the treatment process depends on the initial concentration of the ozone-resistant contaminants as well as the presence of other radical scavengers such as alkalinity.

Overall, our study confirmed the applicability of the membrane contactors for ozone injection in ISCO, but also revealed some limitations. The initiated chain reactions not only enhance the removal of initial BTEX concentrations, they also result in a rapid ozone decomposition directly

at the membrane surface. This limits ozone transport into the groundwater and may consequently result in inhomogeneous BTEX removal, at least until aromatic structures in the vicinity of the membrane are fully oxidized. Our results also showed that the oxidation of monocyclic aromatics, especially at lower ozone dosages, can generate aromatic products that are more persistent than the parent compounds. Further research is recommended to better understand characteristics and toxicity of the formed products. Combining passive membrane injection with H_2O_2 adversely affected removal of ozone-resistant compounds. Similar to the reaction of BTEX, this may be explained by immediate reaction at the membrane surface resulting in only local radical exposures.

ACKNOWLEDGEMENT

This research was conducted in the framework of the German and Israeli Cooperation, funded by the German BMBF and MOST from Israel. The authors thank Zhian Ying and Grigori Gulitski for their helpful experimental support and technical assistance.

REFERENCES

Bein, Emil; Zucker, Ines; Drewes, Jörg E.; Hübner, Uwe (2021): Ozone membrane contactors for water and wastewater treatment: A critical review on materials selection, mass transfer and process design. In *Chemical Engineering Journal* 413 (18), p. 127393. DOI: 10.1016/j.cej.2020.127393.

Huang, Xianfeng; Li, Xuchun; Pan, Bingcai; Li, Hongchao; Zhang, Yanyang; Xie, Bihuang (2015): Self-enhanced ozonation of benzoic acid at acidic pHs. In *Water research* 73, pp. 9–16. DOI: 10.1016/j.watres.2015.01.010.

Ying, Zhian; Yecheskel, Yinon; Huo, Mingxin; Hübner, Uwe; Zucker, Ines (2021): Ozone Consumption by Soils: A Critical Factor in In Situ Ozonation Processes. In *ACS EST Water* 1 (11), pp. 2403–2411. DOI: 10.1021/acsestwater.1c00236.

Project WT1802: NanoWater

Development of plasmonic nanoarray on-chip platform for rapid multiplex monitoring and management of microbial water quality

Sinwook PARK[1], Keren BUHNIK-ROSENBLAU[2], Golak KUNTI[1], Andrea CSAKI[4], Gilad YOSSIFON[1,3], Yechezkel KASHI[2], Fritzsche WOLFGANG[4]*
[1]*Faculty of Mechanical Engineering, Technion - Israel Institute of Technology*
[2]*Faculty of Biotechnology and Food Engineering, Technion - Israel Institute of Technology*
[3]*School of Mechanical Engineering, Tel-Aviv University, Israel*
[4]*Department of Nanobiophotonics, Leibniz IPHT Jena, Germany*
**Corresponding author's e-mail:wolfgang.fritzsche@ipht-jena,de*

ABSTRACT
A plasmonic nanoarray on-chip platform for detection of pathogenic DNA in water was developed. The project consisted of five working packages as following: WP1: In silico oligonucleotide selection; WP2: DNA extractions, Molecular DNA analysis; WP3: Realization Nanoarrays; WP4: Realization of electric-field assisted target preconcentration; WP5: Realization of spectroscopic readout setup. Combining these parallel efforts together promises to provide a platform with enhanced detection specificity and sensitivity of pathogenic DNA from bacteria within water.

KEYWORDS
Plasmonic nanoarray, DNA analysis, Electrokinetics, Microfluidics, Microbial water quality, Fecal coliforms.

INTRODUCTION
Water is essential for life. The amount of fresh water on earth is limited, and its quality is under constant pressure. Preserving the quality of fresh water is important for the drinking-water supply, food production and recreational water use. To evaluate the water quality and potential for pathogenic bacteria and viruses, general tests for contamination are used as indicator for fecal contamination and quality of the water. Tests for specific pathogens are usually not applied in routine screening since the available culture methods are long (up to a week) and are highly expensive. Therefore, there is an urgent need for a rapid, low cost and specific diagnostic technology for pathogen identification in water. Here we suggest to develop a rapid, sensitive monitoring for fecal coliforms (concentrating on *E. coli*) and a specific test for the highly invasive human pathogen, *Vibrio vulnificus*, as a model. *V. vulnificus (*belonging to the *Vibrionaceae* family) is an emerging zoonotic and infectious agent found in water, and a worldwide human pathogen, with one of the highest mortality rates (up to 50%) (Oliver 2006, Jones and Oliver 2009). In the proposed research a microarray detection following a previous DNA amplification (by PCR) will be developed, based on the extensive knowledge of the Israeli biotech partners in DNA-based identification of any targeted bacterial species, as well as their long experience in water quality tests and in water management system together with the expertise of the German partner in microarray chip technology with potential for on-site solutions, and in plasmonic detection. Using localized surface plasmon resonance (LSPR) effects in gold nanostructures, a label-free detection is possible, avoiding the additional steps, costs and problems connected with the introduction of labels. Nevertheless, an optical readout is possible, allowing for a robust on-site detection. LSPR detection

is based on the plasmonic effects introduced by light in noble metal nano-structures (Zhao *et al.*, 2006, Sepulveda *et al.*, 2014). The light will induce a movement of the rather freely movable conduction electrons, and this oscillation can have a resonance, which position (wavelength-wise) depends on the properties of the nanostructure and of the immediate surroundings (Fritzsche and Lamy, 2014). Binding of a molecular layer at the nanoparticle surface is thereby detectable. In the presence of the analyte, it will bind specifically to its binding partner (a cell, protein or DNA) at the particle surface, and this binding will induce a shift in the resonance wavelength of this sensor spot, which will be detected optically (Csaki *et al.*, 2011). A microarray on a solid support (chip) will be developed, that comprises several spots of DNA-modified nanoparticles, each sensing a specific target sequence (Schneider *et al.*, 2013). This approach will be further enhanced using electric-field-based molecular manipulation approaches by the other Israel partner, which will be used to enhance the local concentration of the target molecules at the sensor surface, thereby increasing sensitivity and/or lowering the required assay time.

RESULTS AND DISCUSSION

In silico oligonucleotide selection

In silico oligonucleotide selection was carried out in order to design DNA sequences to be allocated on the microarray, representing the bacterial groups of interests. The selection process aimed at maximizing both specificity and sensitivity of the designed probes to each bacterial group. *E. coli*, one of the leading indicator bacteria for fecal contamination in water, was our first target for *in silico* analysis. Bioinformatics analysis was carried out for several genomic targets chosen based on thorough literature search and *in silico* analysis, and the genes *uidA* and *rodA* were chosen for further analysis. As negative control sequences, we focused on searching for species-specific non-*E. coli* sequences. One such example is Vibrio-specific genes, such as the cholerae toxin sequences or others. Based on literature search and bioinformatioc analysis, we chose two negative control sequences on the Vibrio-specific genes HlyA and CtxA. The next bacterial target was *Vibrio Vulnificus*, an important water-borne pathogen used as a model bacteria. The *V. vulnificus*-specific gene *vvh*, encodes for the virulent factor hemolysin A, was chosen for further analysis. Two genomic locations for *vvh* gene amplification were chosen, generating 100 bp and 205 bp products (Campbell and Wright et al; Panicker et al).

DNA extractions, Molecular DNA analysis

Species specific primers and probes designed in the scope of the previous step were validated by wet lab molecular DNA analysis. Genomic DNA was extracted from both *E. coli* and *V. vulnificus* strains. Representative strains used were *E. coli* O157:H7 HER 1265 belonging to the EHEC (Enterohemorrhagic *Escherichia coli*) group, as well as different *V. vulnificus* strains belonging different biotypes (biotype 1 strains yb164, yb178 and yb172 and biotype 3 strains v239, v241 and yb146; Broza et al). PCR amplification reactions for the *V. vulnificus* and *E. coli* strains targeting the two *V. vulnificus* specific loci (vvh100, vvh205) and the two *E. coli* specific loci (uidA, rodA) were carried out. Both *V. vulnificus* specific amplification reactions presented PCR products in the expected sizes for all *V. vulnificus* strains and no product for the *E. coli* strain, validating the use of both PCR reactions as specific for *V. vulnificus*. Regarding *E. coli*, only locus rodA presented amplification product. Therefore, locus uidA was excluded from further analysis. Next, in order to verify that the designed probes are homologous to the DNA sequences inside the PCR amplification product of each genetic locus, PCR amplification reactions using each probe together with one of the primers of the genetic locus (forward or reverse) was carried out. Products in the expected sizes were obtained for *V. vulnificus* and *E. coli* loci, validating the option to implement the specific probes in the developed array.

Realization Nanoarrays

The Leibniz-IPHT team established an optimized protocol for the nanoarray preparation. For this, spherical gold nanoparticles were selected, but also other shapes are under investigation as they provide higher sensitivities. The surface chemistry for the immobilization such of particles has been addressed. Utilizing a ligand exchange reaction, the particles can be successfully bound to the chips. Immobilization on the glass substrate is realized using a piezo-driven spotting device (spotter). The spot parameters were optimized, the spot size is adapted to the desired integrated design, with 80-200 µm in spot diameter.

Realization of electric-field assisted target preconcentration

To increase the mass transport of target molecules towards the binding sites on the array of spots we have examined several electrokinetic effects. The first was using an interdigitated array of electrodes that can be integrated with the array of spots. The electrodes are used for generation of electro-hydrodynamics. For low conductivity solutions it is mostly alternating-current electro-osmosis (ACEO), while for high conductivity solutions it is electro-thermal (ET) electroconvection. However, the electrodes rapidly degraded at the high conductivity solution that is typical of the real test conditions for detection of the DNA following its amplification. As an alternative approach we have tested two parallel ITO (Indium -Tin-Oxide) electrodes coated on glass slides. However, also here the high conductivity solution reduced the intensity of the electrohydrodyamic flow and with it its effectivity in enhancing the detection sensitivity. Instead, we have recently examined a different electrokinetic phenomenon, using concentration-polarization based preconcentration, and succeeded to obtain a preconcentration value of ~20 fold within 20 seconds of operation at solution conductivities that are very close to the realistic high solution conductivity of the amplified DNA (Fig.1). These results are promising and suggest that it has the potential for enhancing the detection signal. It is our purpose to combine it with plasmonic sensing for demonstrating its benefit.

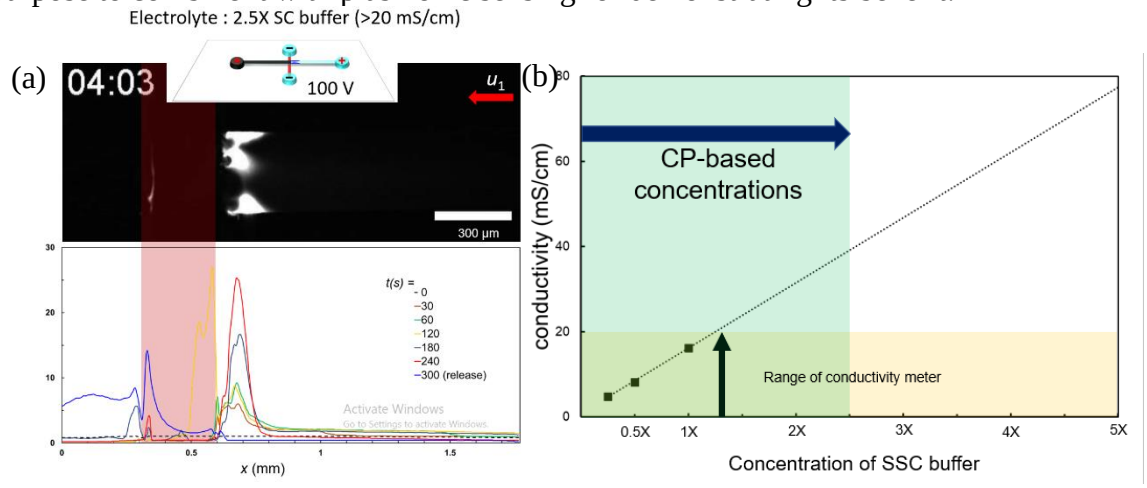

Figure 1. Concentration-polarization based preconcentration of DNA target molecules. (a) a microscope fluorescent image of the preconcentrated molecule plug and corresponding fluorescent intensity profile at different times as obtained using the microfluidic system depicted in the inset consisting of a microfluidic channel with embedded Nafion membrane. Results were obtained at 2.5XSSC buffer. (b) demonstrating the range of solution conductivity where preconcentration is possible.

Realization of spectroscopic readout setup

Pathogens are detected using their DNA as biomarker, which is realized by binding to complementary DNA on the nanoparticles acting as sensor. For readout, UV-VIS spectroscopy is utilized, in order to monitor the spectroscopic behavior (upon binding of target DNA, the resonance of the sensor will shift to greater wavelengths). Different approaches are used in the project. For assay establishment, single spot measurement has been conducted, for simultaneous readout of a spot array, imaging spectrometry is applied (Zopf 2019, Pittner 2019).

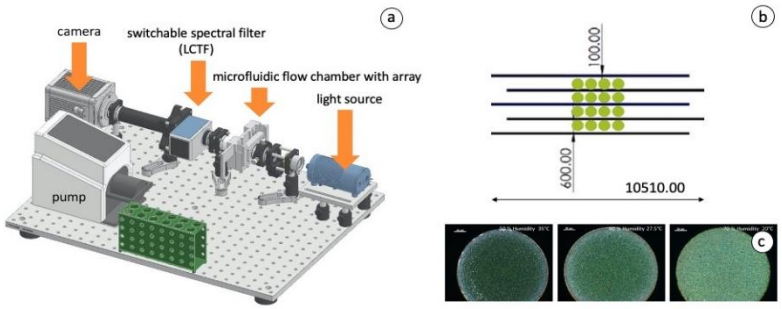

Figure 2: Array-readout realization: For detection of the binding events, an array of gold nanoparticle is uitilzed, and monitored by an imaging spectrometer. A scheme of the setup is shown in a), the array arrangement in b), and microscopic images of single spots in c).

For the multiplex assay an imaging detector was adapted from existing filter-based concept for the parallel readout of 15-100 spots. The spectral information is provided by using a switchable filter based on liquid crystal tunable filter (LCTF) principle, a setup is shown in figure 2. The various components including the pump driving the analyte solution through the flow chamber and thereby through the preconcentration volume and over the array are integrated and all controlled by one software, written in Python language.

Status of project

In the moment, the preconcentration and the array are combined, and will be provided to both sides for final tests. Thereby, the flow chamber was customized to provide the optimized channel height for the preconcentration process. The array position was adapted to align the preconcentration area in the flow chamber with the array position in the light path of the spectrometer readout.

CONCLUSIONS

The project combined an innovative molecular detection setup based on LSPR with a novel preconcentration approach in order to boost the sensitivity. The finalized platform will allow for an enhanced detection ability for water pathogens in a multiplexed (array) fashion, and will be open to adapt to similar analytical applications, such as antibiotic resistance detection in aqueous samples.

ACKNOWLEDGEMENT

The authors acknowledge BMBF grant 02WIL1521and MOST grant 3-15876.

REFERENCES

Boehm AB, Van De Werfhorst LC, Shanks OC, Wang D and Weisberg SB. 2013. Water Res. 47(18):6812-28.
Broza Y., Danin-Poleg Y., Lerner L., Broza M. and Y. Kashi. J Clin Microbiol. 2007 Sep;45(9):2951-9.
Campbell, M. S., Wright, C. A. 2003. Appl Environ Microbiol. 69 (12): 7137–7144.
Csaki T. Schneider, J. Wirth, Jahr N and Fritzsche W. 2011.. Phil Trans A 369, 3483-3496.
Fritzsche W, M. Lamy de la Chapelle. 2014. Molecular Plasmonics Wiley-VCH, Weinheim.
Jones MK, Oliver JD. 2009. Vibrio vulnificus: disease and pathogenesis. InfectImmun 77:1723-1733.
Miti, A., Thamm, S., Csáki, A., Fritzsche, W. and Zuccheri, G.. Biosens Bioelect, 167, 112465 (2020).
Oliver JD. 2006. In F. Thompson et al. (ed.), The biology of vibrios. ASM Press, Washington, DC.
Panicker G., Bej A. K.. 2005. Appl Environ Microbiol. 71(10):5702-9.
Pittner, A., S. Wendt, D. Zopf, A. Dathe, N. Grosse, A. Csaki, W. Fritzsche, O. Stranik. Analytical and Bioanalytical Chemistry 411, 1537-1547 (2019)
Podlesnaia, E., A. Csaki, W. Fritzsche. Nanomaterials 11 (4), 1049 (2021)
Schneider T, Jahr N, Jatschka J, Csaki A, Stranik O, Fritzsche W. 2013. J Nanopart Res 15, 1531
Sepulveda B, Angelome PC, Lechuga LM, Liz-Marzan LM. 2014.. Nano Today 4, 244-251
Zhao J, Zhang X, Yonzon CR, Haes AJ, Van Duyne RP. 2006. Nanomedicine 1, 219
Zopf, D., A. Pittner, A. Dathe, N. Grosse, A. Csaki, K. Arstila, J. Toppari, W. Schott, D. Dontsov, G. Uhlrich, W. Fritzsche, O. Stranik. ACS Sensors 4, 335-343 (2019)

Project WT2003: CatMemReac

CO_2 reduction in the oxidation of micropollutants - energy intensive vs. novel solar-based processes

Amit Imbar[1], Anu Kundu[1], Ashish Sengar[2], Christiane Chaumette[2], Hadas Mamane[1], Benjamin Wriedt[2]*

[1]Tel Aviv University, School of Mechanical Engineering, Tel Aviv-Jaffa, Israel
[2]Fraunhofer Research Institute, 70569 Stuttgart, Germany
**Corresponding author's e-mail: benjamin.wriedt@igb.fraunhofer.de*

ABSTRACT

Trace organic contaminants such as pharmaceuticals have been detected in environmental waters (e.g., rivers, groundwater) in the ng/L to µg/L range. The presence of these pollutants in water sources is concerning as they can lead to unanticipated harmful effects on the aquatic and terrestrial life. The main objective of the present study is to show the usage of photocatalysis (through a photocatalytic membrane reactor) as a complementary method to remove the organic micropollutants (OMPs) from water sources while reducing CO_2 emissions compared to applied technologies such as ozonation and activated carbon.

At the core of the research, a porous substrate was successfully coated with commercial TiO_2 using the EPD method, forming a substrate-catalyst bond that showed high durability to water flow, produced in a short time by a simple apparatus under standard conditions of temperature and pressure. The photocatalytic unit was integrated into a flow system to allow continuous water treatment, irradiated by UV-LEDs. Reactor characterization was conducted using ferrioxlate actinometry. As a benchmark reaction for performance comparison, the degradation of carbamazepine (CBZ, 1 ppm) was assessed in the reactor using different operating conditions such as irradiation intensity, pH, and flow regimes. The fixed bed lab scale photoreactor degraded up to 80% CBZ at a flow rate of 6 L/h. The different operating conditions were optimized as the starting point for upscaling, conducing our goal of reducing CO_2 emission in a pilot-scale application. Currently, a large-scale reactor is designed, manufactured, and placed in the Shafdan facility as a pilot system. Further, continuing lab-scale experiments in parallel aim to assess different catalysts with lower energy input, e.g., composites of TiO_2 and g-C_3N_4.

KEYWORDS

Wastewater treatment; micropollutants; advanced oxidation process; photocatalysis; catalytic membrane; CO_2-reduction.

INTRODUCTION

Climate change, population growth, rising standards of living, and uneven water distribution are the main causes of competition over water resources, water scarcity, poor water quality, and variability of hydrological events. Water sources are commonly exposed to organic micropollutants (OMPs). OMPs reach environmental waters primarily through the discharge of effluents from wastewater treatment plants (WWTPs) (Bavumiragira et *al.*, 2022). OMPs (such as pharmaceuticals) may exert significant health risks to humans on ingesting contaminated water. These pollutants have also been linked to causing adverse effects on aquatic life (Bickley et *al.*, 2017).

Current WWTPs are limited in the removal and degradation of persistent OMPs - as they often involve capital and energy-intensive approaches. Existing technologies such as reverse osmosis (RO) and other advanced oxidation processes (AOPs) effectively degrade OMPs. However, these technologies are energy intensive, RO has membrane fouling issues, and AOPs may even form toxic byproducts (more harmful than the parent OMP) (Foureaux et *al.*, 2019; Pohl et *al.*, 2019). Therefore, the water industry is challenged to develop innovative renewable energy-based technologies to reduce its carbon footprint, especially in energy-demanding technologies, while producing high-quality water and being highly efficient in degrading OMPs.

Photon-based photocatalytic membrane reactors (PMRs) for enhanced OMPs oxidation in water are a simple, effective and low-cost point-of-use **(**POU) technology that we previously demonstrated on a pilot scale in South Africa and Jordan (NATIOMEM project, Nano-structured N-doped TiO_2 photocatalytic membranes for water treatment). Based on our experience with these pilots, we plan to modify the materials and substrates and adapt the design to Israeli and German conditions, including using solar panels to power up arrays of LEDs. Considering the PMR advantages and reduced CO_2 generation potential, the main aim of the present work was to develop a PMR setup and showcase its potential to degrade OMP-CBZ (1 ppm) in water by using solar/LED-based light sources. Further, the operating conditions of the PMR were optimized to minimize the CO_2 production potential.

METHODS

In the present study, a PMR setup was designed to degrade OMP (see Figure 1). The porous membrane was coated with commercial TiO_2 by using the EPD method. The deposition is done under standard temperature and pressure conditions using a simple lab-scale apparatus in a short time frame. The TiO_2-coated membrane and LED array was fitted in the PMR to allow a continuous flow system. CBZ (1 ppm dosing) was selected as the target OMP and its degradation was assessed. The PMR was operated at different operational parameters such as pH, flow rate, and UV irradiation intensity. Further, batch experiments were performed to evaluate the catalytic performance of modified TiO_2 and composites of TiO_2 and g-C_3N_4.

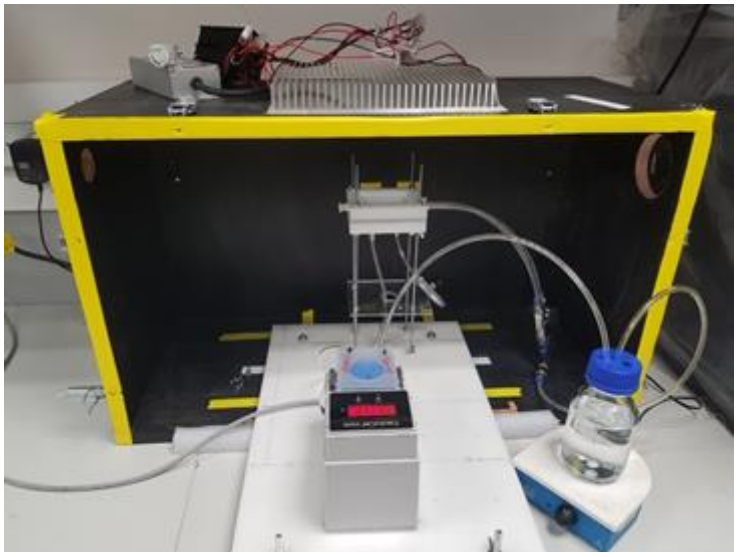

Figure 1: Picture of the lab-scale reactor, opened on the front side. The reactor is in the center of the arrangement, the LED irradiation occurs from the top of the blackened box.

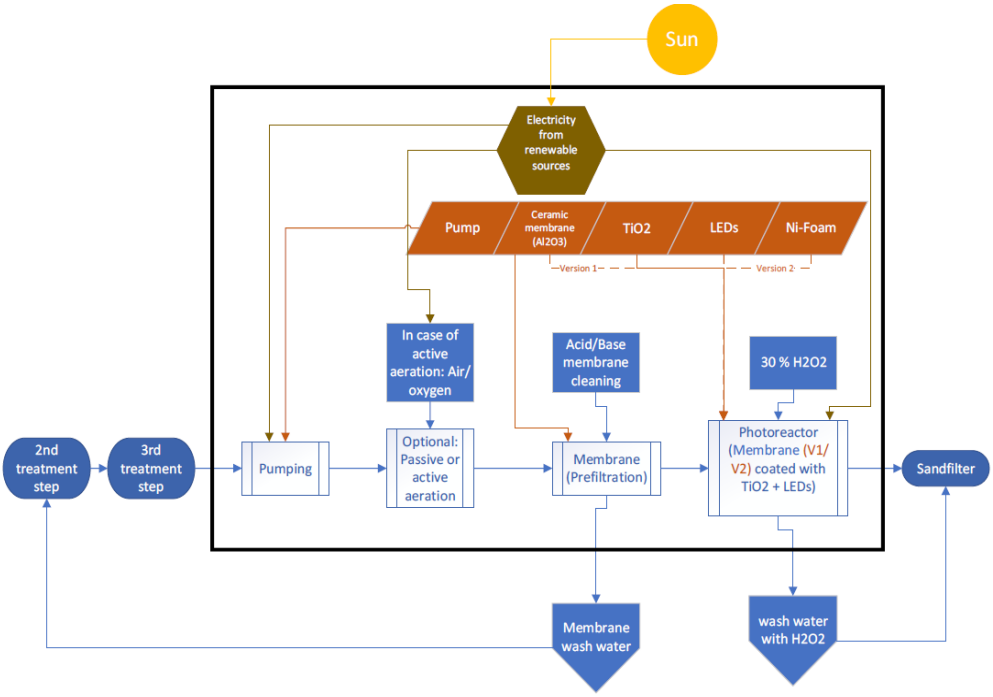

Figure 2: Flowsheet of the catalytic membrane reactor as part of a wastewater treatment plant.

CONCEPT DEVELOPMENT

After a literature review on various AOPs and operating protocols for catalyst preparation and application, the holistic concept of the lab-scale reactor already with regard to the later on-site demonstration was developed. The created and investigated system was chosen to act as a fourth treatment step in a WWTP. A prefiltration with a membrane is necessary to avoid clogging the substrate and the catalyst's active sites. Further, to guarantee the absence of any potential transfer products and remaining compounds after the photocatalytic treatment, a sand filter is installed post-treatment, as demonstrated in the flowsheet elaborated (see Figure 2). Furthermore, the flowsheet outlines the basis for the LCA assessment to concede the carbon footprint of each influencing factor of the reactor system.

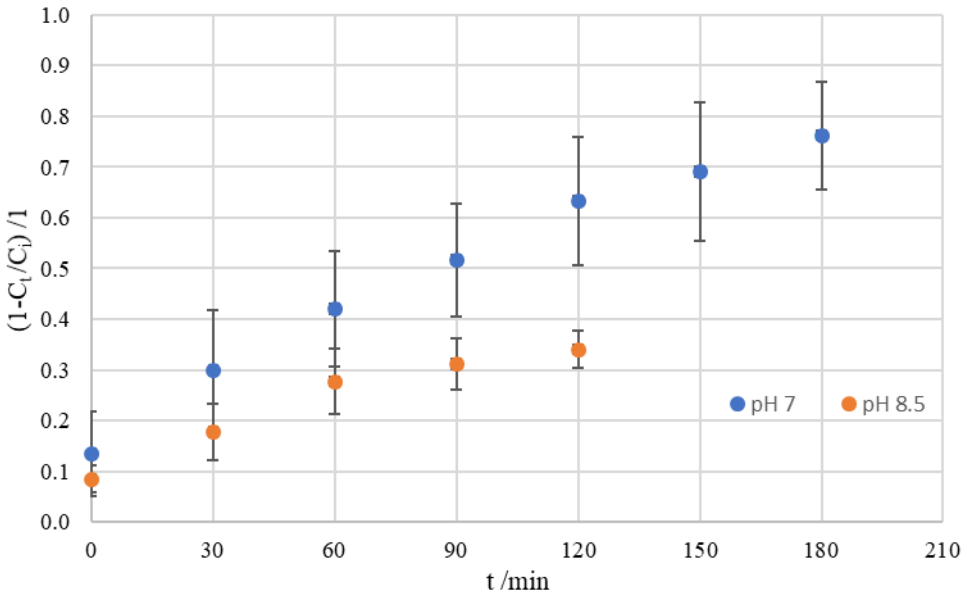

Figure 3: CBZ removal over time at two pH levels.

RESULTS

Catalyst production, coating of the membrane, and integration of the LED array in the reactor were conducted. The PMR operating parameters, such as light intensity, pH, and flow rate, were optimized in a series of experiments. The removal of CBZ was increased using 15 W light intensity (from 7.5 to 20 W). The CBZ degradation rate constant was found to change with different flow rates (maximum value of rate constant achieved at 6 L/h), confirming that the process is in the mass-transfer control regime. Further, the CBZ removal efficiency was evaluated at pH of 7 and 8.5. It was found that pH 7 had better efficiency in the CBZ removal rate (almost 80 % removal), as shown in Figure 3.

OUTLOOK

Based on the lab-scale experiments serving as a proof of concept, it is crucial to investigate the impact of different and probably interfering parameters in real-case scenarios. Hence, the operation conditions will be optimized for using distilled water spiked with multiple OMPs and actual WWTP effluent. Subsequently, the goal is to operate a long-term demonstration of a large-scale pilot plant (>10 L/h) in a wastewater treatment facility. Finally, global impact evaluation regarding the CO_2 balance for different scenarios compared to other treatment methods and sensitivity analysis will be undertaken.

CONCLUSION

The presented work shows that the approach of saving CO_2 emissions by applying a photocatalytic membrane reactor to remove OMPs from wastewater is successful. The developed system has defined reaction engineering properties that qualify it as performant and resistant on a lab scale. The upscaling process and further catalyst development will prove the system to be beneficial on an industrial scale, saving even more energy through a more efficient catalyst composition.

ACKNOWLEDGEMENT

We thank the Israeli MOST (project numbers 3-17762 and 3-17763) and the German BMBF (funding code 02WIL1605) for funding the project CatMemReac in the context of the German-Israeli-Cooperation on Water Technology Research.
We also thank our dear colleagues for contributing to the project: Vered Blass from Tel Aviv University (ISR), Sabine Langkau, Jana Thomann, and Felix Tettenborn from Fraunhofer ISI (GER).

REFERENCES

Bavumiragira, J.P. and Yin, H. (2022). Fate and transport of pharmaceuticals in water systems: A processes review. *Science of The Total Environment*, *823*, 153635.

Bickley, L.K., van Aerle, R., Brown, A.R., Hargreaves, A., Huby, R., Cammack, V., Jackson, R., Santos, E.M. and Tyler, C.R. (2017). Bioavailability and kidney responses to diclofenac in the fathead minnow (Pimephales promelas). *Environmental Science & Technology*, *51*(3), 1764-1774.

Foureaux, A.F.S., Reis, E.O., Lebron, Y., Moreira, V., Santos, L.V., Amaral, M.S. and Lange, L.C. (2019). Rejection of pharmaceutical compounds from surface water by nanofiltration and reverse osmosis. *Separation and Purification Technology*, *212*, 171-179.

Pohl, J., Ahrens, L., Carlsson, G., Golovko, O., Norrgren, L., Weiss, J. and Örn, S. (2019). Embryotoxicity of ozonated diclofenac, carbamazepine, and oxazepam in zebrafish (Danio rerio). *Chemosphere*, *225*, 191-199.

Project WT1901: MoDiCon

Online monitoring and digital control in drinking water distribution systems

Jonas SCHUSTER[1*], Leonid KADINSKI[2*], Hao CAO[3*], Gopinathan R. ABHIJITH[2], Anissa GRIEB[1], Pu LI[3], Avi OSTFELD[2], Mathias ERNST[1]

[1] *Institute of Water Resources and Water Supply, Hamburg University of Technology, 21073 Hamburg, Germany*
[2] *Faculty of Civil and Environmental Engineering, Technion – Institute of Technology, 32000 Haifa, Israel*
[3] *Institute of Automation and Systems Engineering, Technical University Ilmenau, 98693 Ilmenau, Germany*
**Corresponding author's e-mail: jonas.schuster@tuhh.de; kleonid@campus.technion.ac.il; hao.cao@tu-ilmenau.de*

ABSTRACT
The objective of MoDiCon project is to develop an integrated framework for continuously monitoring and simulating selected organic and bacteriological water quality parameters. Thereby, abnormal deviations in water quality behavior in water distribution systems can be detected and responded to in real-time. Furthermore, an appropriate and autonomous control framework for response and recovery from a contamination event will be developed. Both goals are directly targeted towards contribution to a digital transformation of the water sector. Working towards this goal, TUHH is working with flow cytometry and fluorescence spectroscopy as leading edge sensor technologies to determine organic and microbiological substances in drinking water in a highly efficient manner. Laboratory batch experiments have shown the successful generation of individual organic and microbiological fingerprints. Adapting parallel factor analysis (PARAFAC) was approved as a sensitive tool to detect even little changes in organic drinking water compositions. Technion is focusing on an interface of experimental values and simulations as well as data-driven technologies and developing highly complex mathematical models for water quality simulations. First results indicate the successful integration of experimental values in the developed bacterial growth model. The water quality model was applied on a variety of water network examples and coefficients are calibrated. Additionally, the created model will be continuously tested on a test bed facility, while water quality data will be collected and used for an anomaly detection system. Using model-based optimization, TU Ilmenau is developing and an optimal control framework for contamination mitigation response. First optimization results show the mechanism by which the flow in the pipeline affects the concentration of chemical materials (here: free chlorine) in simulated water networks, such that the specified water quality can be recovered.

KEYWORDS
Flow cytometry; fluorescence spectroscopy; water quality simulation; bacterial regrowth model; water quality control; optimal control strategy

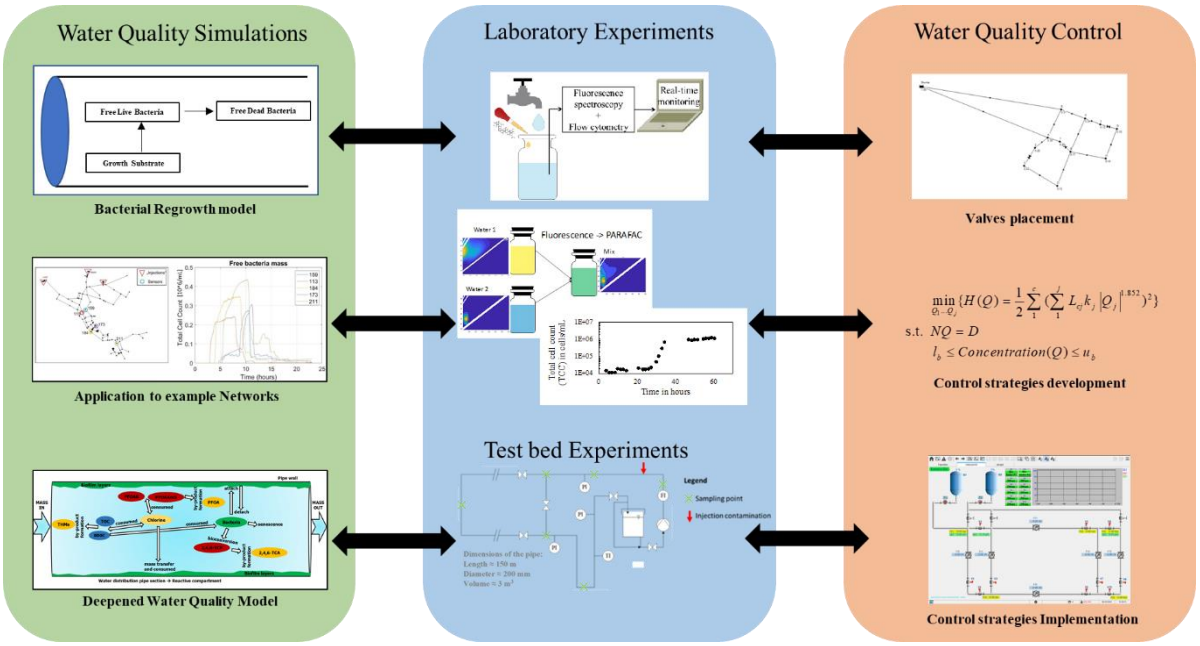

INTRODUCTION

Guaranteeing high drinking water quality in the entire water distribution network (WDS) is one main objective for ensuring public health. Regarding an evolving event of contamination, an early detection and reaction procedure is required. The interaction and risks between both microorganisms and natural organic matter (NOM) is reported by Sillanpää, 2014 and Camper *et al.*, 2003.

Flow cytometry is known as a sensitive method to monitor microorganisms in terms of total cell count (TCC) as well as nucleic acid content (Macey, 2007; Prest *et al.*, 2013). However, data evaluation remains challenging and needs further standardization procedures (Safford & Bischel, 2019). Regarding bacterial growth potential in drinking water, the monitoring of dissolved organic matter (DOM) is crucial. Fluorescence spectroscopy in combination with parallel factor analysis (PARAFAC) is known as a rapid and sensitive method for generating organic fingerprints of several water bodies (Andersen and Bro, 2003; Coble, 1996; Wünsch and Murphy, 2021). According to Heibati *et al.* (2017), studies about characterizing DOM in drinking water via fluorescence spectroscopy are very few. Combining both methods is promising regarding the monitoring of water quality as well as the generation of data generation which can be applied for further water quality data simulation.

Besides actual monitoring of water quality parameters, the simulation of bacterial growth behaviour within the WDS became a powerful tool to evaluate eventual hazardous risks. There has been a lot of research on placing water quality sensors in a WDS and simulating water quality in terms of a contamination event of a chemical contaminant (Eliades *et al.*, 2014; Klosterman *et al.*, 2014; Ostfeld *et al.*, 2008; Schwartz *et al.*, 2014). However, there has only been limited research on monitoring and simulation of organic water quality parameters and detecting biological contamination or relevant inconsistencies in water quality. Further development of building data-driven event detection algorithms as well as deepened, more complex water quality simulations with chemical and biological compounds is part of this work. Based on the water quality monitoring and bacterial growth behaviour, the contamination in WDS can be determined and control strategies developed to restrict the contaminated area using pumps and valves as the main manipulators, and then flush the pipeline to ensure that the water quality in WDS remains within reasonable limits (Berglund *et al.*, 2020). These are on going tasks to be studied. Furthermore, the optimized control strategy can be applied on an established test bed as a comparison with simulation results.

MATERIALS AND METHODS

Monitoring of water quality parameters via flow cytometry and fluorescence spectroscopy

In laboratory batch experiments, drinking water samples from different water utilities as well as samples spiked with organic nutrient medium were investigated by flow cytometry and fluorescence spectroscopy. Individual fingerprints were generated and the bacterial growth was observed by simultaneous real-time analysis. Therefore, flow cytometer CyFlowTM Cube 6 V2 with onCytTM OC-300 automation add-on was used. Total cell count (TCC) was determined by applying SYBR® Green I fluorescent dye and cells were further discriminated into low nucleic acid (LNA) and high nucleic acid (HNA) cells. Fluorescence spectroscopy measurements were performed by Aqualog® fluorometer from HORIBA and spectroscopic data was evaluated via multi-way decomposition PARAFAC method.

Simulation of water quality parameters

The chosen bacterial regrowth model of Zhang et al. (2004) was adjusted for the purposes of this work by excluding the chlorine compounds from the water quality simulation. The main compounds that are simulated are the mass concentration / TCC of bacteria in the drinking water as well as the concentration of the substrate which is utilized for the bacterial growth. To validate and interface the water quality simulations with bacterial growth experiments in the laboratory, assimilable organic carbon (AOC) introduced by van der Kooij *et al.* (1982), which was measured in batch experiments, was used to determine the growth parameter and dependencies needed for an accurate regrowth model. The simulations are conducted using EPANET 2.0 including a MATLAB Toolkit for EPANET toolkit (Eliades *et al.*, 2017) via MATLAB 2020a.

Controlling of contamination events

An approach for the control of chlorine concentration in WDSs by formulating and solving a nonlinear optimization problem based on a hydraulic and water quality model has been developed. To formulate the optimization problem, the mass and energy conservation laws are used to describe the hydraulic properties of a WDS. The one-dimensional advective transport model (partial differential equation (PDE)) is solved analytically to describe the decay of chlorine in the pipelines. The chlorine concentration limits at the nodes are formulated as inequality constraints which will be satisfied by manipulating the flows and their directions in the pipelines. Furthermore, a test bed has been established to illustrate the process of control and mimic of a real water distribution system. To validate the optimization results, Simulations were conducted using EPANET 2.0 including a MATLAB Toolkit for EPANET toolkit (Eliades *et al.*, 2017) via MATLAB 2019a.

RESULTS AND DISCUSSION

Fingerprinting of different water

For all samples, a seven component model was developed by applying parallel factor analysis (PARAFAC). An overview of organic fingerprints for six different drinking waters is shown in Figure 1. Components 1 - 4 were identified as humic-like substances while components 5 - 7 as protein-like substances. Furthermore, respective flow cytometric results (TCC) and TOC analysis results of each water is shown in Table 1.

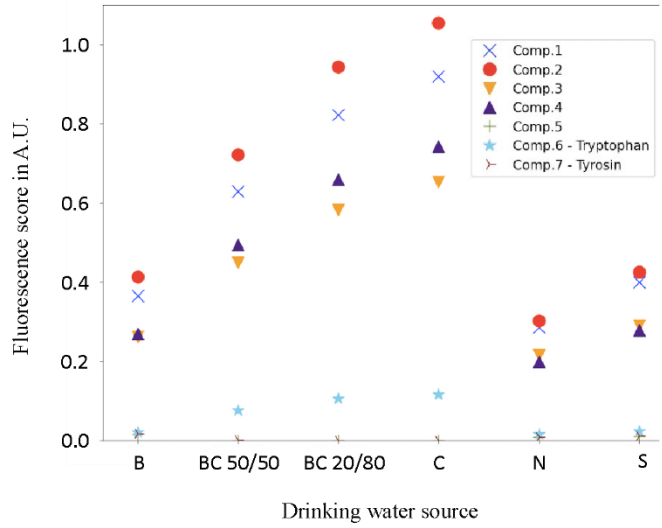

Figure 3: Fluorescence score of seven different components decomposed by PARAFAC method. Drinking water samples were taken from different water utilities in Hamburg, Germany.

Table 1: TOC and TCC of drinking water samples from different water utilities in Hamburg, Germany.

Drinking Water Sample	TOC mg/L	TCC cells/mL
B	1.0	3.4×10^4
BC 50/50	2.0	1.1×10^5
BC 20/80	2.9	1.7×10^5
C	3.3	1.9×10^5
N	0.8	4.6×10^4
S	1.1	7.5×10^4

There is a clearly visible difference between the organic compositions of each drinking water sample. The fluorescence score of humic-like substances (1 - 4) can be related to the respective TOC amount of each sample (Table 1 - left column). Compared with flow cytometric results from Table 1 - right column, we identified Component 6 - Tryptophan as an index for the respective TCC of each drinking water sample. This enables the opportunity of a further use of this PARAFAC model in combination with flow cytometry regarding real-time analysis in treatment systems as well as in distribution networks.

Bacterial growth behaviour and water quality simulation model

For the example application, Monod Kinetics (Zhang *et al.*, 2004) are used to model the bacterial growth in the water network inside of the simulation tool EPANET-MSX. The various equation coefficients, such as maximum TCC and maximum growth rate (µmax), are taken from the laboratory experiment evaluation described in Schuster *et al.* (2022). Figure 2 shows one simulated scenario of the developed bacterial growth model. The left-hand side of the figure shows the water network model Net3 with the respective injection nodes where the substrate was injected into the system. Furthermore, it shows the locations of the water quality sensors which are assumed to record the free bacteria mass of the system. The right sides of the figures show the readings of the water quality sensors where the TCC (in 10^6 cells/mL) is plotted over the simulation time which is 24 hours.

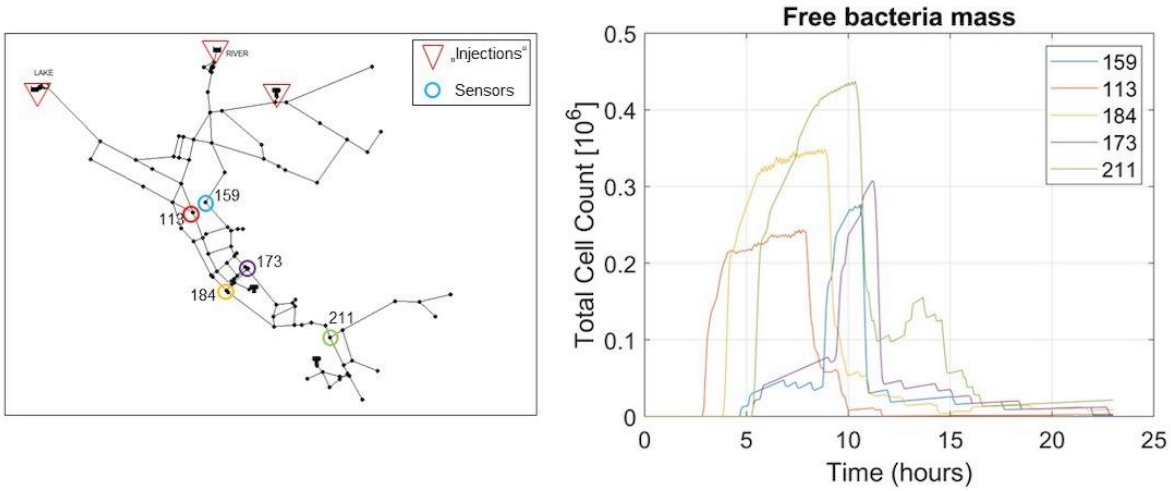

Figure 4: Application of bacterial regrowth model on EPANET network example. The water network model Net3 on the left side showing the positions of the substrate "injections" and the water quality sensors. The readings of the bacterial growth in 10^6/mL of the sensors are shown on the right.

Simulation of chlorine contamination in a test network

By solving the nonlinear optimization problem, we can obtain new values and directions of flow rates for each pipe. These results will be realized as references for the placement of flow control valves (FCVs) and determining their setting values. In a first case study, the network model shown in Figure 3 was analyzed. Table 2 shows an optimal solution and simulation result of a case with 3 loops. Assume in the initial operation, node E has a free chlorine concentration higher than 0.3 mg/L. After optimization and FCVs placement, all nodes with demand will have an acceptable chlorine concentration. The concentration at node G and H show a little decrease, but still above the lower bound of the specification.

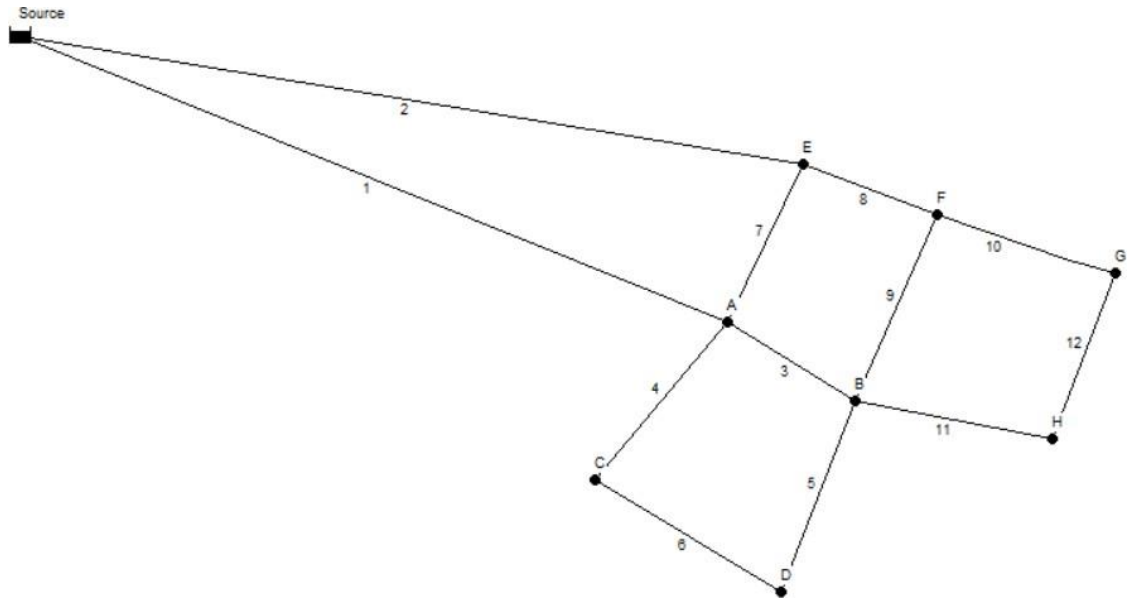

Figure 5: Water distribution system with three loops.

Table 2: Chlorine concentration and flow rate results of contamination simulation case study.

Node ID	Demand m^3/h	Chlorine concentration mg/L		Pipe ID	Flow rate m^3/h	
		Original system	After FCV placement		Original system	After FCV placement
Reservoir		1.2	1.2	1	90.02	93.52
A	0	0.32	0.36	2	89.97	87.28
B	30	0.21	0.17	3	53.98	34.72
C	10	0.21	0.23	4	41.80	40.44
D	30	0.12	0.12	5	1.80	0.24
E	30	0.35	0.30	6	31.80	30.34
F	20	0.25	0.23	7	5.76	18.25
G	30	0.13	0.10	8	54.21	75.43
H	30	0.11	0.10	9	4.01	29.24
				10	30.19	26.09
				11	29.80	34.10
				12	0.19	4.00

CONCLUSIONS

Adapting real-time monitoring of water quality parameters into a real WDS requires detailed testing and evaluating of flow cytometric and fluorescence spectroscopic analysis. During the first half of this project, methodology was developed for laboratory batch circumstances. Fingerprinting via both methods was successfully conducted and allowed detailed real-time characterizing. As a next step we will apply these methods into a real flowing system. If access to the Hamburg test bed is assured (depending on the COVID conditions in coming autumn/winter), we will simulate contamination experiments. Different drinking water as well as raw water sources shall be used as „contaminants“. Besides the simulation of a contamination case, revealed information about the microbial growth behavior from batch experiments should be validated in a flowing system.

The successful establishment of an interface between the laboratory experiments and the water quality simulations leads to the next step of validating the model through a sensitivity analysis using mentioned flow experiments. After the validation, the model will be fused with deepened simulations (see Abhijith et al. (2021)) and expanded continuously for developing a control model in cooperation with the partners from TU Ilmenau. This model will be explored further on the mentioned test bed at the water utility in Hamburg, Germany in course of the MoDiCon project and the output will be continuously compared to the in-situ flow experiments (flow cytometry and fluorescence spectroscopy). Additionally, the measurement data is collected to improve a data-driven model for anomaly detection, which was built with water quality data which was provided by Hamburg Wasser.

To develop optima the control strategies of combating contamination events, a mixed-integer nonlinear programming (MINLP) problem will be formulated in the next step, aiming at finding the on-off-switches of the valves in the WDS. Our goal is to minimize the operation time from the time point of the detected contamination to that of the recovery of the water quality to the specified state. This control strategy will be implemented on the developed test bed.

ACKNOWLEDGEMENT

This project was funded by the Israeli Ministry of Science and Technology (MOST) and the German Federal Ministry of Education and Research (BMBF). The project numbers are 3-17011 (MOST) and 02WIL1553A (BMBF).

REFERENCES

Abhijith, G. R., Kadinski, L., and Ostfeld, A. (2021). Modeling bacterial regrowth and trihalomethane formation in water distribution systems. Water (Switzerland), 13(4).

Andersen, C. M., & Bro, R. (2003). Practical aspects of PARAFAC modeling of fluorescence excitation-emission data. Journal of Chemometrics: A Journal of the Chemometrics Society, 17(4), 200–215.

Berglund, E., Pesantez, J., Rasekh, A., Shafiee, E., Sela, L., Haxton, T. (2020). Review of Modeling Methodologies for Managing Water Distribution Security. Journal of Water Resources Planning and Management. 146. 03120001. 10.1061/(ASCE)WR.1943-5452.0001265.

Camper, A. K., Brastrup, K., Sandvig, A., Clement, J., Spencer, C., & Capuzzi, A. J. (2003). Effect of distribution system materials on bacterial regrowth. Journal / American Water Works Association, 95(7). https://doi.org/10.1002/j.1551-8833.2003.tb10412.x

Coble, P. G. (1996). Characterization of marine and terrestrial DOM in seawater using excitation-emission matrix spectroscopy. Marine Chemistry, 51(4), 325–346. https://doi.org/10.1016/0304-4203(95)00062-3

Eliades, D. G., Lambrou, T. P., Panayiotou, C. G., & Polycarpou, M. M. (2014). Contamination event detection in water distribution systems using a model-based approach. Procedia Engineering, 89, 1089–1096. https://doi.org/10.1016/j.proeng.2014.11.229

Eliades, G., Demetrios, Kyriakou, Marios, Vrachimis, Stelios, & Polycarpou, M., Marios. (2017). EPANET-MATLAB Toolkit: An Open-Source Software for Interfacing EPANET with MATLAB. Computer Control for Water Industry (CCWI), Amsterdam. https://doi.org/10.5281/zenodo.437751

Heibati, M., Stedmon, C. A., Stenroth, K., Rauch, S., Toljander, J., Säve-Söderbergh, M., & Murphy, K. R. (2017). Assessment of drinking water quality at the tap using fluorescence spectroscopy. Water Research, 125, 1–10. https://doi.org/10.1016/j.watres.2017.08.020

Klosterman, S. T., Uber, J. G., Murray, R., & Boccelli, D. L. (2014). Adsorption model for arsenate transport in corroded iron pipes with application to a simulated intrusion in a water distribution network. Journal of Water Resources Planning and Management, 140(5), 649–657. https://doi.org/10.1061/(ASCE)WR.1943-5452.0000353

Macey, M. G. (2007). Flow cytometry: Principles and applications. Flow Cytometry: Principles and Applications, 1–290. https://doi.org/10.1007/978-1-59745-451-3

Ostfeld, A., Über, J. G., Salomons, E., Berry, J. W., Hart, W. E., Phillips, C. A., … Walski, T. (2008). The battle of the water sensor networks (BWSN): A design challenge for engineers and algorithms. Journal of Water Resources Planning and Management, 134(6), 556–568. https://doi.org/10.1061/(ASCE)0733-9496(2008)134:6(556)

Prest, E. I., Hammes, F., Kötzsch, S., van Loosdrecht, M. C. M., & Vrouwenvelder, J. S. (2013). Monitoring microbiological changes in drinking water systems using a fast and reproducible flow cytometric method. Water Research, 47(19), 7131–7142. https://doi.org/10.1016/j.watres.2013.07.051

Schuster, J., Huber, J., Stumme, J., Grieb, A., & Ernst, M. (2022). Combining real-time fluorescence spectroscopy and flow cytometry to reveal new insights in DOC and cell characterization of drinking water. Frontiers in Environmental Chemistry, 0. https://doi.org/10.3389/fenvc.2022.931067

Schwartz, R., Lahav, O., & Ostfeld, A. (2014). Integrated hydraulic and organophosphate pesticide injection simulations for enhancing event detection in water distribution systems. Water Research, 63, 271–284. https://doi.org/10.1016/j.watres.2014.06.030

Sillanpää, M. E. T. (2014). Natural organic matter in water: Characterization and treatment methods (p. 383).

Van der Kooij, D., Visser, A., & Hijnen, W. A. M. (1982). Determining the concentration of easily assimilable organic carbon in drinking water. Journal - American Water Works Association, 74(10), 540–545. https://doi.org/10.1002/J.1551-8833.1982.TB05000.X

Wünsch, U. J., & Murphy, K. (2021). A simple method to isolate fluorescence spectra from small dissolved organic matter datasets. Water Research, 190. https://doi.org/10.1016/j.watres.2020.116730

Zhang, W.; Miller, C. T.; DiGiano, F. A. (2004). Bacterial regrowth model for water distribution systems incorporating alternating split-operator solution technique, Jour. Environmental Engineering, 130 (9), 932-941.

Project WT1902: NEMWARE

Nano-electro Membrane Processes for Micropollutant Removal in Water Reuse

Siqi LIU[1], Abed Alhakeem AZAIZA[2], Hilla SHEMER[2], Rapheal SEMIAT[2], Andrea Iris SCHÄFER[1], Daniel MANDLER[3]*

[1]*Institute for Advanced Membrane Technology, Karlsruhe Institute of Technology, 76344 Eggenstein-Leopoldshafen, Germany*
[2]*Wolfson Department of Chemical Engineering, Technion - Israel Institute of Technology, Haifa 3200003, Israel*
[3]*Institute of Chemistry, The Hebrew University of Jerusalem, Jerusalem, Israel 9190401*
**Corresponding author's e-mail: daniel.mandler@mail.huji.ac.il*

ABSTRACT

The issue of water pollution and scarcity of secure drinking water, as well as water for agriculture, has been widely recognized. The monitoring and removal of contaminants, including numerous micropollutants, are global challenges for safe water reuse. The main objective of this project is to address these issues by developing novel electrochemical membrane processes.

The Israeli partner at the Technion focused on the electro-removal of a model micropollutant compound, propoxur (PR), from a secondary effluent reverse osmosis concentrate (ROC). The electro-oxidation of PR was carried out using a graphite fiber-felt (GF) cathode and a Ti/RuO_2/IrO_2 anode, catalyzed by amorphous ferric oxi/hydroxide agglomerates (AOAs).

The research group at the Hebrew University of Jerusalem has focused on an electrochemical membrane (EM) for the removal of a model micropollutant compound 4-nonylphenol (4-NP). A flow-through electrochemical cell was constructed for investigating the monitoring and removal of this compound. A limit of detection (LOD) within 0.2 nM was achieved. 4-NP could be detected very efficiently due to its adsorption on the carbon nanotubes (CNTs) followed by its electrochemical oxidation. Afterwards, the electro-Fenton (EF) reactions with different carbonaceous-based membranes was tested, which demonstrated different electron-transfer mechanisms for the formation of H_2O_2 and water.

A flow-through electrochemical filtration system with an effective membrane area of 20 cm^2 was designed and constructed by research group in KIT, allowing to evaluate the performance of a variety of ultra- and micro-filtration (UF and MF) EMs for the micropollutant removal. The photocatalytic degradation of β-estradiol (E2) on a poly(vinylidene fluoride) (PVDF) membrane immobilized with TiO_2 nanoparticles (PVDF-TiO_2) was examined at environmentally relevant concentration (100 ng/L). The result showed that a E2 removal of 80% could be achieved at optimized conditions. Preliminary investigation of E2 degradation with an electrochemical CNTs membrane was carried out.

KEYWORDS

Fenton-oxidation, electro-chemistry, membrane; photo-Fenton, micropollutants

INTRODUCTION

The occurrence and fate of organic micropollutants (MPs) is of concern worldwide due to their potential toxicological effects on human health and the environment. Micropollutants include

pharmaceutical and personal care products (PPCPs), pesticides, surfactants, industrial additives, and plasticizers. The removal of MPs in wastewater treatment plants (WWTPs) is generally influenced by the physicochemical properties of the compound; by the type of wastewater treatment technology (conventional and non-conventional), and by process-specific factors such as sludge retention time, temperature, and organic loading rates. The most common conventional wastewater treatment is activated sludge that has not been specifically designed for removing MPs (Dordio *et al.*, 2010).

Advanced oxidation processes (AOPs) utilize powerful hydroxyl radicals as a major oxidizing agent. AOPs are broadly studied for treatment of different types of wastewaters because the strong oxidants can readily degrade recalcitrant organic pollutants. AOPs attack organic compounds through four pathways: hydrogen abstraction, combination or addition of radicals, and electron transfer (Deng and Zhao, 2015). The use of iron species as free catalysts for producing HO· in Fenton processes has widely been studied, but its application on wastewater such as tertiary treatments in real conditions is restricted since the required pH is 2-4. For this reason, studies have proposed three modified Fenton process: heterogeneous Fenton, photo-Fenton, and electro-Fenton (Gernjak *et al.*, 2003).

The general objective of this project is to study the removal of micropollutants from polluted water by developing novel electrochemical membrane processes.

RESULTS

Electro-removal of propoxur micropollutant

Initially, the synthesized AOAs were characterized, and their catalytic activity was compared to the benchmark catalysis by Fe^{2+} (Fenton) or Fe^{3+} (Fenton-like) in batch and continuous flow ceramic membrane reactor (CMR) experiments (Figure 1a). As seen in Figure 1b and 1c, the AOAs exhibited a layered, porous, scattered aggregated iron structure with agglomerate sizes ranging from 33 to 50 µm and a pH_{PZC} of 6.1. The heterogeneous PR oxidation efficiency was equalized to its Fenton-like oxidation by increasing the hydrogen peroxide and AOAs concentrations, so as to obtain a molar ratio of 1:1 H_2O_2 to iron (Figure 1d).

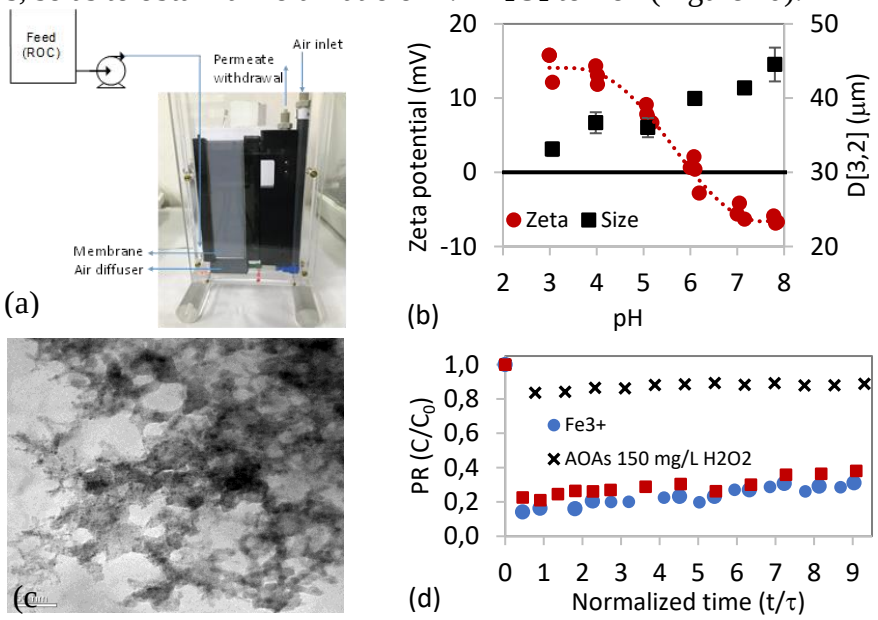

Figure 1: (a) The submerged ceramic membrane reactor, (b) AOAs zeta potential and agglomerate sizes, (c) TEM image of the AOAs, (d) PR removal from ROC catalyzed by Fe^{3+} and AOAs in CMR experiments.

Next, the effects of pre-treatment of the GF, its thickness, electrolyte pH, oxygen/air purging, applied current, and electrolyte composition on the in-situ generation of hydrogen

peroxide were studied. Despite the fact that a voltammetry measurements did not reveal the oxygen reduction peak, at (-0.4)–(-0.6) V vs. SCE, which is characteristic of carbonaceous substrates, hydrogen peroxide was electro-generated in both Na_2SO_4 and ROC solutions, with higher concentrations obtained in the former. Superior hydrogen peroxide electro-production was obtained with a 2 mm-thick GF, pH 3-4, 50 mL/min of O_2 purging, and a -2.4 V applied current.

The electro-oxidation of PR catalyzed by Fe^{2+} (electro-Fenton), Fe^{3+} (electro Fenton-like) and the AOAs (heterogeneous electro Fenton-like) were compared. The electro-oxidation of PR catalyzed by AOAs had the lowest removal efficiency, followed by Fe^{3+} and Fe^{2+} (Figure 2a). Nonetheless, the PR removal was equalized to that catalyzed by Fe^{2+} by increasing the AOAs concentration and prolonging the reaction time (data not shown). The current potential enhanced the of PR removal (Figure 2b). The electro-Fenton was found to be more efficient than the Fenton oxidation, as it requires less catalyst and shorter reaction time for the three iron catalysts (Table 1). Overall, the results point to the potential of heterogeneous electro Fenton-like oxidation as a sustainable process for the efficient removal of PR from secondary effluent ROC.

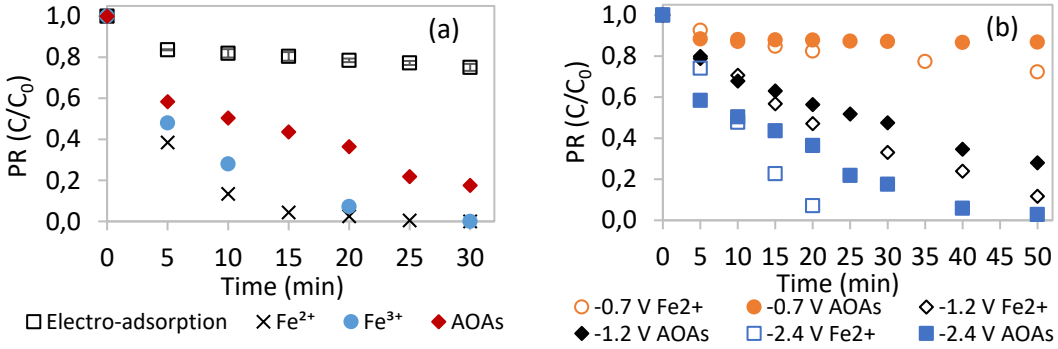

Figure 2: PR electro-removal by (a) adsorption and oxidation catalyzed by Fe^{2+}, Fe^{3+}, and AOAs, (b) at different applied currents

Table 1: Comparison between Fenton-oxidation and electro-oxidation in terms of reaction time, H_2O_2 and catalysts dosages for 80% PR removal ($[PR]_0$= 1 mg/L, molar ratio 1:1 H_2O_2 to Fe).

	Fenton	Fenton-like	AOAs Fenton-like	Electro-		
				Fenton	Fenton-like	AOAs Fenton-like
Reaction time (min)	<10	120	120	10	15	30
Catalyst (mg/L)	26.5	82.0	245.0	4.8	20.1	20.8
H_2O_2 (mg/L)	40.3	50.0	150.0	5.6	5.2	10.5
pH	2.5	3.0	4.0	3.0	3.0	4.0

Degradation of 4-nonylphenol on the CNTs membrane

Figure 3 shows the EM system for 4-NP monitoring and removal. A larger system with a surface area of 5 cm^2 was constructed and tested. The level of detection for the system was estimated to be $1.92 \cdot 10^{-10}$ M (equals to 42.3 ppt) of 4-NP. The EM could also be used for the 4-NP removal. Yet, the oxidation of the 4-NP fouls the CNT membrane, and therefore a second membrane was added, and an entire flow-through cell was 3D printed.

The EF reactions carried out in a static cell with different carbonaceous-based membranes showed that the oxygen can be reduced by a two-electron process (Eq. 1) to form H_2O_2, a four-electron process (Eq. 2) to form water, and a three-electron process to give $OH^{\cdot}$ radicals (Eq. 3). The faradaic efficiency and selectivity of the different EMs for producing H_2O_2 and OH radicals are currently being examined.

$$O_2 + 2H^+ + 2e^- \rightarrow H_2O_2 \qquad (1)$$

$$O_2 + 4H^+ + 4e^- \rightarrow 2H_2O_2 \quad (2)$$

$$O_2 + 2H^+ + 3e^- \rightarrow 2OH\cdot + OH^- \quad (3)$$

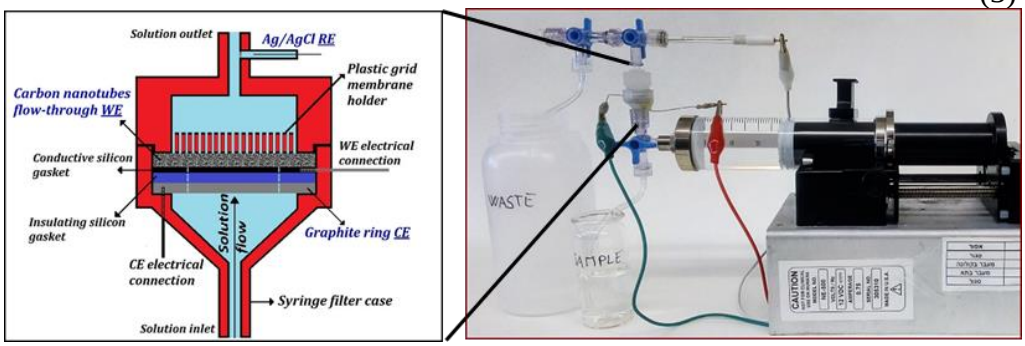

Figure 3: Left schematics of the electrochemical membrane; right the entire system.

Degradation of β-estradiol with photocatalytic membrane

Figure 4 shows the E2 removal on a pristine PVDF or a PVDF-TiO_2 membrane *via* adsorption, photolysis, or photocatalysis degradation. The photocatalysis was repeated five times to confirm the reproducibility.

As seen in Figure 4, the E2 was not removed by the PVDF-TiO_2 membrane by adsorption. The E2 removal by photolysis, and photocatalysis were 11 and 80%, respectively. These results indicated the potential the PVDF-TiO_2 membrane for E2 micropollutant treatment, even though the ambitions guideline of 1 ng/L (WHO, 2022) cannot yet be achieved *via* photocatalysis which is now investigated *via* electrochemical processes.

Unverified results with and electrochemical CNTs membrane (Zhu *et al.*, 2018) showed a E2 removal comparable to photocatalysis. Improving these results beyond the performance of photocatalysis is in progress following extensive method development.

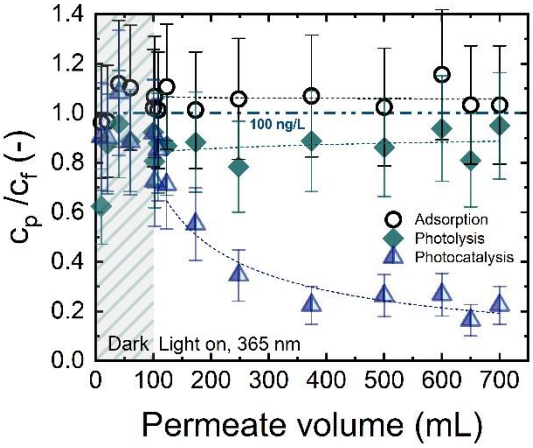

Figure 4: Permeate to feed concentration ratio c_p/c_f vs. cumulated permeate concentration for adsorption, photolysis, and photocatalysis. Adsorption: PVDF-TiO_2 membrane in dark; photolysis: pristine PVDF membrane with light irradiation; photocatalysis: PVDF-TiO_2 membrane with light irradiation, I_{UV} = 10 mW/cm^2, 365 nm, c_f=100 ng/L, J_w = 600 L/m^{2}h, 1mM $NaHCO_3$, 10 mM NaCl, 27.2 mg/L EtOH, 79.2 mg/L MeOH pH 8.3±0.1, and 24±2 ºC (to be submitted).

CONCLUSIONS

Carbonaceous-based membranes electro-generate hydrogen peroxide and hydroxyl radicals.
Electro-Fenton was found to be more efficient than Fenton oxidation for propoxur removal from a secondary effluent reverse osmosis concentrate.
A dual-purpose flow through an electrochemical system was developed for efficient detection and removal of 4-nitrophenol. Yet, Electro-oxidation of the 4-NP fouls the CNT membrane.
The electro-chemical CNTs membrane performed similarly to photocatalysis in terms of β-estradiol removal.

ACKNOWLEDGEMENT

The authors wish to thank the funding of the NemWare project (WT1902) by the German Ministry of Education and Research (BMBF) and Israeli Ministry of Science & Technology (MOST) within the framework of the German-Israeli water technology cooperation.

REFERENCES

Dordio A., Carvalho A.P., Teixeira D.M., Dias C.B., Pinto A.P. (2010). Removal of pharmaceuticals in microcosm constructed wetlands using Typha spp. and LECA. *Bioresour. Technol.*, 101, 886–892.

Deng Y., Zhao R. Advanced Oxidation Processes (AOPs) in wastewater treatment. (2015). *Curr. Pollut. Rep.*, 1, 167-176.

Gernjak W., Krutzler T., Glaser A., Malato S., Caceres J., Bauer R., Fernández-Alba A.R. (2003). Photo-Fenton treatment of water containing natural phenolic pollutants. *Chemosphere*, 50(1), 71-78.

Zhu, X., Dudchenko A.V., Khor C.M., He X., Ramon G.Z., Jassby D. (2018). Field-induced redistribution of surfactants at the oil/water interface reduces membrane fouling on electrically conducting carbon nanotube UF membranes. *Environ. Sci. Technol.*, 52, 11591-11600.

World Health Organization, https://www.who.int/news/item/01-07-2021-billions-of-people-will-lack-access-to-safe-water-sanitation-and-hygiene-in-2030-unless-progress-quadruples-warn-who-unicef Access date: 04/30/2022.

Project WT2001: LowGHGWatt

Reduction green-house gas emissions in the water treatment sector by integrated technologies for biofouling mitigation

Leilah KROUNBI[1], Akachukwu NWAOBI[1], Roy BERENSTEIN[1*], Steffen WITZLEBEN[2*], Edo BAR-ZEEV[1] , Eran EDRI[3*] and Martin SIEBER[2]

[1]*Ben-Gurion University, Zuckerberg Institut of Water Research, 84990 Beer Sheva, Israel*
[2]*Bonn-Rhein-Sieg University, Institute of Technology, Resource, and Energy Efficient Engineering, 59379 Rheinbach, Germany*
[3]*Department of Chemical Engineering, Ben-Gurion University of the Negev, Be'er-Sheva 8410501, Israel*
**Corresponding author's e-mail: royber@bgu.ac.il; Steffen.Witzleben@h-brs.de; edrier@bgu.ac.il*

ABSTRACT

Reverse osmosis (RO) desalination is one of the main solutions to bridge the shortfall between water needs and the dwindling freshwater worldwide. However, desalination is an energy-intensive technology that contributes a major fraction of the total GHG emissions of the water technology sector. Currently, the energy consumption of RO membranes is much higher than the theoretical energy demand for membrane desalination. One of the main reasons for the superfluous energy demand is biofouling. Biofouling can be mitigated by disinfection. Specifically, ozone disinfection is an environmentally-friendly and energy-efficient disinfection agent. Nevertheless, RO membranes are not stable against ozone. This research aims to lower the energy demands of reverse osmosis (RO) desalination. Specifically, we are developing an ozone-stable polyamide RO membrane with protective ultrathin metal oxide (MO) layer using atomic layer deposition (ALD).

Commercial RO membranes were modified using ALD, in which an organo-metallic molecule comprised of alumina and ethylene glycol (i.e., alucone) is deposited in molecular layers. Long-term ozone exposure tests were carried out by storing the membranes in ozone solution for up to 16 weeks at 50 ppb (the maximum ozone concentration permitted by the EU Drinking Water regulations) and 150 ppb. FT-IR spectra of the untreated membranes following the long-term ozone treatment showed changes in the band of 1750 cm^{-1}, indicating the onset of oxidation of the polyamide chain in the active layer. On the other hand, the spectra of the coated membranes with 10 layers of alucone showed only minimal changes in the 1750 cm^{-1} IR band. In addition, even after storage in ozone for 16 weeks, negligible changes in intensity were detected.

The performance (permeability and salt rejection) of the alucone-coated RO membranes was tested before and after exposure to high ozone concentrations up to 120 mg $L^{-1}h$. RO membranes coated with alucon withstand degradation at high ozone concentrations relative to pristine membranes, which were readily destroyed. However, their performance following ALD coating was significantly reduced. Pretreating the membrane with glycerol that prevents pore collapse under the strong vacuum conditions within the ALD restricted the reduction in performance, but the ozone stability was not maintained. The results of this study indicate that ALD can be used to improve the membrane stability to oxidation, but the coating should be optimized to minimize its effect on the membrane performance.

KEYWORDS

Desalination; Reverse Osmosis; Ozone; Atomic layer deposition; Polyamide membranes

INTRODUCTION

Increased water scarcity in the world is an acute problem. One solution to bridge the shortfall between water needs and the dwindling freshwater is desalination. As a result, the current desalination capacity in the world is approx. 100 million m^3/day, and it is expected to grow by 40% until 2030. However, desalination is an energy-intensive technology that contributes a major fraction of the total GHG emissions of the water technology sector. In particular, the specific energy consumption of seawater RO desalination, which is the most energy-efficient desalination technology, is 3-5 kWh/m^3. Developing sustainable desalination technologies that consume less energy and have lower GHG emissions requires new technologies which rely on alternative renewable energy and improve the energy consumption of the current ones.

In particular, biofouling is one of the main reasons for the excessive energy demand of RO desalination. Biofouling, the consequence of biofilm formation on the membrane's surface, is responsible for approx. 15% of the specific energy demand in RO desalination plants and thus increases operational costs and GHG emissions. Biofouling also increases the energy cost of RO due to the need for intensive pretreatments and chemical cleaning of the fouled membranes. Hence, mitigating, or significantly hindering biofouling by low-energy approaches, can help attain the theoretical energy demand of RO desalination. One alternative to mitigate biofouling is ozone disinfection of the feed water before desalination. Unfortunately, the common polyamide RO membranes are sensitive to oxidation; therefore, this approach has not been applied to date. This study focuses on developing membranes that are stable against oxidation, specifically ozone-stable membranes, for biofouling mitigation in RO desalination.

EXPERIMENTAL

Commercial RO membranes (ESPA1, Hydranautics) were used in this study. The ALD experiments were conducted according to previous studies (Chaudhury et al., 2020; Wormser et al., 2021). Metal deposition via ALD is enhanced on more hydrophilic surfaces. Thus, hydroxyethyl methacrylate (HEMA) was grafted onto RO membranes (Bernstein et al., 2010) to increase the concentration of the surface OH groups prior to ALD. Alucone-coated membranes were imaged using scanning electron microscopy (SEM) with EDS capabilities for surface chemical information. Membrane performance following ALD coatings and ozonation was evaluated by salt rejection (1 g NaCl/L) and water permeability (DDW) in a dead-end filtration cell (Bernstein et al., 2010). Salt rejection was calculated as $\%R = (1-\Lambda_f/\Lambda_p)$, where Λ is the feed (f) and permeate (p) conductivity. Water permeability was calculated as $Lp=Jv/P$, where J_v is the water flux (L/m^2h), and P is the applied pressure (bar). O_3 concentration was measured using a colorimeter method with Indigo dye.

RESULTS AND DISCUSSION

Long-term low oxidation studies

The setup of these experiments used an existing polymer electrolyte membrane (PEM)-ozone generation test device for exposing materials to ozone. The test facility consists of two components: ozone is generated electrochemically with the help of an Innovatec microcell in the first unit. The gaseous ozone is then transferred via a hose connection to the second component containing RO membrane samples (Fig.1). The second cell in which membrane

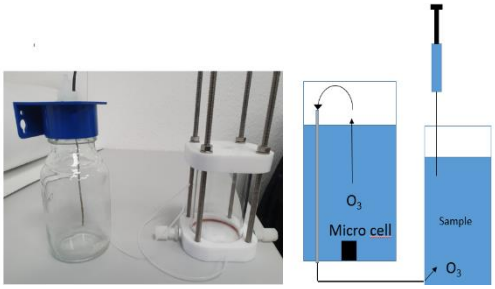

Figure 1: Experimental system for materials' exposure toO_3 .

samples are exposed to ozone is sampled and checked for ozone concentration, pH, and electrical conductivity. If there is a deviation from expected values, ozone production is readjusted, or the water is replaced. Membranes had been rinsed in ethanol to remove anti-microbial coatings and any other preservatives deposited by the manufacturer. All these materials were evaluated for ozone resistance. O_3 resistance tests commenced using membranes coated with 10 cycles of alucone. These samples were exposed to dissolved ozone at 50 and 150 µg/L for up to 4 months. Additional steps for optimizing ALD coatings, including HEMA-grafting, glycerol-dipping, and various coating cycles, were not evaluated in these preliminary long-term tests at low ozone concentrations. Ozone resistance was evaluated via FT-IR and light microscope. The microscopic examinations revealed slight color changes. However, no changes in structure or surface were observed with microscopy (results not shown).

Performance of alucone-coated RO membranes

Further studies focused on the effect of alucone coatings and related surface modifications on RO membrane performance. Figure 2A presents the salt rejection (R) and water permeability (Lp) of membranes before (Pristine) and after alucone coating, with and without HEMA grafting (HEMA-alu and Alu). It can be seen that the membrane permeability decreased significantly following alucone coating. However, based on previous studies, alucone should not compromise membrane performance (Chaudhury et al., 2020). It was speculated that the flux decreased due to the drying process (Hermans et al., 2015) and high vacuum, which are essential for the ALD. To overcome this problem, membranes were soaked in glycerol for 30 min to prevent pore collapse and preserve adequate water flux. Figure 2B shows that the decline in the membrane flux was solely due to the drying step and that soaking the membrane in glycerol before the drying step mitigated this problem. The glycerol-soaked and alucone- coated membranes in Figure 2A further confirm that coating with alucone ALD following the pre-soaking with glycerol does not compromise membrane performance, even after 25 coating cycles.

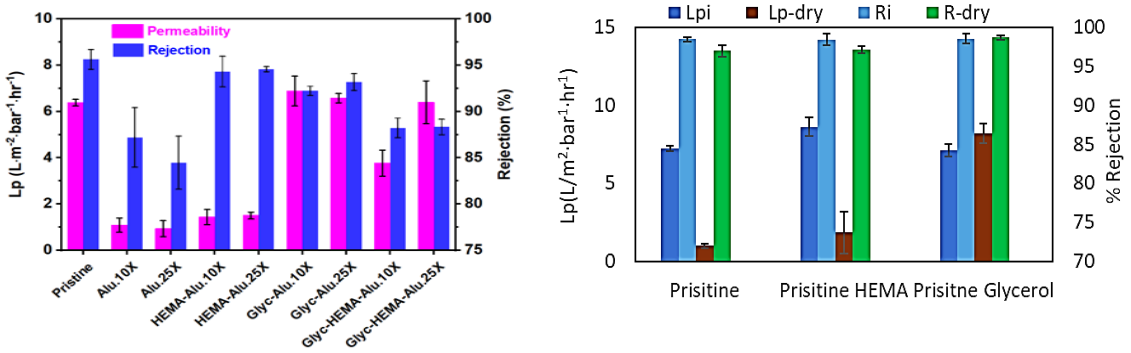

Figure 2: (A)Rejection (%R) and permeability (Lp) of pristine, 10 and 25 cycles coated (Alu10x and Alu 25x); HEMA grafted (HEMA-alu); dipped in glycerol (Glyc-Alc) HEMA grafted with, glycerol dipped (HEMA-glyc.-Alu) memebranes (B)Performance of pristineand pretreated memebranes.before (i) and after (dry) drying. n>3

Enhanced oxidation studies

The effect of the alucone coating on membrane stability after ozonation was studied. All membranes were evaluated, regardless of salt rejection or water permeability values after coating, as the goal was to measure membrane performance before and after ozonation
First, the ozone dose required to destroy the pristine RO membrane was determined. It was found that at an ozone dose of approx. 120 mg-$O_3 \cdot L^{-1} \cdot$min, the membrane water permeability increased while salt rejection decreased, indicating that the membrane surface was oxidized. The alucone-coated membranes were exposed to a similar ozone dose. Figure 3 presents the membrane permeability and salt rejection ratio before (L_{pi} and R_i) and after exposure to the ozone dose (L_{pO3} and R_{O3}). A decrease in the permeability ratio and an increase in the salt rejection ratio indicate membrane oxidation. Figure 3 shows that alucone coatings mitigate the increase in water permeability and the decrease in salt rejection, especially after 25 cycles. Specifically, the salt rejection ratio (R_i/R_{O3}) of HEMA-grafted membranes, glycerol-dipped, and alucone coated with 10 cycles was ≈1. Moreover, both the salt rejection and water permeability ratio (R_i/R_{O3} and Lpi/L_{pO3}) of HEMA-grafted, glycerol-dipped, and alucone coated with 25 cycles (glycerol-HEMA-Alu25x) were ≈ 1, suggesting that alucone protected membranes from ozone damage.

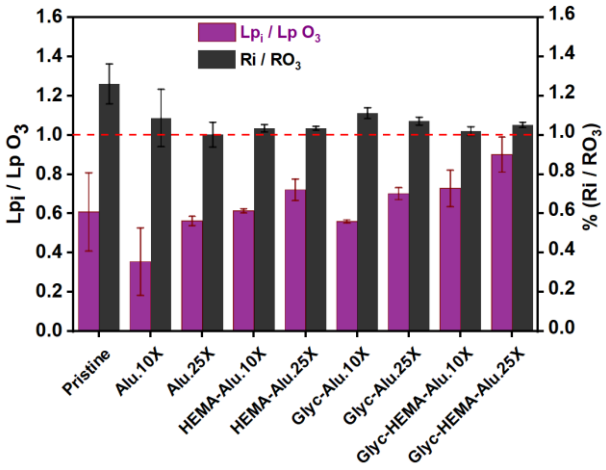

Figure3 : Water permeability (L_p) and salt rejection (%R) ratio of pristine and alucone-coated membranes .before (i) and after (O_3) exposure to ozone

Additional experiments were carried out to test the effect of 50 cycles of alucone coating. Figure 4A presents the water permeability and salt rejection of pristine and glycerol-dipped membranes coated with alucone for 0, 10, 25, and 50 cycles before and after ozone exposure. Figure 4B presents these results as a ratio of values AFTER ozonation vs. before and after normalization to the ratio of pristine membranes to assess the relative 'damage' to membranes after ozonation compared to the pristine membrane.

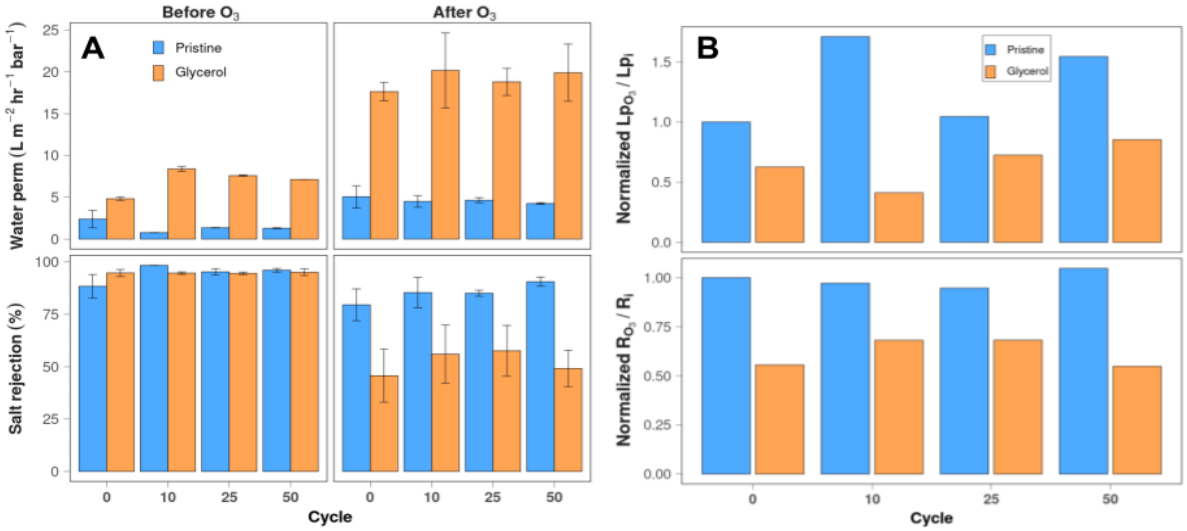

Figure 4: (A) Water permeability and salt rejection of pristine and glycerol-coated membranes coated with alucone for 0-50 cycles before and after ozone exposure. (B) The ratio of the water permeability and salt rejection AFTER vs. BEFORE ozonation. All ratios have been normalized to the ratio of the pristine, uncoated membrane (pristine 0x).

Figure 4B shows that the salt rejection of pristine membranes coated for 50 cycles was slightly higher after ozonation. The water permeability was also higher, indicating that membrane surfaces were damaged. However, this damage did not seem to affect the ability of the membrane to filter out salt, which is the main interest in desalination. Glycerol-dipped membranes could preserve good water permeability before ozonation but appeared more susceptible to damage after ozonation, as indicated by the sharp increase in water permeability and decrease in salt rejection.

The membranes were also imaged with SEM and scanned with EDS to gain surface chemical information (Figs. 5 and 6). It was found that the alucone coating fills the vacuole spaces, creating a smooth, continuous layer, which likely leads to decreased water permeability before ozonation in pristine membranes.

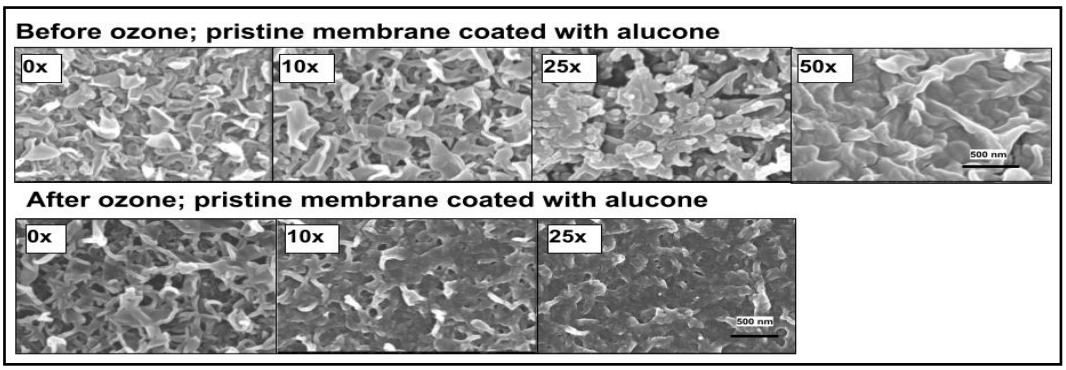

Figure 5: SEM images of pristine membranes coated with alucone for 0, 10, 25, and 50 cycles before and after exposure to ozone.

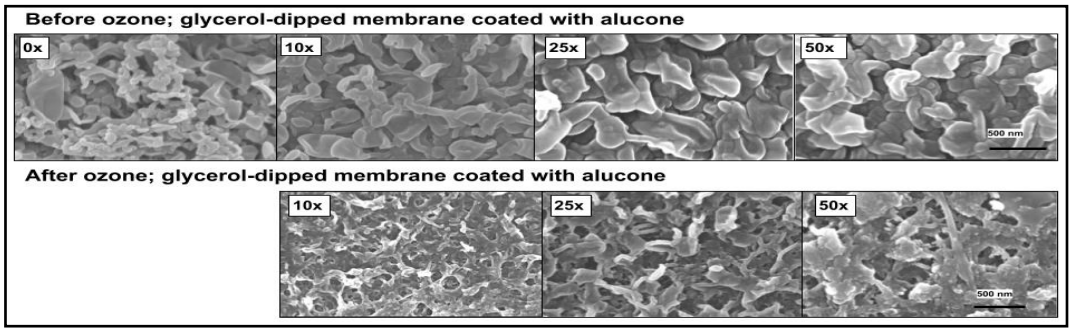

Figure 6: SEM images of glycerol-dipped membranes coated with alucone for 0, 10, 25, and 50 cycles before and after exposure to ozone.

The effect of alucone in protecting membranes from ozonation is still unclear. What is clear is that the alucone coating appears stable under ozonation. Figure 7 presents the ratio of chemical information of membrane surfaces after ozonation vs. before for pristine and glycerol-dipped membranes coated with alucone for 10, 25, and 50 cycles. Ozonation only slightly lowers the content of alumina, the active ingredient in alucone, across various cycle numbers.

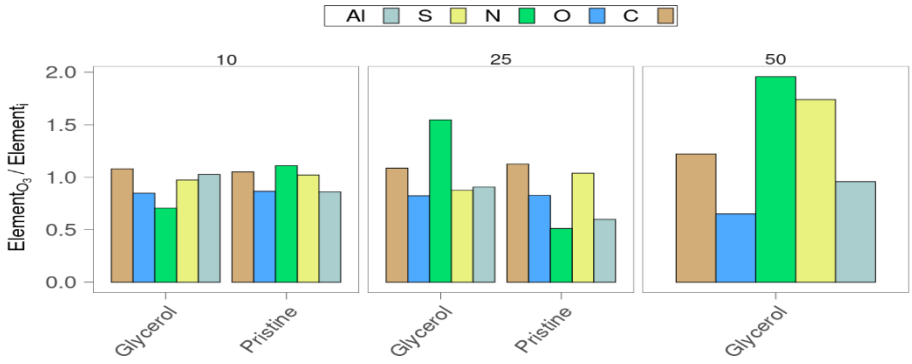

Figure 7: The ratio of AFTER vs. BEFORE ozone exposure of elemental concentration by weight percent of aluminum (Al), sulfur (S), nitrogen (N), oxygen (O), and carbon (C) on the surface of membranes. Membranes were glycerol dipped or not dipped (pristine) and coated with alucone for 10, 25, and 50 cycles.

CONCLUSION

RO membranes were treated with different ozone concentrations. This procedure made it possible to check ozone resistance in various application areas. A long-term test was carried out on membranes in which ozone concentrations are permitted under the EU Drinking Water regulations (50 ppb) and with a threefold higher ozone concentration (150 ppb). In this scenario, permanent use

was tested. The FT-IR spectra of the untreated membranes (ESPA membrane) showed small changes in the band of 1750 cm-1 at concentrations of 50 ppb and 150 ppb, indicating a starting oxidation of the polymer chain after storage for 16 weeks. The spectra of the treated RO membranes (ESPA membrane MCO-Alu 10x) showed only minimal changes in the IR band at the concentration levels of 50 and 150 ppb at 1750 cm^{-1}. Even after storage in ozone for 16 weeks, only very small changes in intensity occurred.

The membranes' salt retention and permeability were investigated after enhanced oxidation experiments using high ozone concentrations. The results show that alucon coating reduces the membrane performance, but the effect can be eliminated by pretreatment with glycerol. It was also found that pretreatment using HEMA did not significantly affect the coating degree. The enhanced ozone oxidation experiments revealed that while the pristine RO membranes quickly lose their performance, it remains almost stable following ALD coating. This indicates that coating the membrane with a metal oxide layer can protect the membrane against ozone attack. However, the exact coating conditions still need to be optimized. Specifically, it was found that glycerol pretreatment preserves the membrane performance but then, although the coating remains intact, the layer's anti-oxidizing ability does not. This can be due to the high porosity of the alucon coated on a pretreated glycerol membrane. Therefore, other metal oxides will be investigated as a protective layer for ozone.

ACKNOWLEDGEMENTS

The research is supported by grants from The Ministry of Innovation, Science & Technology and the German Federal Ministry of Education and Research (BMBF): The German-Israeli Water Technology Cooperation Program. L.K thanks the Jacob Blaustein Center for Scientific Cooperation for a postdoctoral fellowship.

REFERENCES

Bernstein R., Belfer S., Freger V. (2010). Surface modification of dense membranes using radical graft polymerization enhanced by monomer filtration. Langmuir 26 (14), 12358-12365

Chaudhury S., Wormser E., Harari Y., Edri E., Nir O. (2020). Tuning the ion-selectivity of thin-film composite nanofiltration membranes by molecular layer deposition of alucone. ACS applied materials & interfaces 47, 53356-53364.

Hermans S., Bernstein R., Volodin A., Vankelecom IFJ. (2015) Study of synthesis parameters and active layer morphology of interfacially polymerized polyamide–polysulfone membranes Reactive and Functional Polymers 86, 199-208.

Wormser E., Nir O., Edri E. (2021). Low-resistance monovalent-selective cation exchange membranes prepared using molecular layer deposition for energy-efficient ion separations. RSC Advances, 11, 2427-2436.

Project WT2002: Red-CO2-PNA

Reducing CO_2 Emissions from Municipal Wastewater Treatment – Comparing Different Partial Nitritation/Anammox Applications

Michal GREEN[1], Sheldon TARRE[1]*, Samah ABASI[1], Qi LI[2], Oliver DAS[2] and Susanne LACKNER[2]

[1]Faculty of Civil and Environmental Engineering, Technion, Haifa, 32000, Israel
[2]Department of Civil and Environmental Engineering Sciences, Institute IWAR, Water and Environmental Biotechnology Group, Technical University of Darmstadt, Darmstadt, 64277, Germany
**Corresponding author's e-mail: shelly@technion.ac.il*

ABSTRACT
Conventional wastewater treatment plants (WWTPs) are energy intensive and about 25% of their total energy consumption is spent on nitrogen removal. Instead of the traditional nitrification/denitrification processes used today, partial nitritation and anammox (PN/A) can offer significant energy savings and a lower WWTPs CO_2-footprint when applied to mainstream municipal wastewater (MWW). While PN/A is a proven technology for MWW side-stream treatment, the technology has not yet been effectively applied to the much larger market of MWW mainstream treatment due to the high COD/N ratio of MWW, lower temperatures, and low and fluctuating ammonium concentrations.

The objective of this research project is the investigation of two different process strategies to overcome the limitations of the partial nitritation/anammox (PN/A) process for application in mainstream MWW treatment. The first strategy is based on an ion exchange (IX) in combination with a bioregeneration process for the selective removal and treatment of ammonium from mainstream MWW (Israeli side). The premise for this strategy is that the removal of ammonium from mainstream by IX eliminates bacterial competition from carbon removal in mainstream WW and provides an IX regenerant with high ammonium concentrations for stable and controlled PN/A operation. In the second strategy, biofilm reactors (German side) will be used in one and two-stage PN/A configurations. Of particular interest is the impact of organic carbon on the operation of PN/A in mainstream and the associated N_2O emissions. First data shows promising results, especially with regards to the saline anammox reactors in Israel and with the performance of the biofilm reactors in Germany. High nitrogen removal can be achieved with both systems while keeping N_2O emissions low. Optimizing process operation, i.e. C:N ratio, aeration patterns, reactor control, etc., will be the focus of the next phase of research.

KEYWORDS
Mainstream wastewater treatment; partial nitritation; anammox; ion exchange; biofilm reactors

INTRODUCTION
Conventional wastewater treatment plants (WWTPs) are energy intensive and are responsible for the emissions of more than 27 Mtonnes of CO_2 year-1 in Europe alone. About 25% of the

total energy consumption in wastewater treatment is spent on removal of inorganic nitrogen compounds. Partial nitritation and anammox (PN/A) for nitrogen removal in mainstream municipal wastewater (MWW) instead of the conventional nitrification/denitrification processes has the potential for significant energy savings and lowering of the CO_2-footprint of WWTPs. While PN/A is a proven technology for MWW side-stream treatment, the technology has not been effectively applied to the
much larger market of MWW mainstream treatment due to the high COD/N ratio of MWW, lower temperatures, and low and fluctuating ammonium concentrations. The overall objective of this research project is thus to investigate and compare two different process strategies to overcome the limitations PN/A processes are still facing when applied in mainstream MWW treatment.

METHODOLOGICAL APPROACH

Both research groups developed, constructed and started-up their experimental setups and reactors early in the project. For the Israeli research group, the top priorities were to 1) successfully establish both ammonia oxidizing bacteria (AOB) and anammox bacterial populations suitable for the saline conditions of the ion exchange and partial nitritation-anammox (IX-PN/A) process, and 2) initiate PN and PN/A reactor operation. Anammox bacteria are particularly difficult to cultivate due to a slow growth rate, a low cell yield and a high sensitivity to changing environmental conditions.

The Germany research group focuses on biofilm reactors. In phase I, the potential of stable nitrite production (partial nitritation, PN) with Membrane Aerated Biofilm Reactors (MABR) was tested. Four MABRs were operated with synthetic feed (containing ammonium at a concentration of 50 mg-N L-1) under different intermittent aeration regimes. MABR-1/-2 had one aeration cycle per hour (2min/h) and MABR-3/-4 had two aeration cycles per hour (2min/0.5h). This operation mode enabled the setting of a certain ratio of oxygen to substrate (here NH4-N) to investigate optimal conditions for PN. In phase II, two MABRs, one with intermittent aeration and one with continuous aeration, were operated to test the impact of the C:N ratio on total nitrogen removal performances and N_2O emissions. During the first months of operation, a C:N ratio of 1.7 was chosen to mimic carbon limitation.

RESULTS AND DISCUSSION

Enrichment of AOB and anammox bacteria under saline conditions

Sludge taken from a sea water (4%) aquaculture denitrification filter was used to inoculate fixed bed reactors filled with volcanic scoria (retentive media). The reactors, fed sea water amended with ammonium and nitrite, showed good anammox activity and nitrogen removal performance after several months. Biomass harvested from the saline reactor was used to quickly start-up other anammox based reactors under 4% salinity. Microbial community analysis of the saline anammox reactor by next generation sequencing (NGS) revealed the obligately halophilic bacteria from the genus *Candidatus Scalindua*, known for its presence in the ocean. Given that anammox can be active under 4% salinity (hyper saline conditions) and higher salinity offers the benefit of more efficient ion exchange regeneration, 4% salinity was chosen for the regenerant saline concentration of the IX-PN/A process. To complement the anammox bacteria grown under 4% salinity, enrichment of AOB for nitritation was undertaken at 4% salinity and successfully carried out in similar fixed bed reactors. The microbial community analysis of the nitritation reactors revealed bacteria from the obligately halophilic *Nitrosococcus* genus and the

halotolerant *Nitrosomonas* genus as the dominant AOB. *Nitrosococcus* is a well-known marine AOB and *Nitrosomonas* is also known to be active under saline conditions. Nitrite oxidizing bacteria (NOB) appeared in the nitritation reactor at free ammonia (FA) concentrations less than 1 mg/L (Fig. 1). When nitrite oxidation occurred, the NOB identified was from the genus *Nitrospina*, a known marine NOB. The activity of NOB under 4% salinity could be inhibited by maintaining FA concentrations in the range of 1 to 10 mg/L (Fig. 1).

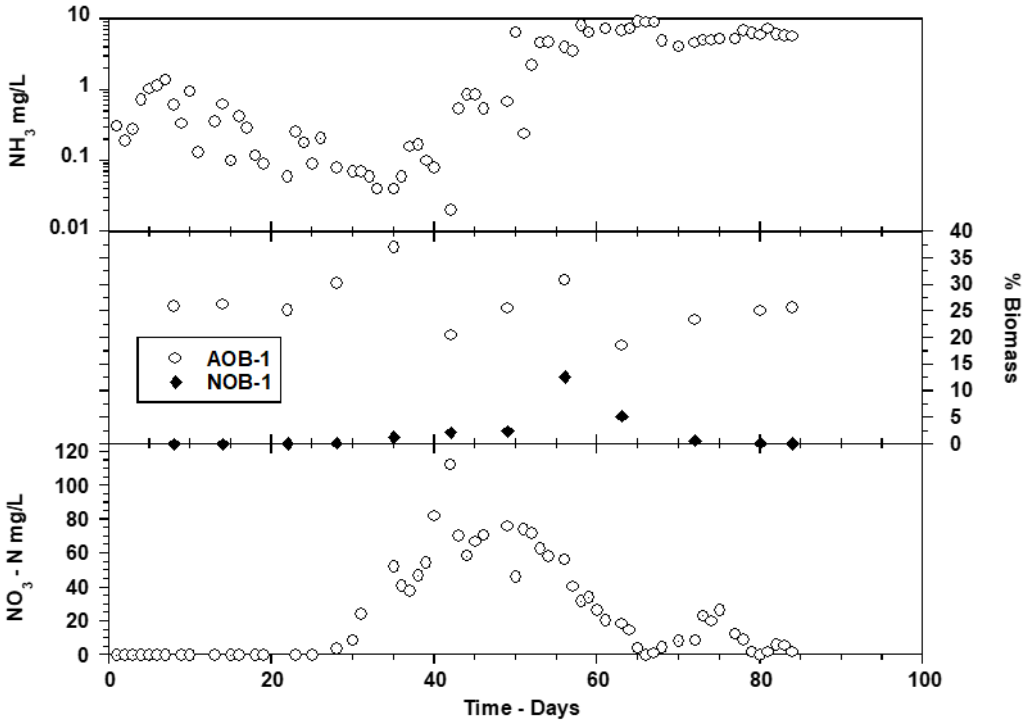

Fig. 1. Partial nitritation reactor, the effect of free ammonia (FA) concentration on the appearance of nitrates: bottom pane effluent nitrate concentration, middle pane %AOB and %NOB of biomass, and top pane FA concentration.

Operation of one stage and two stage PN/A reactor systems

After enriching AOB and anammox biomass, both one stage and two stage (separate reactors for nitritation and anammox) PN/A reactor systems were constructed and operated under saline conditions with influent concentrations simulating the bioregeneration stage of the IX-PNA process. One stage PN/A deammonification rates are inherently limited due to low reactor dissolved oxygen concentrations used to prevent toxicity to anammox bacteria. Sparging the one stage PN/A reactor with 2.5 and 5% oxygen gas mixtures resulted in relatively high deammonification rates when compared to other one stage PN/A systems reported in the literature (Fig. 2). While the two stage PN/A reactor system showed even higher nitrogen removal rates, lower N_2O emissions were observed from the one stage PN/A reactor particularly when effluent ammonium concentrations were kept low (Fig. 3). However, lower operating ammonium concentrations to minimize N_2O emissions may enhance NOB proliferation especially in separate partial nitritation reactors where higher dissolved oxygen concentrations are present. N_2O emissions were not affected by changes in loading rates or transient events.

Operation of the IX-PN/A system

An IX column was filled with 1L of zeolite (chabazite) for ammonium removal and 48 absorption and bioregeneration cycles using synthetic wastewater (50 mg/L NH_4; 200 L/cycle) were carried out. The IX column was regenerated with a 4% brine solution (24 L/cycle) starting with sea water. Sodium loss during absorption was compensated by adding NaCl to the

regenerant. After IX column regeneration, the average regenerant brine ammonium concentration was 207.5 mg/L. The ammonium rich brine regenerant was fed to the PN/A reactor and more than 90% of ammonium was successfully removed. Stable operation of the PN/A reactor was observed with no apparent growth of nitrite oxidizing bacteria (NOB). However, the build-up of calcium in the recycling regenerant (see Fig. 4, circles) to very high concentrations (3000 mg/L as Ca) due to minimal regenerant blowdown (field capacity only; approximately 1%) eventually impaired the anammox bacteria in the PN/A reactor function as evidenced by the appearance of N-NO_2 concentrations.

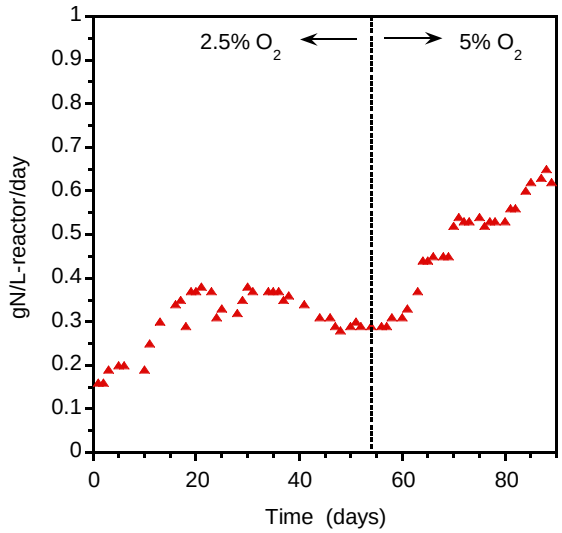

Fig. 2. Single stage PN/A reactor deammoniafication rates using 2.5 and 5% oxygen gas mixtures.

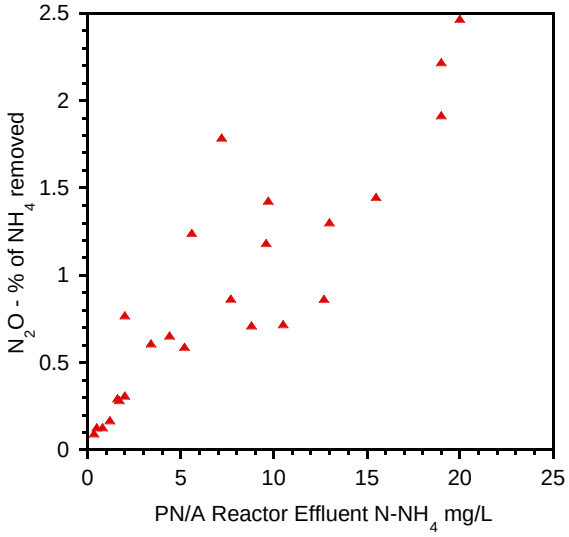

Fig. 3. N_2O emission as % of total NH_4 removed from a PN/A reactor as a function of reactor [NH_4^+].

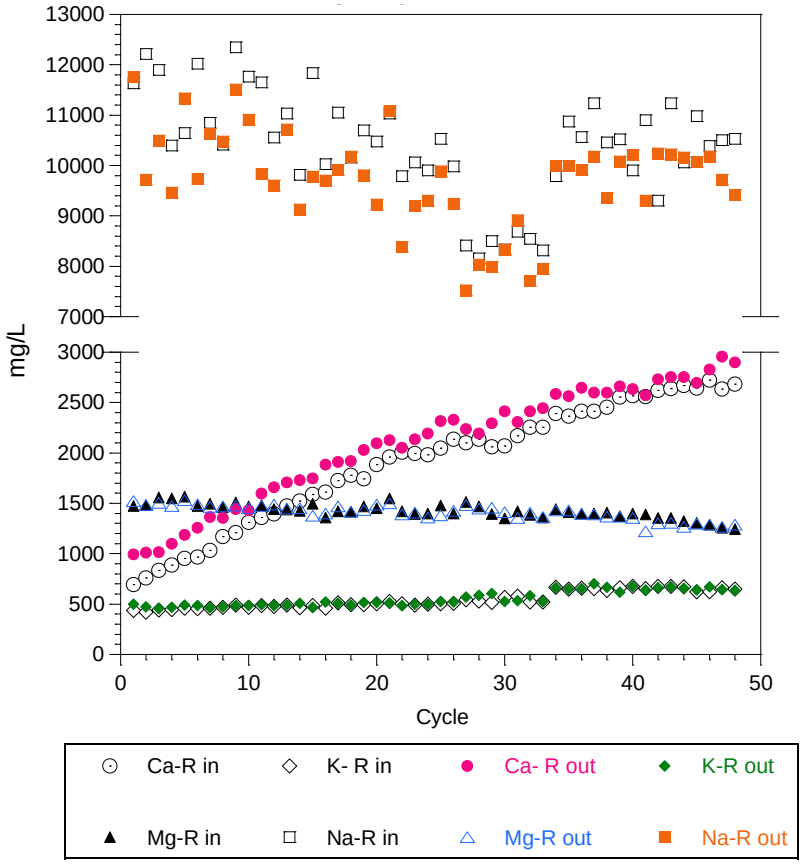

Fig. 4. Cation composition of regenerate before and after PN/A reactor treatment

MABR start-up and operation

The MABR trials delivered the following results. Phase I (PN) showed that stable nitrite production was sustained in all four MABRs during the first 50 days of operation (see Fig. 5). Afterwards the nitrite concentration declined under both intermittent aeration strategies. It was possible to recover nitrite production in MABR-1 and -4 from around day 80 onwards. The aeration time of only 2 min every hour seemed most suitable to achieve a somewhat stable nitrite production (see MABR-1).

The nitrogen balance in this reactor suggests some anammox activity present. With the residual ammonium concentration, such an effluent is also suitable for subsequent anammox reactors.

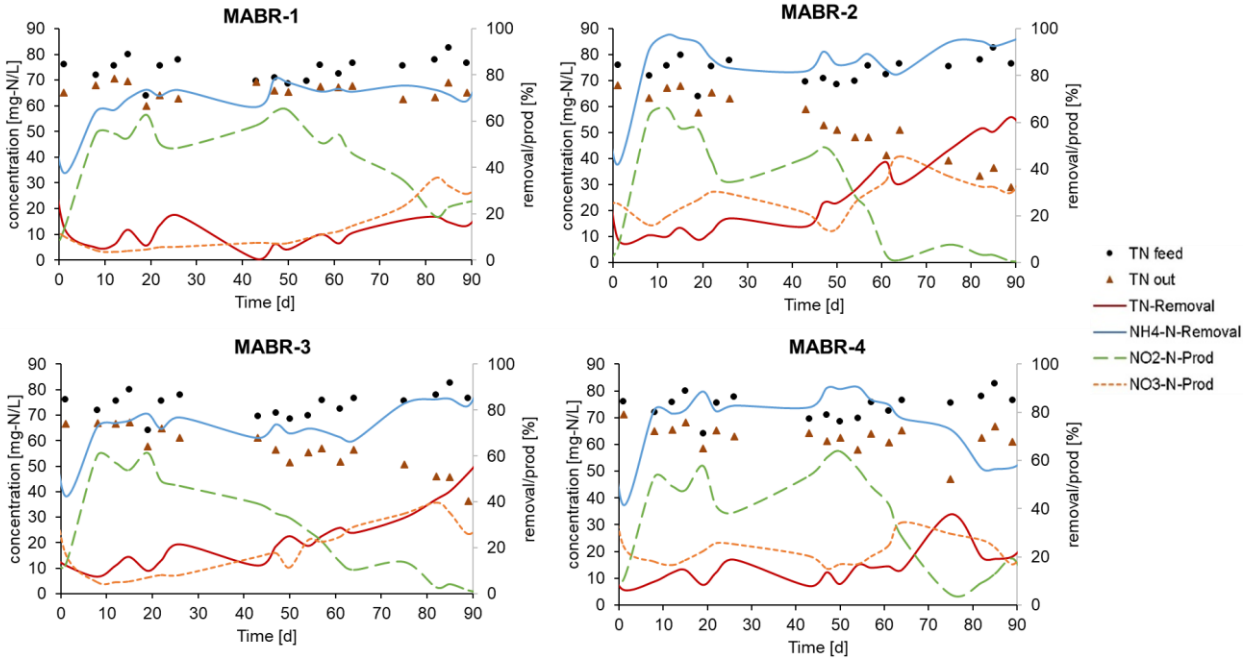

Fig. 5. Nitrogen balance within the 4 different MABRs.

One of the main disturbances in mainstream PN/A comes from influent COD. Thus, phase II introduced COD to the reactor influent and furthermore a change of the aeration strategy to intermittent (MABR-1) and continuous (MABR-2) aeration. Using a C:N ratio unfavourable for complete denitrification as is expected when the ultimate goal is PN/A, the main focus of phase II during the first months was to determine potential N_2O emissions from the MABRs. N_2O was measured in the gas-outlet of the MABRs as well as in the bulk liquid. With the use of these data, N_2O production rates could be determined which are shown in Fig. 6. Now, the performance of a continuously and an intermittently aerated MABR was compared. N_2O emissions were detectable in both systems but generally low, and even lower in the intermittently aerated MABR (MABR-1). Also, the N_2O concentrations were approximately 10-time higher in the bulk liquid as compared to the gas phase. Batch activity tests were performed to get some more insights into the microbial community and the activities of the different bacterial groups. Evaluation of these batch tests is underway.

CONCLUSIONS AND OUTLOOK

Both one stage PN/A and two stage (separate reactors for nitritation and anammox) PN/A systems are operational and under investigation. A combined IX-PN/A system demonstrating the complete process of ammonium absorption from mainstream wastewater by IX and IX bioregeneration by PN/A is presently under investigation using actual wastewater with an emphasis on establishing stable calcium concentrations in the IX regenerant solution.

The biofilm reactors (MABR) showed promising results, and the performances so far also suggest that a single stage PN/A system, incorporating PN and anammox in the same biofilm, might be easier to operate, as sustaining stable PN and nitrite production seems challenging. First experiments with carbon disturbances revealed low levels of N_2O emissions. Intermittently aerated MABRs are more promising to establish stable PN/A, but might be more limited in their removal capacities compared to continuously aerated systems. Optimizing and adopting the aeration regime for varying inflow conditions (C:N ratios) while minimizing N_2O emissions and maintaining high TN removal will be subject of the coming months.

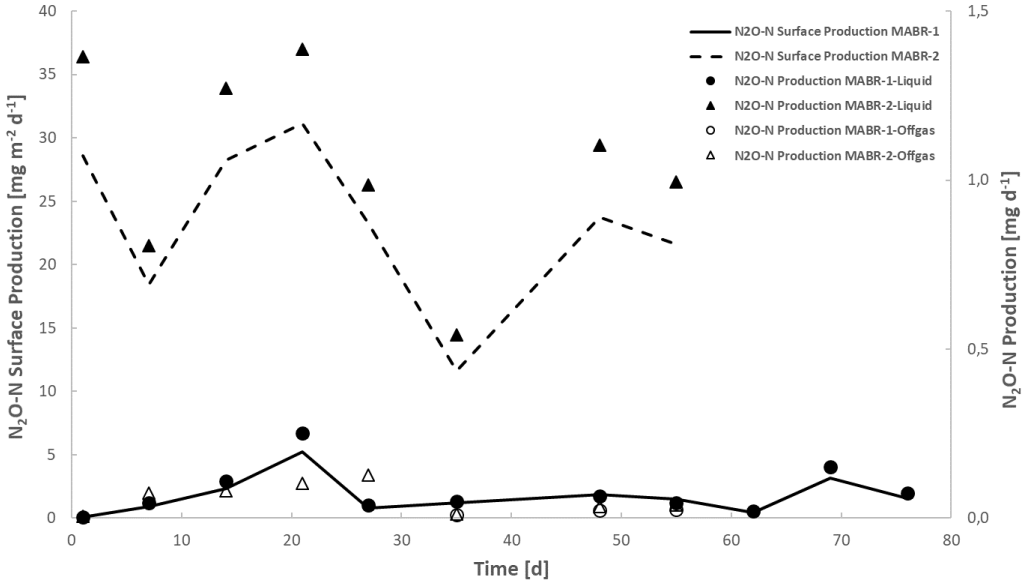

Fig. 6. N_2O production in the gas and liquid phase of the two MABRs

The cooperation between the partners will further focus on; 1) analyses and comparison of microbial communities under saline (Israel) and fresh water (German) conditions, 2) N_2O measurements, 3) investigation of N_2O production from Israel/German biomass and determination of reactor conditions for minimizing N_2O emissions, and 4) conditions for nitrite oxidizing bacteria (NOB) inhibition.

ACKNOWLEDGEMENT

This study is being supported by NSF-BSF (Grant No. 2019-708) and BMBF-MOST (Grant No. WT2002).

Project WT2004: EconWatSim-Project

Developing an economic simulation-modelling framework as a decision-support tool for policymakers in the water sector

Israel FINKELSHTAIN[1], Iddo KAN[1], Jonas LUCKMANN[2]*, Ami REZNIK[1], Yehuda SLATER[1]

[1]*Department of Environmental Economics and Management, The Hebrew University of Jerusalem, Israel*
[2]*International Agricultural Trade and Development Group, Humboldt-Universität zu Berlin*
**Corresponding author's e-mail: luckmann@hu-berlin.de*

ABSTRACT
In this study economic simulation models are linked to investigate the implications of different water pricing schemes on the Israeli economy. Preliminary model results suggest that the current pricing scheme can be optimized from an efficiency perspective. However, an increase of agricultural water prices as currently under discussion, may have unanticipated consequences in terms of distributional effects and welfare. The study demonstrates the potential of the model-linking approach to provide complementary results in terms of spatial and economy-wide perspectives, which go beyond the capability of the single models. This allows for a more holistic assessment of the implications of changes in the water sector. In this project, it is intended to enhance the linkages between the two models and to develop a novel economic simulation-modelling framework as a decision-support tool for policymakers in the water sector. The project will help to design coherent policies for the water and other sectors and thereby contribute to a more efficient and sustainable use of scarce water resources in Israel.

KEYWORDS
Water policy, economic simulation modelling, water price reform, Ramsey-Boitex pricing, marginal pricing, economies of scale

INTRODUCTION
In recent decades, population and income growth have led to increased water demand and the exacerbation of water scarcity across the globe. This issue is expected to be further aggravated by climate change. To meet these challenges, international organizations are promoting reinforcement of the traditional arsenal of quantitative instruments for water allocation, such as quotas or riparian rights, with price-based policies, such as user charges and fees (OECD, 2010). Two main arguments are raised to justify these policy reforms: 1) pricing constitutes essential incentives for efficient water use, and 2) fees are necessary for cost recovery, funding the water system's operation and maintenance, and facilitating investment in infrastructure. Accordingly, in 2010, the Israeli water law was changed, such that the cost-coverage principle came into force. From then onwards the water tariffs are supposed to cover the pumping and supply costs, including the investments required for the efficient development of the water sector. However, a typical water sector tends to exhibit scale economies, mainly as a result of the substantial share of capital investments in total costs. Also, physics and hydrology contribute to create

economies of scale in the conveyance of the water. With a simple proportional pricing, cost-covering requires to set the price at the average cost level,

while economic incentives call for marginal pricing. Scale economies imply that the two differ. Indeed, based on 2010 data, Reznik et., al (2016) report significant economies of scale in the Israeli water sector and estimated substantial deadweight losses as a result of the above pricing conflict in Israel.

Acknowledging the fact that under these conditions a pricing rule that implements the first best is infeasible, Ramsey (1929) and Boitex (1971) suggested a pricing rule that minimizes the deadweight losses, according to which the relative markup of the water price above the marginal cost should be proportional to the inverse demand elasticity of water. Thus, water consumers with less elastic demand pay more. Dierker (1991) formulated the conditions, under which the Ramsey-Boitex pricing rule indeed achieves the second best and is thus optimal under the cost coverage requirement. Much in the spirit of the above Ramsey-Boitex pricing rule, since the 2010 reform, the water economy in Israel was characterized by intersectoral cross subsidization, where the lower demand elastic urban sector subsidizes the agricultural sector with a larger demand elasticity as described in Luckmann, et al (2014).

However, as of 2022, the Israeli Water Authority (IWA) suggests a new pricing reform, increasing the water tariffs in the agricultural sector by 40% in order to abolish the intersectoral cross subsidization (IWA, 2021). In this study we investigate the implications of marginal water pricing, Ramsey-Boitex pricing as well as the effects that the 2022 water tariff reform is expected to have on the Israeli economy using a high-resolution nation-wide model of the water sector and a computable general equilibrium (CGE) model.

METHODS

The first model used in this study is the water sector economic model MYWAS (Multi Year Water Allocation System Model), which depicts a high level of topological detail, distinguishing 21 urban and 18 agricultural consumption areas and differentiates 46 sources of water, including desalination and wastewater treatment. Also, the conveyance infrastructure connecting supply and demand is depicted in detail. The second model is the CGE model STAGE_W (Luckmann et al., 2014). This model allows for linkages of the water sector with the rest of the economy, by depicting all relevant economic agents, such as households, firms and the government, which are linked through economic transactions on commodity-and factor-markets. The model differentiates 46 economic activities, 41, production factor categories, 10 household groups and considers a wide range of taxation instruments. It has been expanded specifically to capture the relevant peculiarities of the Israeli water sector, including use of different water qualities and sources (natural fresh water, desalination, reclaimed wastewater, brackish water) as well as price-differentiation between users.

For this study both models have been updated and calibrated to the year 2019 as base-year. While both models are not fully consistent, due to diverging modelling assumptions, calibrating the models to the same data achieves a high level of consistency. The models are run in a consecutive setup: MYWAS is used to optimize the water sector under marginal pricing as well as under Ramsey-Boitex pricing. The resulting water prices are then plugged into STAGE_W to investigate the economy-wide and distributional implications. In a third scenario, both models are used to analyse the implications of the 2022 water price reform.

PRELIMINARY RESULTS

MYWAS

To accommodate the balanced budget requirement, water rates were increased significantly during the previous decade. The price of fresh water for agriculture increased in real terms by more than 30% and the rates of reused water increased by more than 70% (Ahitov, 2022). However, even with this increase, agricultural water tariffs were lower than average cost implying cross subsidization by urban consumers. In this section we compare this policy to the first- and second-best pricing rules in the Israeli water economy and conclude that the actual policy, that involves the intersectoral cross subsidization was close to the second-best tariffs and therefore nearly optimal. **Fehler! Verweisquelle konnte nicht gefunden werden.** presents the results.

Table 3: Comparison of water pricing rules

	Pricing Rule:	**Actual Pricing 2019**	**Marginal Pricing (First best)**	**Ramsey-Boitex Pricing (Second-best)**
Water Consumption (MCM)	Urban	883	949	883
	Agriculture	1,141	1,342	1,315
	Neighbors	140	140	140
	Environment	0	0	0
	Total	2,164	2,431	2,339
Water Supply (MCM)	Fresh	818	1,071	1,021
	Brackish	131	108	107
	Desalinated Groundwater	1	2	1
	Treated Wastewater	556	593	552
	Desalinated Seawater	657	657	657
	Total	2,164	2,431	2,339
Efficient Prices (NIS/CM)	Urban	9.06	4.55	9.31
	Agriculture	1.84	1.41	1.47
Costs and Payments (M NIS)	Urb. Water Payments	8,000	4,319	8,221
	Ag. Water Payments	2,101	1,895	1,937
	Total Payments	10,100	6,214	10,158
	Total Variable Costs	5,846	6,227	5,907
	Total Fixed Costs	4,251	4,251	4,251
	Total Costs	10,097	10,479	10,158
Welfare (M NIS)	Urban Water Consumers	3,247	3,656	3,222
	Agriculture Water Consumers	8,846	9,052	9,010
	Agricultural Products Consumers	36,836	37,783	37,763
	Welfare (Surplus-Water Cost)	38,832	40,012	39,837

The first notable result is that the actual agricultural and urban water tariffs are higher than the efficient prices, which are equal to marginal cost, including a scarcity rent. This of course creates deadweight losses, which are estimated at 1.2 billion NIS (comparing total welfare in column 1 and 2 of Table 1), about 12% of the water sector's total cost. Interestingly, a large share of the welfare loss is associated with decreased surplus of consumers of agricultural products. However, it can be seen that the first best marginal pricing policy is infeasible, since it leads to a reduction in water payments by 4.2 billion NIS and to a deficit of the water sector. Note that this is mainly the result of the large fixed cost. In contrast, Boitex-Ramesy pricing ensures a balanced budget and entails much smaller welfare losses that amount to 200 million NIS, compared to marginal pricing. Note that the agricultural water price under the second-best pricing is very similar to the optimal one, the difference is about 4%, but it is 20% lower than the actual 2019 price. Thus, comparing to the 2019 prices, the Ramsey-Boitex second best

solution calls for a significant, 20%, reduction in the agricultural water price, and a minor increase in the urban price. Moreover, this analysis provides economic justification for the intersectoral cross subsidization, that has been applied in the Israeli water sector for the past two decades and questions the plan to abolish it, which is intended by the 2022 water tariff reform.

Table 4 presents the MYWAS-results of the water tariff reform. The bottom line is that the reform will decrease total welfare by 200 million NIS annually. Water use in agriculture will decrease by 90 million cubic meters, implying a demand elasticity of about 0.38. Yet, this elasticity was not taken into account when the tariff reform was designed. Therefore, the reform will reduce cross subsidization by 75%, but will not fully abolish it.

Table 4: Implications of the proposed 2022 water tariff reform

		Baseline	**Price Reform**
Prices (NIS/CM)	Urban	9.06	9.06
	Agriculture	1.57	2.23
Water Supply (MCM)	Fresh	828	746
	Brackish	139	131
	Treated Wastewater	465	465
	Seawater Desalination	657	657
	Total	2,089	1,999
Water Consumption (MCM)	Urban	883	883
	Agriculture	1,066	906
	Neighbors	140	140
	Environment	0	70
	Total	2,089	1,999
Welfare (M NIS)	Urban Net Consumer Surpluses	3,631	4,041
	Farmers' Profits	4,121	3,641
	Change in Agriculture Consumer Surpluses	0	-138
	Total	7,752	7,544
Costs and Payments (M NIS)	Revenues	9,546	9,867
	Variable Costs	5,838	5,749
	Fixed Costs	4,251	4,251
	Water Suppliers Profits	-544	-134
	Total	12,004	11,796

STAGE_W

STAGE_W allows to study the economy-wide and distributional implications of the water tariff changes. Interestingly, the marginal pricing scenario results in a situation in which despite of lower water prices in the agricultural sector, output prices increase (not shown). This is due to the strong urban water price decline, which results in a general boast of the economy, increasing the demand for production factors and thus the cost of production in all sectors, resulting in an increased price level, which is shown in **Table 5**. The efficiency gains in the marginal pricing scenario, lead to an increase of household and government income. However, with Ramsey pricing, the gains in the agricultural sector are outweighed by production reduction in other sectors, for which water prices increase, resulting in only a very minor increase in GDP.

Similarly, the increase of agricultural water prices (Price Reform), leads to reduced production and hence reduced income and GDP.

Table 5: Macroeconomic indicators

		Marginal Pricing		Ramsey-Boitex Pricing		Price Reform	
		million NIS	%-change	million NIS	%-change	million NIS	%-change
Factor income	Labour	23,662	3.0%	-1,160	-0.1%	-687	-0.1%
	Capital	9,627	2.9%	-488	-0.1%	-198	-0.1%
	Land	38	11.5%	12	3.5%	-62	-18.4%
Enterprise income		1,854	3.2%	-170	-0.3%	267	0.5%
Production	Agriculture	128	0.2%	59	0.1%	-341	-0.7%
	Industry	2,205	0.2%	-95	0.0%	10	0.0%
	Services	1,664	0.1%	-38	0.0%	-268	0.0%
	Total	3,997	0.1%	-75	0.0%	-600	0.0%
Household consumption		240	0.03%	-59	-0.01%	27	0.00%
Government income		7,309	1.6%	-566	-0.1%	419	0.1%
Real GDP		140	0.01%	10	0.00%	-70	0.01%

The distributional effects of the water tariff reforms are visible in **Figure 6**. While Ramsey-Boitex pricing only has very minimal implications for household welfare, due to the relatively small change in water prices, the other two scenarios result in a distribution in which poor households loose welfare, while rich households gain. For the marginal pricing scenario, this can be explained by the overall boast to the economy, resulting in an increase of income on the one hand, but also raising consumer prices on the other hand. Thereby, income of richer households increases over proportionally, due to their larger share of income from the ownership of enterprises, which is more positively affected, while poorer households depend to a larger extend on fixed government transfers, such that price increases outweigh their income gains. For the price reform scenario, the main cause is raising agricultural prices, which affects poor households with a high share of subsistence consumption over proportionally and increasing enterprise incomes benefitting mainly rich household groups.

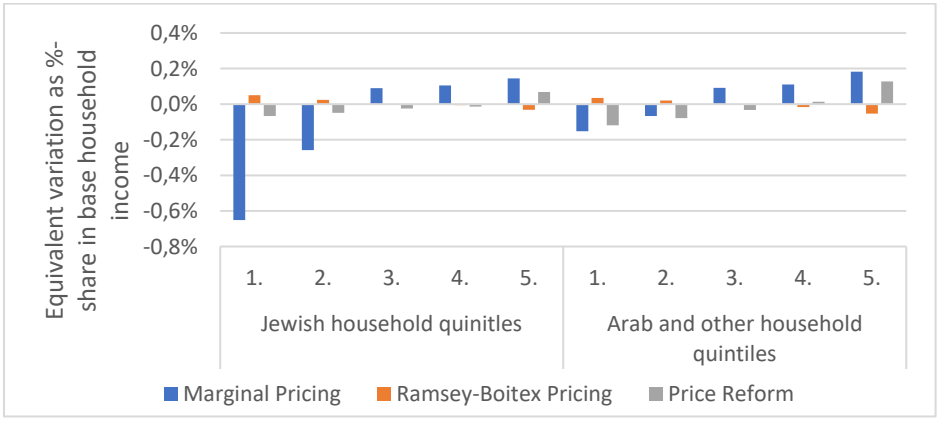

Figure 6: Change in household welfare

DISCUSSION, CONCLUSIONS AND OUTLOOK

Model results show that the suggested water tariff reform leads to welfare losses, while marginal pricing and Ramsey-Boitex pricing may improve efficiency in the water sector and welfare from an economy-wide perspective. In order to achieve a more pro-poor distribution of

welfare gains, complementary social policies could be designed to redistribute some of the efficiency gains in the latter two scenarios.

While the results presented in this analysis are preliminary as the models are work in progress, the study demonstrates the potential of the approach of model-linkage in providing complementary perspectives and hence allowing for a more holistic assessment of the implications of changes in the water sector.

In the further cause of this project the model integration is to be developed further, also allowing for feedback from STAGE_W to MYWAS e.g., in terms of energy-price changes, which in turn influence the optimization-process in the water sector. The final aim is the development of a fully integrated consistent economic simulation-modelling framework as a decision-support tool for policymakers in the water sector. This tool will allow for ex-ante analyzes of water policies as well as other direct or indirect changes to the water sector in a holistic way and in unprecedented detail. The project will help to design coherent policies for the water and other sectors (e.g. agricultural subsidies, tariffs) and thereby contribute to a more efficient and sustainable use of scarce water resources in Israel, considering all dimensions of international water benchmarking. Another novelty is that the framework will be able to take into account that different water sources produce water of varied quality. The modelling framework will be able to optimize both the quantity and quality of the water supplied, observing constraints imposed by regulations and capacity limits through two new mechanisms: i) selecting cost-efficient purification methods and ii) blending water from different sources, where feasible.

ACKNOWLEDGEMENT

Financial support in the framework of the German-Israel Water Technology Cooperation by the Israeli Ministry of Science, Technology and Space (MOST) and the German Federal Ministry of Education and Research (BMBF) under the funding code 02WIL1606 is gratefully acknowledged.

REFERENCES

Ahitov, A. (2022). Professional review to the depths of the water - What is the right way to design the optimal policy for the water sector for agriculture in Israel (in Hebrew). https://www.yfpp.org.il/article/146.

Boitex, M. (1971). On the management of public monopolies subject to budgetary constraints. *Journal of economic Theory* 3(3), 219-240.

Dierker, E. (1991). The optimality of Boiteux-Ramsey pricing. *Econometrica* 59 (1), 99-121.

IWA (2021). Call for public preliminary consultation (in Hebrew). https://www.gov.il/BlobFolder/reports/water-agriculture-18-4-21/he/council_calls_agriculture-water-18-4-21a.pdf

Luckmann, J., Grethe, H., McDonald, S., Orlov, A. and Siddig, K. (2014). An integrated economic model of multiple types and uses of water. *Water Resources Research* 50 (5), 3875–3892, https://doi.org/10.1002/2013WR014750.

OECD (2010). *OECD Review of Agricultural Policies: Israel 2010*, OECD Review of Agricultural Policies, OECD Publishing, Paris, https://doi.org/10.1787/9789264079397-en.

Ramsey, F. (1927). A Contribution to the Theory of Taxation. *The economic journal* 37 (145), 47-61.

Reznik, A., Feinerman, E., Finkelshtain, I., Kan, I., Fisher, F., Huber-Lee, A., Joyce, B., (2016). The Cost of Covering Costs: A Nationwide Model for Water Pricing. *Water Economics and Policy* 02 (04), 1650024. https://doi.org/10.1142/S2382624X16500247.